Tracing Degradation Effects in Organic Solar Cells

Tesis doctoral presentada por

Safakath Karuthedath

Para optar al título de Doctor en Ciencias Físicas

Departamento de Física de la Materia Condensada
Universidad Autónoma de Madrid
Madrid, Septiembre de 2015

Tracing Degradation Effects in Organic Solar Cells

Doctoral thesis presented by

Safakath Karuthedath

for the degree of Doctor of Philosophy in Physics by Universidad Autónoma de Madrid

Department of Condensed Matter Physics
Universidad Autónoma de Madrid
Madrid, September 2015

Directors of thesis:

Supervisor: Dr. Larry Lüer (IMDEA Nanociencia, Spain)

Co-host supervisor: Prof. Gytis Juška (Vilnius University, Lithuania)

Tutor: Prof. Nicolás Agraït (UAM, Spain)

Ph.D co-supervisors:

Dr. Reinhold Wannemacher (IMDEA Nanociencia, Spain)

Dr. Juan Cabanillas Gonzalez (IMDEA Nanociencia, Spain)

Dr. Johannes Gierschner (IMDEA Nanociencia, Spain)

Dr. Kristijonas Genevičius (Vilnius University, Lithuania)

Dr. Andreas Distler (Belectric OPV GmbH, Germany)

Thesis committee:

Prof. Vidamantas Gulbinas (Center for Physical Science &Technology, Lithuania)

Prof. Roberto Pacios (IKERLAN, Spain)

Dr. Reinhard Schwoediauer (Johannes Kepler University, Austria)

Dr. Felix Zamorra (Universidad Autónoma de Madrid/IMDEA Nanociencia, Spain)

Dr. Beatriz Romero (Universidad Rey Juan Carlos, Spain)

Dr. Mariano Campoy (ICMAB, Spain)

Dr. Cristina Flors (IMDEA Nanociencia, Spain)

This research was funded by the European Union Seventh Framework Program (FP7/2011 under grant agreement ESTABLIS no 290022)

Acknowledgements

I would like to thank many people, in many countries, who so kindly contributed to the work presented in this thesis.

First and foremost, I wish to thank my supervisor Dr. Larry Lüer at IMDEA Nanociencia for accepting me in his group to do a PhD. It has been an honour to be his first PhD student at IMDEA. He offered his continuous advices, encouragements, caring, patience, and systematic guidance and provided me excellent facilities for doing research throughout the course of this thesis. I learned a lot from him not only about ultrafast spectroscopy and global, target analysis but also about how a good scientist should be. During my tenure, he contributed a rewarding PhD experience by giving me intellectual freedom in my work, supporting my attendance at various conferences, engaging me in new ideas and keeping me covered during my entire PhD period. I am forever grateful.

I would like to thank my co-supervisors Dr. Reinhold Wannemacher, Dr. Juan Cabanillas and Dr. Johannes Gierschner at IMDEA Nanociencia for their continuous assistance. I especially thank Dr. Reinhold Wannemacher for helping me with experiments during first year of my PhD. Thanks to my co-host supervisors; Prof. Gytis Juška, Dr. Kristijonas Genevičius and Prof. Kestutis Arlauskas at University of Vilnius, Lithuania for providing good facility to learn opto-electrical techniques from masters. Thanks to my tutor Prof. Nicolás Agraït at Departamento de Fisica de la Materia Condensada, Universidad Autonema de Madrid.

Every result described in this thesis was accomplished with the help and support of fellow lab mates and collaborators in the ESTABLIS consortium. I greatly thank Dr. Tobias Sauermann, Dr. Andreas Distler, Dr. Dargie Deribew and Dr. Simon Dowland of Belectric OPV GmbH, Nuremberg, Germany for providing me excellent organic solar cells time to time, worthy science exchanges and the training I received from you guys during my stay at Belectric. I especially thank Dr. Hans-Joachim Egelhaaf of ZAE Bayern (former R&D head, Belectric OPV) for the intense scientific collaboration, the discussions happened online and offline and advices during my entire PhD term. Thanks to Dr. Graham Morse of Merck Chemicals, Southampton, UK, Isabel Fraga of IPREM, Clermont-Ferrand, France, Hasina Ramanitra and Alberto Gregori of UPPA, Pau, France for sending me your materials for the ultrafast studies.

My deepest gratitude to the project ESTABLIS and its co-ordinators, Dr. Roger C. Hiorns, Dr. Paul Topham, Dr. A J Sutherland and Dr. Mélanie Pédeutour for this wonderful project, training I received, and great workshops we together had all-around the Europe. I also thank all the ESTABLIS project leaders, supervisors and associates. It was really nice to collaborate with you. And my dearest ESTABLIS fellows; Hugo, Hasina, Anna, Alberto, Aurelien, Meera, Isa, Jenia, Joanna, Mamadou, Meera, Stefan, Graham, Dargie, Simon, Hari; thank you very much for the nice time we had together. It was enjoyable to work with you, live with you and play with you. Sorry for the tackles and fouls I did during the football matches. Your Shaffy is deeply thanking you. Thanks Meera and Anna, the best colleagues I ever had. It was really a pleasant time in Vilnius with you Meera and I enjoyed the trips with you. Thank you Meera. Anna, you were my best guest ever. Really nice to share office with you, thanks for the travels, dinners, discussions, crazy goes we had. It's always a pleasure to be your friend.

I deeply thank my colleagues and friends at IMDEA Nanociencia. Guilin, Benedict, Rameesha, Abasi, Lungfie, Jun Shi, Santanu, Rim, Diana, Siya, Aitor, Pawel, Shinto, Patricia and Mike; thank you guys for making my PhD life vibrant and enjoyable. Special thanks to Diana for helping me with Spanish translations for my thesis. Thanks Cristina, Enrico, Reinhold, Begoña, and Feng for your advices, helps and for the lunch time discussions. I would like to thank Juan Carlos for helping me to learn Spanish and his advice to eat more potatoes. Thanks Antonio for getting me liquid Nitrogen time to time. Thanks to the IMDEA administration team; Patricia for the hectic VISA and residence card procedures, Isabel for financial and reimbursements, Dr. Marije Villa for helping with contracts. I also thanks to the whole IMDEA team and the institute for the nice time I had and hosting me for my PhD.

Thanks to all my friends in Kerala and in India for giving me energy to continue. Thanks Manoop, Anoop, K.K, Navas, Faiz, Sharaf, all FIRSTians and Gulanders for the Skype and Hangout calls we had during the weekends and support.

Thanks to everybody whome I forgot to mention!

Finally, I thank the Almighty for the health and wellbeing that were necessary to complete my PhD work. I would like to thank my family; my parents, my sisters and my brother for supporting me spiritually throughout writing this thesis and my life in general. Last, but not least, I would like to thank my wife Rameesha for her understanding and love during the past few years. Her support and encouragement was in the end what made this dissertation possible.

Table of Contents

Acknowledgements iv

Resumen (ES) ix

Abstract (EN) xiii

1 Introduction 1

1.1 History of organic solar cells 1

1.2 Bulk hetero-junction organic solar cells 3

1.3 Device physics 4

1.3.1 Photon absorption and exciton generation 5

1.3.2 Exciton diffusion and dissociation 7

1.3.3 Charge carrier pair dissociation 8

1.3.4 Charge carrier transport 10

1.3.5 Charge Carrier recombination 11

1.3.6 Charge carrier extraction 12

1.4 Characteristic values of a solar cell 12

1.5 Degradation in organic solar cells 14

1.5.1 Physical stability 15

1.5.1.1 Morphological stability 16

1.5.1.2 Flexibility and stability 17

1.5.1.3 Delamination 17

1.5.2 Chemical degradation 18

1.5.2.1 Photochemical stability 18

1.5.2.2 Barrier effects of layers 19

1.5.3 Electrode degradation 20

1.6 Aim of the thesis 21

2 Materials and methods 22

2.1 Materials 22

2.1.1 P3HT 22

2.1.2 Si-PCPDTBT 22

2.1.3 PDTSTzTz (KP115) 23

2.1.4 BDT-DPP polymers 23

2.1.5 $PC_{60}BM$ 24

2.1.6 Intermediate layers 25

2.2 Device preparation and degradation 25

2.2.1 Coating method: Doctor blading 27

2.3 Experimental setups 27
2.3.1 Transient absorption spectroscopy (TAS) 28
2.3.1.1 Femtosecond pump-probe spectroscopy 29
2.3.1.2 Microsecond transient absorption spectroscopy 31
2.3.2 Transient electrical measurements 32
2.3.2.1 Transient photovoltage (TPV) 33
2.3.2.2 Transient photocurrent (TPC) 33
2.3.2.3 Charge extraction by linearly increasing voltage (CELIV) 33
3 Photo-physics of P3HT:PCBM solar cells 36
3.1 Introduction 37
3.2 Experimental 38
3.3 Results and discussion: Photoexcitation dynamics in pristine films and solar cells 40
3.3.1 Femtosecond transient absorption spectroscopy 40
3.3.2 Microsecond transient absorption spectroscopy 42
3.3.3 Determining recombination dynamics in an operating P3HT:PCBM solar cell 43
3.3.4 Recombination dynamics in P3HT:PCBM devices and films: A comparison 45
3.3.5 Lateral diffusion of polarons in P3HT:PCBM solar cells induced by high-conductivity PEDOT 48
3.4 Summary 52
4 The effect of oxygen induced degradation in P3HT and Si-PCPDTBT solar cells 53
4.1 Introduction 54
4.2 Experimental Section 54
4.3 Results 56
4.3.1 Transient absorption spectroscopy 57
4.3.2 Photo-CELIV 60
4.4 Discussion 62
4.4.1 Transient absorption spectroscopy 62
4.4.2 Photo-CELIV 68
4.5 Summary 69
5 Photo-oxidation effects in silole-based polymer:PCBM solar cell 71
5.1 Introduction 72
5.2 Experimental 72
5.3 Results and discussion 73
5.3.1 Current density-voltage characteristics 73
5.3.2 UV-Vis absorption spectra 75
5.3.3 Picosecond transient absorption spectroscopy 76

5.3.4 Microsecond transient absorption spectroscopy 79
5.3.5 Transient photovoltage decay 83
5.3.6 Transient photocurrent decay 84
5.4 Summary 87
6 Improved thermal stability of low band gap polymer solar cells: Relating device performance to blend morphology 89
6.1 Introduction 90
6.2 Experimental 92
6.3 Results and discussion 93
6.3.1 Electrical performance in the pristine state and after thermal degradation 93
6.3.2 Generation of extractable carriers 95
6.3.3 Charge extraction and nongeminate recombination 104
6.4 Conclusions 107
7 Conclusiones y outlook (ES) 109
7.1 Conclusiones 109
7.2 Outlook 112
8 Conclusions and outlook (EN) 114
8.1 Conclusions 114
8.2 Outlook 116
9. **References** 118
Appendix 1 129
Appendix 2 135
Appendix 3 139
Publications 142

Resumen

Durante la última década notables avances en el campo de las celdas solares orgánicas (OSC, por sus siglas en inglés) han sido alcanzados. Las OSC compuestas por polímeros han logrado una eficiencia de conversión de energía de más del 10% y ya valores del 15% están a su alcance. La química de polímeros ha jugado un papel importante en este logro y será la clave para su desarrollo ulterior. Por otra parte, los mecanismos subyacentes en el proceso de conversión fotovoltaica son aún objeto de debate en las celdas solares de polímeros. Una cuestión fundamental que debe ser mejorada en las celdas solares orgánicas es su tiempo de vida útil. La caracterización de corriente-voltaje es el método más directo para monitorear la pérdida de rendimiento inducida por la degradación en las celdas solares orgánicas. Pero una curva I-V sólo da una estimación aproximada del mecanismo de degradación. La eficiencia cuántica externa (EQE, por sus siglas en inglés) de una OSC depende de la eficiencia de absorción (φ_{abs}), la eficiencia de la disociación del excitón (φ_{diss}), la eficiencia de la separación del par polarón (φ_{sep}) y la eficiencia de la extracción de carga (φ_{extr}). Estos procesos suceden en una OSC en una amplia gama de escalas de tiempo que varían de pocos femtosegundos a milisegundos.

Los efectos de la degradación química y el estrés térmico en la capa activa de las OSC son aún poco conocidos. Por lo tanto esta tesis trata de profundizar sobre los efectos de la luz inducida por foto-oxidación y el tratamiento térmico en un sistema polimérico modelo, P3HT y una serie de nuevos materiales de pequeña banda prohibida incorporados con fullereno. Las mediciones opto-eléctricas resueltas en el tiempo son excelentes herramientas para la identificación de los mecanismos de degradación. Al realizar estudios de espectroscopía de absorción resuelta en el tiempo (TAS, por sus sigla en inglés) se tiene acceso a la población de excitones y especies cargadas, los referidos estudios se pueden llevar a cabo tanto en filmes que comprenden solo la capa activa, así como en dispositivos completos. Esta técnica es la única que es capaz de cubrir todas las escalas temporales en las cuales pueden tener lugar los procesos de pérdida, desde femtosegundos hasta milisegundos. Además cuando se combina con herramientas de análisis de matrices como el análisis global y el análisis objetivo, esta técnica es capaz de proporcionar información cuantitativa sobre la dinámica de todo el estado foto-excitado que puede ser relevante, como pueden ser excitones individuales, tripletes, estados de carga, estados de transferencia de carga, etc. Esto permite identificar las razones de las pérdidas de rendimiento de las celdas solares orgánicas. Además de

espectroscopía de absorción resuelta en el tiempo (TAS, por sus sigla en inglés), técnicas eléctricas transitorias complementarias como la medición del foto-voltaje resuelto en el tiempo (TPV, por sus siglas en inglés), la medición de la foto-corriente resuelta en el tiempo (TPC, por sus siglas en inglés), la medición de la extracción de carga al incrementar linealmente el voltaje (CELIV, por sus siglas en inglés) también se utilizan para controlar las pérdidas de rendimiento por degradación inducida en la celda solar orgánica.

El objetivo principal de esta tesis ha sido el estudio de la fotofísica, por medio de técnicas resueltas temporalmente, de celdas solares orgánicas recién construidas y ya una vez degradadas. El Capítulo 1 ofrece una introducción al mundo de las celdas solares orgánicas y a la fotofísica fundamental de las mismas luego de la absorción de fotones. En el mismo a continuación se detallan los factores desencadenantes más importantes que pueden afectar el rendimiento de las OSC. El Capítulo 2 trata acerca de los materiales estudiados en esta tesis y de las técnicas experimentales utilizadas para investigar la fotofísica de las celdas solares orgánicas.

En el Capítulo 3, se estudia la fotofísica de celdas solares recién construidas, así como de filmes delgados de P3HT:PCBM. Diferentes técnicas de resolución temporal, denominadas, espectroscopía de absorción resuelta en el tiempo (TAS, por sus siglas en inglés) y foto-voltaje resuelto en el tiempo (TPV, por sus siglas en inglés), se han utilizado para desentrañar la dinámica de estado excitado del P3HT:PCBM. Los resultados obtenidos en el rango de los microsegundos empleando la TAS, sugieren una dinámica de recombinación bimolecular de los portadores de carga dependiente de la intensidad. En este capítulo también se investiga el efecto de la altamente conductora capa intermedia de PEDOT:PSS en el transporte de portadores de cargas. Se ha encontrado que la presencia de esta capa intermedia de PEDOT:PSS facilita los movimientos laterales de los portadores de carga junto con la difusión vertical.

En el capítulo 4, los efectos de la foto-oxidación en las celdas solares de P3HT y Si-PCPDTBT se investigan por medio de la espectroscopía de absorción resuelta en el tiempo (TAS, por sus sigla en inglés) y la medición de la extracción de carga al incrementar linealmente el voltaje (CELIV, por sus siglas en inglés). Los estudios arrojaron una reducción drástica de la corriente de cortocircuito (Jsc, por sus siglas en inglés) ya a niveles muy bajos de foto-oxidación. Antes de que cambios apreciables en la absorción tengan lugar, la foto-oxidación conduce a una fuerte reducción en la recombinación y la extracción de portadores

de carga debido a una disminución de la movilidad de los portadores de carga y a un aumento en la concentración del fondo de portadores, mientras que la generación de portadores de carga no se ve afectada. Se demuestra que la extracción ocurre con un mayor retraso que la recombinación, posiblemente debido a una reducción de la extracción de cargas por el fondo de portadores.

En el capítulo 5, los efectos de la degradación inducida por el oxígeno en muestras de KP115:PCBM en presencia de la luz se explica por medio de técnicas resueltas en el tiempo. Los estudios revelaron que la enorme pérdida en la corriente de cortocircuito (Jsc, por sus siglas en inglés) es debido a los efectos combinados de la reducción de la movilidad efectiva y la formación de zonas aisladas de donante-aceptor. Curiosamente, la foto-oxidación en estos materiales no altera el orden de recombinación y no crea un fondo de portadores. También se observa que incluso en el caso en que los dispositivos se encuentran recién construidos la extracción de carga no es completa, hecho que indica que la morfología no es la óptima.

El Capítulo 6 se ocupa de los efectos de la degradación térmica, que son tan críticos para la vida operativa de los dispositivos como los efectos de la foto-oxidación, pero que en contraste con este último no puede ser controlado por medio de la encapsulación, sino que más bien depende de la evolución de la morfología de la capa activa. Debido a esto, se estudió una serie de celdas solares de los polímeros BDT:DPP con diferentes cadenas laterales, lo que proporciona la oportunidad de investigar diferentes morfologías pero con una estructura electrónica muy similar. La inmediata formación de tripletes, incluso en el caso de los dispositivos recién construidos, parece ser un problema importante en este tipo de celdas solares. El tratamiento térmico aumenta el rendimiento de la formación de tripletes, reduciendo así el rendimiento de los dispositivos. La degradación térmica reduce fuertemente la generación de carga ultrarrápida, mientras que las vías retardadas para la difusión muestran que reducen la eficiencia de generación de carga. Esto podría ser debido a la reducción de la vía ultrarrápida debido al crecimiento de dominios ricos en presencia del material donante. La reducida producción de portadores de carga de esta vía retardada se atribuye a procesos de disminución de los excitones como, la reducción de aceptores molecularmente disueltos en la fase en que existe la presencia de dominios ricos de material donante. Adicionalmente, resultados obtenidos en el rango de los microsegundos muestran que, parte de la pérdida del rendimiento eléctrico observado es debido a un mayor tiempo de extracción y recombinación de los portadores de carga, lo que indica su movilidad reducida. Estos procesos son menos

notables en las celdas solares que emplean polímeros con cadenas laterales de alquilo, las cuales demuestran una estabilidad mejorada de la mezcla bajo estrés térmico.

Por último, los comentarios concluyentes sobre las celdas solares estudiadas y sus perspectivas se dan en el Capítulo 7 y 8, el cual es seguido por la sección bibliográfica.

Abstract

Remarkable progress has been made in the field of organic solar cells (OSCs) over the last decade. Polymer based OSCs have achieved power conversion efficiencies of more than 10% already and 15% is within reach. Polymer chemistry has played a significant part in this achievement and will be the key to the further developments. On the other hand, the underlying mechanisms in the photovoltaic conversion process are still under debate in polymer solar cells. A critical issue to be improved in organic solar cells is their operational lifetime. Current-voltage characterization is the most direct method to monitor degradation induced performance loss in organic solar cells. But an I-V curve gives only a rough estimation to the degradation mechanism. The external quantum efficiency (EQE) of an OSC is dependent on efficiency of absorption (φ_{abs}), efficiency of exciton dissociation (φ_{diss}), efficiency of polaron pair separation (φ_{sep}) and efficiency of charge extraction (φ_{extr}). These processes are happening in an OSC in a wide range of time scales varying from few femtoseconds to milliseconds.

The effects of chemical degradation and thermal stress on the active layer of OSCs are still poorly understood. Therefore this thesis attempts to shed more light on the effects of light induced photooxidation and thermal annealing on a model polymer system, P3HT and a series of new low optical band gap materials containing fullerene. Transient opto-electrical measurements are excellent tools for identifying the degradation routes. Transient absorption spectroscopy (TAS) studies give access to the time-resolved population of excitons and charged species, and can be performed in films of the active layer as well as in complete devices. It is the only technique which is capable of addressing all relevant time scales in which loss processes can occur, from femtoseconds to milliseconds. When combined with matrix analysis tools like global and target analysis, it is able to provide quantitative information on the dynamics of all relevant photo-excited states, such as singlet excitons, triplets, charged states, charge transfer states etc. This allows to identify the reasons for performance loss of organic solar cells. In addition to TAS, complementary transient electrical techniques like transient photo-voltage (TPV), transient photo-current (TPC), charge extraction by linearly increasing voltage (CELIV) were also used to monitor degradation induced performance losses in organic solar cell.

The main goal of this thesis has been to study the photophysics of pristine and degraded organic solar cells by means of time-resolved techniques. Chapter 1 gives an introduction to

the world of organic solar cells and the fundamental photophysics of OSCs upon photon absorption followed by detailing the major degradation triggers affecting the performance of OSCs. Chapter 2 deals with the materials studied in this thesis and experimental techniques used to probe the photophysics of organic solar cells.

In Chapter 3, the photophysics of pristine P3HT:PCBM solar cells and thin films are studied. Different time-resolved techniques, namely transient absorption spectroscopy (TAS) and transient photovoltage (TPV), have been used to unravel excited state dynamics of P3HT:PCBM blends. Microsecond TAS results suggested an intensity dependent bimolecular recombination dynamics of charge carriers. This chapter also investigates the effect of the highly conductive PEDOT:PSS interlayer on the charge carrier transport. It is found that the presence of highly conductive PEDOT:PSS facilitates the lateral movement of charge carriers, in addition to vertical diffusion through the bulk.

In Chapter 4, the effects of photooxidation on P3HT and Si-PCPDTBT solar cells were investigated by means of TAS and charge extraction by linearly increasing voltage (CELIV). A drastic reduction of short circuit current (Jsc) was observed already at very low levels of photooxidation. Before any appreciable changes in absorption occurs, photo-oxidation leads to a strong reduction in the recombination and extraction of charge carriers due to a decrease of charge carrier mobility and an increase in the background carrier concentration, whereas the generation of charge carriers is not affected. Extraction is shown to be retarded even more strongly than recombination, possibly by a reduction of the extraction field by the background carriers.

In Chapter 5, effects of oxygen-induced degradation in KP115:PCBM in the presence of light is explained by means of time-resolved transient techniques. Studies unveiled that the huge loss in J_{sc} is due to combined effects of reduction in the effective mobility and formation of isolated donor-acceptor islands. Interestingly, the photooxidation of these materials does not alter the recombination order and creates no background carriers. It is also observed that even in the pristine case the charge extraction is not complete, indicating the morphology is not optimum.

Chapter 6 deals with the thermal degradation effects, which are as critical for the operational lifetime of the devices as the effects of photooxidation but in contrast to the latter cannot be controlled by encapsulation but rather depend on the morphology evolution of the active layer. Therefore, we studied a series of BDTDPP polymer solar cells having different

sidechains, which provides the opportunity to investigate different morphologies but very similar electronic structure. Immediate triplet formation even in the pristine case seems a major problem in these solar cells and thermal annealing increase the triplet yield, reducing the performance of the devices. Thermal degradation is found to strongly reduce the ultrafast charge generation, while the diffusion-mediated delayed pathway also shows reduced charge generation efficiency. This could be due to the reduction of the ultrafast pathway with the growth of donor-rich domains. The reduced charge carrier yield of the delayed pathway is attributed to exciton quenching processes like quenching at molecularly dissolved acceptors in the donor-rich phase. Microsecond transient measurements show that additionally, part of the observed electrical performance loss is due to an increased charge carrier extraction and recombination time, indicating their reduced mobility. These processes are less pronounced in solar cells employing polymers with alkyl side chains which demonstrate an improved stability of the blend under thermal stress.

Finally, conclusive remarks on the studied solar cells and outlook are presented in Chapters 7 and 8.

Chapter 1

Introduction

The growth of global greenhouse gas emissions between 2000 and 2010 has been greater than in the previous three decades. The energy production occupies the major part of growth in emissions accounting for 35% of total emissions globally.[a] In Lima Climate Change Conference -December 2014, member countries agreed on an important resolution to reduce CO_2 emission. One of the mitigation measures is to use low or no carbon energy sources for energy production.[a] Besides the environmental issues, fast depletion of fossil fuel resources and increased energy needs are also demanding sustainable and renewable energy resources.[1,2] Solar energy is one of the most important sustainable energy resources with low carbon release. The earth's surface receives~ $63x10^{15}$W of energy from sun light, which is a thousand times higher than our energy needs.[3,4]

Light is made up of packets of energy, called photons. The energy of photons depends upon the frequency of the light and it is sufficient to excite an electron from the ground state to an excited state, or to a vacuum state where they are free to move, which was explained by Albert Einstein in 1905.[b] This phenomenon is called photoelectric effect. When the material absorbs light, the excited electrons quickly decay from the higher energy states to the ground state. In a photovoltaic device, the excited state electrons (and holes) are split and attracted and guided to the separate electrodes and subsequently to the external circuit because of the asymmetry of the built-in electric field. The effectiveness of light for electricity conversion depends on the choice of light harvesting units, light sources, the way the light is impinging on the material, the way the charge carriers are moving to the electrodes, etc.[3,5,6]

1.1 History of organic solar cells

Chapin, Fuller and Pearson made the first solar cell from silicon p-n junction in 1954.[7] Later on many research groups all around the world developed solar cells based on different inorganic semiconductors.[8–10] The levelized cost of electricity (LCOE) for solar

[a] http://unfccc.int/meetings/lima_dec_2014/meeting/8141.php

[b] Albert Einstein - Facts. Nobel Media AB, 21 Aug. 2013

photovoltaics is still fairly high compared to alternatives based on conventional energy resources such as fossil fuels for competitive commercial production.[11,12]The current photovoltaic market consists of a variety of technologies such as thin film solar cells and wafer based silicon.[13]One can group the development of the photovoltaic (PV) technology into three categories, namely first generation, second generation and third generation photovoltaics as depicted in figure 1.1.

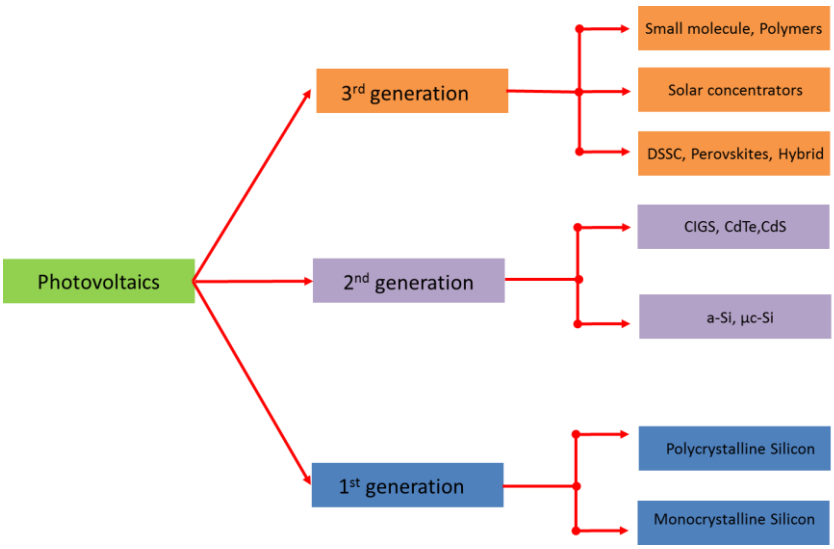

Figure 1.1: Different categories of the photovoltaic technology. Scheme adapted from [c]

Nowadays 90% of the photovoltaic market is dominated by 1st generation photovoltaics (1G).[6,12] Inorganic mono- or polycrystalline silicon-based solar cells with market efficiency around 20% have already been demonstrated.[6] First generation solar cells are inherently stable, and simple in constitution. 1G solar cells are widely used for roof top and free standing applications. The non-scalability and expensive production are the main drawbacks of 1G. Cost of the 200-300 µm thick silicon wafer consumes more than half of the cost of 1G solar cells. So, cutting down the thickness would offer better price, since light absorption takes place in the top few tens of microns.[12] The next cost driving factor is production and installation expenses.[11]

Second generation solar cells (2G) employ better manufacturing conditions and aim to use less materials by reducing layer thickness around few microns.[14,15] This is possible only when the active material has high absorption yield. Materials like cadmium telluride (CdTe), amorphous silicon (a-Si) and copper indium gallium selenide (CIGS) are good candidates for thin film photovoltaics application.[6] On the other hand, these materials, except a-Si, are

[c] http://www.heliatek.com

considered as toxic and harmful which makes the recycling process difficult and costly.[16,17]Moreover, some vital materials for this 2nd generation PV are rare elements which add to the overall cost of the PV module.[18] Because of the high production, maintenance, installation and recycling costs of the 1st and 2nd generation PV devices, new paths to harvest solar energy in cheap and safe ways are being investigated.[19] The third generation (3G) solar cells include dye-sensitized (or Grätzel type) solar cells (DSSC), tandem solar cells, solar concentrators and polymer or small molecule solar cells and perovskites solar cells.[6]

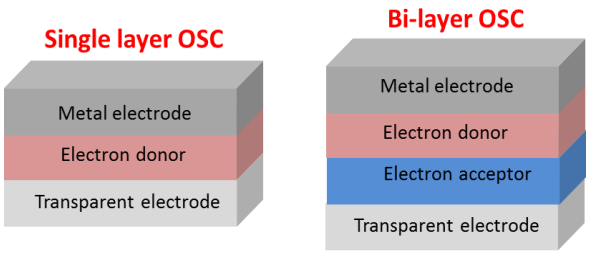

Figure 1.2: Schematics of single layer and bi-layer organic solar cell.

1.2 Bulk hetero-junction organic solar cells

Organic solar cells are also called excitonic solar cells, because optical excitation creates strongly bound electron hole pairs (Frenkel excitons).[20] Because of the small diffusion length, the excitons do not dissociate into charges in single layer OSCs (figure 1.2). Consequently single layer organic solar cells have power conversion efficiency (PCE) far less than1%.[21] Introduction of a second organic semiconductor creating a so-called donor-acceptor system was a turning point in terms of overall performance (figure 1.2). The first organic bi-layer solar cell was realized by C.W Tang in the mid-eighties.[22] The main advantage of bi-layer OSC's is a smaller probability of recombination as compared to single layered organic solar cells. In two-layer organic solar cells, light is absorbed by one of the semiconducting layers (usually by the donor) and the generated singlet excitons diffuse within the donor material toward the planar interface with the second material, the electron acceptor. The acceptor is usually electronegative supplying the energy needed for the exciton dissociation. The resulting separated electrons move onto the acceptor, whereas the holes remains in the donor material. By using appropriate electrodes, one can extract charge carriers to an external circuit.[5]

A potential electron acceptor is the buckminsterfullerene and its derivatives because of their spherical shape and high electronegativity.[23] However, only the excitons created within a distance lower than the diffusion length from a donor-acceptor interface will have the chance

to reach the interface and separate into a free electron-hole pair. The typical exciton diffusion length of conjugated polymers is 5-10nm.[24,25] Hence only about 10% of excitons can reach the interface and contribute current.[5,6] To overcome this issue, the donor material should have a layer thickness comparable with the exciton diffusion length. By doing so, one will compromise the absorption yield or need to use high absorption coefficient materials as donor materials.

In order to overcome issues with small exciton diffusion length and the thickness required for the light absorption, a new concept of blend architecture or bulk heterojunction (BHJ) was introduced.[26] In this architecture, the donor and acceptor are intermixed in order to get a large interfacial area. This, in turn, enables the excitons to reach the interface within their diffusion length. The main disadvantages of the BHJ solar cells are: (i) increased probability of recombination (compared to that in bi-layer devices) and (ii) disrupted charge percolation pathways due to the increased disorder of the system.[5] The high exciton dissociation efficiency and, as a result, overall device performance outweigh these drawbacks.

Efficiencies above 8% have already been reported for bulk heterojunction organic solar cells.[27,28] The operational lifetime (stability) and further improvements in power conversion efficiency are the two main issues yet to be solved. To achieve stable and efficient OPVs intense study of the fundamental electronic interactions between donor and acceptor materials as well as, in the complete device, active layer morphology, fundamental processes happening after the absorption of light, etc. are necessary.[29–33] Depending on the device architecture, there are two types of BHJ solar cells, namely normal or conventional architecture devices and inverted architecture devices (figure 1.3).

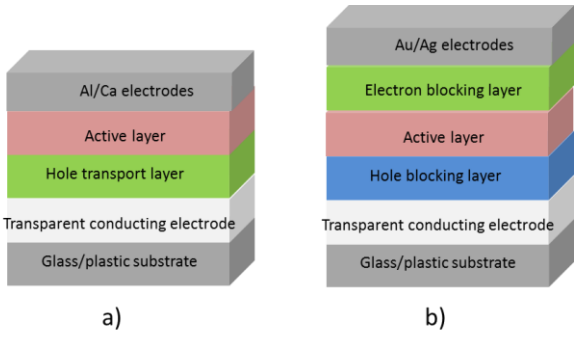

Figure 1.3: Schematic architecture of a) normal b) inverted bulk hetero junction solar cell.

1.3 Device physics

After absorption of a photon from the incoming light and excitation of an electron from the highest occupied molecular orbital (HOMO) to the lowest unoccupied molecular orbital

(LUMO), a series of photo-physical processes happens, resulting in current generation. These fundamental processes are schematically outlined in figure 1.4.

a. Photon absorption and exciton generation;
b. Exciton diffusion and dissociation;
c. Charge carrier (polaron) pair dissociation;
d. Charge carrier transport ;
e. Charge carrier recombination;
f. Charge carrier extraction.

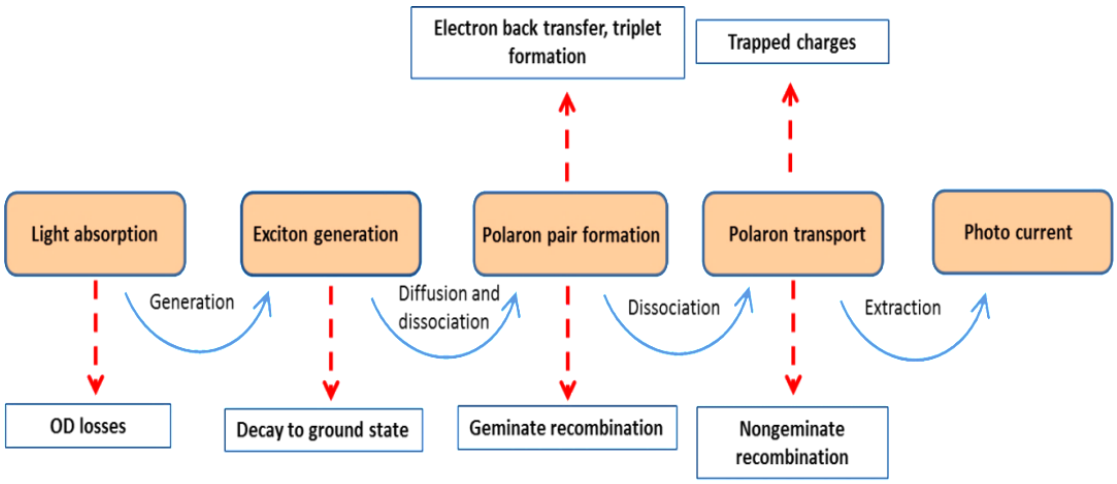

Figure 1.4: Schematic representation of elementary processes in organic solar cell. White rectangles indicate loss mechanisms.

1.3.1 Photon absorption and exciton generation

In organic donor–acceptor solar cells, the donor material usually absorbs the light, in most cases a conjugated polymer. In analogy with many organic dyes, organic solar cells also exhibit high absorption coefficient, 10^7/m, therefore a thickness of 100-300 nm is enough for good absorption of sunlight.[5,6] For comparison, to obtain a similar absorption in crystalline silicon, the layer should be two orders of magnitude thicker. Unlike in organic semiconductors, many organic semiconductors show a spectral mismatch with the AM1.5 solar spectrum (solar spectrum at solar zenith angle of Z=48.2°), which limits the absorption only to the visible part of the solar spectrum.[34,35] By lowering the band gap of the organic material, it is possible to harvest more sunlight and therefore achieve higher photocurrent. For this reason much research effort is currently put into obtaining organic polymers with an optical band in the near infra-red (NIR), so called low bandgap polymers.[36] But, still a lot of work has to be done in terms of optimisation and stability of these materials.[3,37,38]

From the absorbed light, excitons (bound electron-hole pairs) are formed in the organic semiconductors, where the electrons reside in the LUMO and the holes in the HOMO of the donor material. In organic semiconductors the electrons and holes are strongly bound because of their strong Coulomb interaction owing to the small dielectric constant of the materials.[6] The dielectric constant of the organic semiconductors is around 3-4, whereas inorganic ones have much higher dielectric constant.[3,5,6] For efficient energy conversion, this electron-hole pair must overcome the mutual Coulomb attraction V, and separate into long-lived dissociated charge carriers. In an isotropic medium, the Coulomb attractive potential V is given by,

$$V = -\frac{e^2}{4\pi\varepsilon_0\varepsilon_r r_c} \tag{1.1}$$

where e is the charge of an electron, ε_0 is the permittivity of vacuum, ε_r is the dielectric constant of the surrounding medium and r_c is the electron-hole pair separation distance. Considering the Coulomb attraction of an electron-hole pair to get a rough estimate for the exciton binding energy, a separation of 1nm in a material with the dielectric constant of 3, the Coulomb binding energy is equal to 0.5eV.[5] The exciton binding energy far exceeds the thermal energy at room temperature. Such excitons are usually referred to as Frenkel excitons, whereas weakly bound excitons in inorganic crystalline semiconductors are called Mott-Wannier excitons.[39]

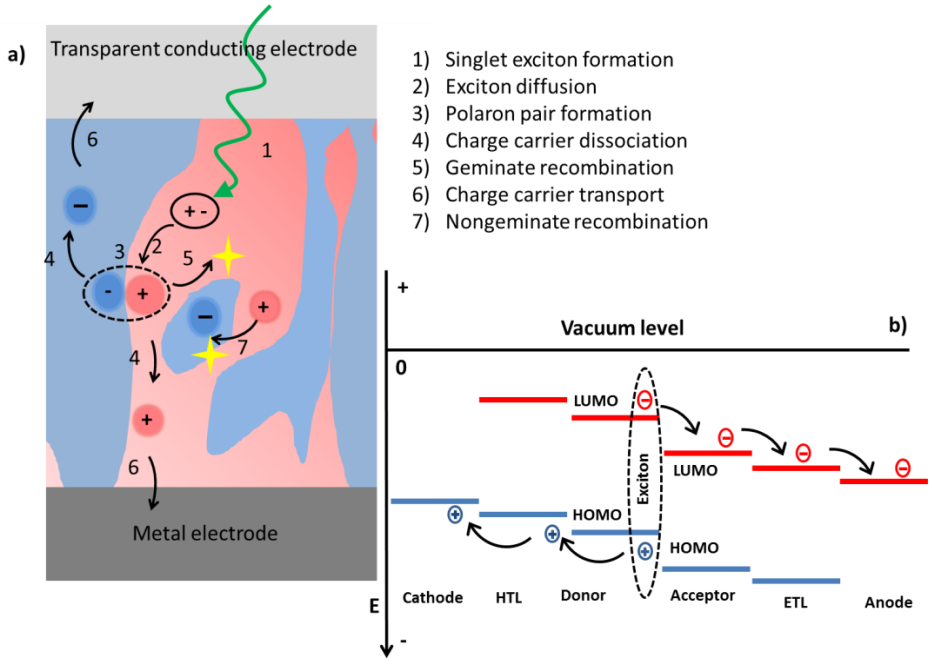

Figure 1.5: Fundamental processes towards the photocurrent generation in a BHJ solar cell. a)Kinetic point of view, b)corresponding simplified energy level diagram. Scheme adapted from reference 6 and 7.

The combined spin state of the two charges forming the excitons is highly important. Singlet excitons have a total spin state of zero, whereas triplet excitons have a combined spin state of 1.[5,40,41] Excitons have a certain lifetime, after that they recombine radiatively or non-radiatively. In organic semiconductors singlet excitons have a lifetime of about 1 nanosecond, with photoluminescence as one of the subsequent recombination pathways.[5,6] Because the weak spin-orbit interaction is required for transitions to the singlet ground state triplets have a much longer lifetime if compared to singlet excitons, and their radiative recombination occurs on microsecond-millisecond time scale.[42]

1.3.2 Exciton diffusion and dissociation

As mentioned above, the exciton binding energy is higher in organic semiconductors, and lies between that of highly delocalized Wannier-Mott excitons in inorganic semiconductors and localized Frenkel excitons in molecular crystals.[43] Because of high binding energy, the thermal energy (*kT*) is not sufficient for exciton dissociation at room temperature. In order to facilitate the charge carrier separation, a driving force is needed. Buckminster fullerene and its derivatives are best acceptors so far because of their high electronegativity and spherical shape, leading to a small reorganization energy, which assists charge separation and reduces recombination. Polymer acceptors and other small molecule acceptors have shown less efficient charge generation so far.[44,45] This could be due to low electron mobilities or LUMO levels not being electronegative enough for charge generation.[5,46] Before the electron transfer from donor to acceptor, excitons have to move to the donor-acceptor interface within its lifetime, τ_{Exc}. This exciton diffusion is an ultrafast process happening on the time scale of picoseconds. Exciton trapping and deactivation are the major loss process during this process. Transport of the exciton occurs by diffusion and the distance an exciton is able to cross, L_{Exc},is expressed as follows;

$$L_{Exc} = \sqrt{D_{Exc}.\tau_{Exc}} \tag{1.2}$$

whereD_{Exc} is the exciton diffusion coefficient.[47]

In general, rather disordered materials like poly [3-hexyl thiophene] (P3HT), [6,6]-phenyl-C61-butyric acid methyl ester (PCBM), poly [2-methoxy-5-(2-ethylhexyloxy)-1,4-phenylenevinylene] (MEH-PPV), etc., which have τ_{Exc} about several nanoseconds and exciton diffusion length between 5-10nm, are typically used as active layers in OSC.[3,5,6,24] Shaw et al. calculated the exciton diffusion length of annealed P3HT: PCBM by analysing spatial Fourier transform of transmission electron microscopy (TEM) images.[47] The

annealing results in demixing of phases and the two-dimensional diffusion length was estimated about 12 nm by using the formula $L = \sqrt{2D\tau}$.[47] This implies that only excitons formed within L_{Exc} can contribute to the photo current. The intermixing of donor and acceptor in the active layer creates many interfaces, and hence the probability of exciton separation is high. This is why the BHJ concept is favourable for better performance.[3,48]

Once the exciton reaches the interface, an electron can be transferred to the acceptor and the hole remains in the donor molecule, as given in the figure 1.5a step (3). The energy gained from charge transfer to the acceptor should be higher than the exciton binding energy. This charge transfer process is very fast, on the order of few tens of femtoseconds.[49,50] These charge carrier pairs, also called polaron pair (PP) or charge transfer state (CTS), are still Coulomb bound, but the binding energy is less than the one in excitons, albeit still higher than *kT*. The observation that complete charge separation occurs anyway at high yields, has been explained by hot exciton dissociation or different polaron energy in amorphous and ordered phases.[51,52,53,54]

1.3.3 Charge carrier pair dissociation

To gain free charge carriers, the polaron pairs have to separate with the assistance of an external field.[55] The schematic representation of charge transfer state dissociation to free polarons is shown in figure 1.5a (4). A frequently used model to explain charge carrier pair dissociation is the Onsager-Braun model.[56] This is an extension of Onsager theory introduced in 1938.[57] In his original publication, Onsager used this model to calculate the separation probability of a Coulomb bound pair of ions of opposite charges under the assistance of an external electrical field with a given initial distance. Onsager's original work was modified in 1984 by Braun. In his extension; he accounted for the finite lifetime of the CT states. Onsager theory contains the boundary condition that, if the separation between the two charges becomes zero, then recombination occurs and the pair irreversibly disappears. Braun stated that because of the finite lifetime, dissociation of CT states into free carriers is a reversible process.[56] The polaron pair dissociation according to Onsager-Braun (OB) model is depicted in figure 1.6.

In this model, three transition rates are used. Polaron pair can either recombine to ground state with a rate constant k_f or be dissociated into free charges with a rate constant k_d. The free charge carriers can meet each other and form back polaron pair again with a rate constant k_r. So, in this assumption, the separated charge carriers never recombine directly to the

ground state, first they have to form again a polaron pair and then they recombine to the ground state.

According to the OB model, the field dependent dissociation probability P(F) of a polaron pair is given by

$$P(F) = \frac{k_d(F)}{k_d(F)+k_f} \tag{1.3}$$

where, F is the electric field, $k_f = \tau_{pp}^{-1}$ the recombination rate to the ground state, k_d is the dissociation rate.[5,56]

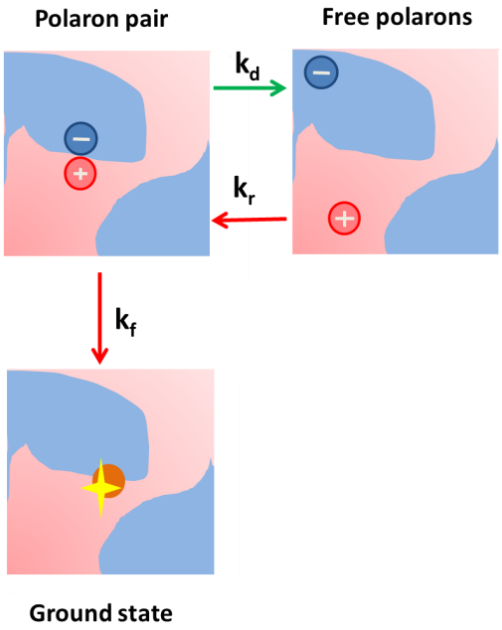

Figure 1.6: Schematic representation of polaron pair dissociation in organic solar cells. k_d is the polaron pair dissociation rate to become free polarons, k_r is the recombination rate of free polarons to polaron pairs and k_f is the recombination rate of polaron pairs to the ground state [scheme adapted from reference 5].

Although the OB model explains the polaron pair dissociation, it is a simplified model and does not account for all phenomena in the device, for example, high local mobility, energetic disorder, nanocrystalline regions in the donor or acceptor phase, etc. The Onsager-Braun model cannot address the high yield of short-lived (about10 ns) polaron pair dissociation at low levels of electric field.[58] Several new models were introduced to explain this high yield at low field. Arkhipov et al. suggested the analytic dark dipole model, which is based on the experimental finding of the vacuum level shift at the heterojunction of oligomer/fullerene bilayers.[59] Puemans et al. have shown that a large initial separation of the polaron pair implies high dissociation yield.[60] Hot polaron pair formation with excess kinetic energy needed for dissociation was also proposed as a model.[61,62] Groves et al. explained the unexpected high dissociation rate with high local mobility within the ordered domains of

disordered blend.[63] Deibel and co-workers ascribed the efficient polaron pair dissociation in BHJ solar cells, which is responsible for the high performance of OSC's, to the conjugation length of the polymers by using Monte- Carlo simulation.[61]

Polaron pairs which are not dissociated can undergo geminate recombination, which is a loss process for the photocurrent generation. Electron back transfer from the acceptor, formation of triplet states, and dissociation of polaron pairs to the wrong electrode are the other loss processes at this stage of the photoelectric conversion.

1.3.4 Charge carrier transport

For efficient photocurrent generation, electron transport in the acceptor and hole transport in the donor is a crucial step. Unlike in inorganic semiconductors where the carrier transport is described by the band model, in organic semiconductors transport happens stochastically by hopping from one localized state to another localized state.[64,65] This is because of lack of long range order.[61] Due tothe stochastic (diffusive) nature of the hopping process and energetic disorder one can expect low charge carrier mobility and slow carrier transport in organic semiconductors.

For the effective transport of charge carriers to the corresponding electrodes, uninterrupted percolation paths called 'wirings' are needed.[52] Broken percolation paths, presence of impurities and other external factors such as oxygen and water, influence the nanomorphology of the blend and leads to slowing down the charge transport and overall performance.[3, 32,62,67,64] Therefore perfect morphology in BHJ solar cells is a balance between strongly intermixed donor-acceptor interfaces for efficient exciton dissociation and extended phases and percolation paths for efficient polaron pair dissociation and for yielding good carrier transport.[3,52,61] Annealing and introduction of additives and good encapsulation would preserve the morphology to some extent.[67,69,70] These issues are detailed in section 1.5.1.

The charge carrier mobility μ is the proportionality constant between carrier drift velocity and the electric field.[71] The charge carrier mobility μ is given by,

$$\mu = \frac{v_d}{F} \tag{1.4}$$

Here, v_d is the drift velocity and F is the electric field.The mobility of most of the organic semiconductors is between10^{-4} and 10^{-3} cm^2/Vs.[65,71,72] In order to avoid a buildup of a space charge region, balanced electron and hole mobilities are desirable.[73] The polaron pair dissociation increases with increase in mobility, so the higher mobility materials yield better

solar cells performance. Low mobilities cause space charge build up due to inefficient extraction and limits performance of the device. In P3HT:PCBM based OSC's photo-oxidation causes severe damage in the extraction process.[32] Energetic traps formation due to external degradation triggers, and mechanical stresses also hinder the smooth hopping transport of the charge carrier to the electrodes.[3,33,61,74] These effects are introduced later in this chapter and detailed in the following chapters of this thesis.

1.3.5 Charge Carrier recombination

Charge carrier recombination can take place during the charge carrier transport to the electrodes. This is schematically shown in figure 1.5a (7). In contrast to the geminate recombination during the polaron pair dissociation this process is called non-geminate recombination since the contributing electrons and holes do not share the same precursor. If two independent mobile charge carriers encounter and recombine, then the recombination process is termed bimolecular recombination and it is a second order process. Recombination of a mobile carrier with a trapped counterpart is considered as a first order process, as the trapped carrier density exceeds the mobile carrier density and the trapped carriers are generally not generated by the illumination, at least not by the photons generating the mobile carriers. This kind of recombination is called trap-assisted recombination.[75]

The number of participants determines the recombination order and thus it is important for understanding the loss mechanism.[5] Assuming Langevin recombination and replacing the bulk hetero structure by an effective homogeneous medium the charge carrier dynamics can be represented by the continuity equation, shown here for electron concentration *n*.

$$\frac{dn}{dt} = G - k_L nn - \mu n \frac{E_{bi}}{d} \tag{1.5}$$

where *n* is the charge carrier concentration, μ is the effective charge carrier mobility, *G* is the photo-induced generation rate of extractable charge carriers and k_L is the bimolecular charge recombination coefficient:

$$k_L = 2e\mu_{eff} f_{LV}/(\varepsilon\varepsilon_0) \tag{1.6}$$

Herein, $\mu_{eff}=\mu_e+\mu_h$ is the sum of the mobilities for positive and negative charges, respectively, ε is the relative dielectric constant, ε_0 is the dielectric constant in vacuum, and f_{LV} accounts for sub-Langevin recombination, as often observed in BHJ active layers. Mozer et al. observed a time-dependent mobility of extracted charge carriers by photo-CELIV technique and they attributed this phenomenon to energy relaxation of the charge carriers

towards the tail states of the density of states distribution.[76] The mobility in general also depends on the charge carrier concentration, temperature, reaction order, etc,.[77] Electron and hole mobility in solar cells should be reasonably well balanced in order to reduce the recombination loss.[78] Thus understanding of the recombination losses is crucial for developing efficient and stable organic photovoltaic devices.[32]

1.3.6 Charge carrier extraction

Charge carrier extraction by the electrodes is the final step in the photocurrent generation process in an organic solar cell. For efficient photo current production, carriers of opposite types should drift towards opposite electrodes. Charges at the 'wrong' electrode are lost for the photocurrent generation. To guide the generated charges to the corresponding electrode, a hole transport layer (HTL) and an electron transport layer (ETL) are used as interlayers.[79] If the extraction rate is too low, it may cause piling up of charge carriers and formation of space charge region at their respective electrodes. This leads to S-shaped current-voltage (J-V) characteristics in organic solar cells, as already reported in the literature.[5,6,80] Excess background carrier concentration can also lead to shielding of the built-in-potential and limits the extraction of carriers. The formation of excess background carriers is identified as one of the potential reasons for performance loss in P3HT: PCBM solar cells upon photooxidation.[32]

1.4 Characteristic values of a solar cell

There are three main characteristic values which determine the quality of a solar cell.[6] They are:

a) Current –Voltage (I-V) characteristics under illumination
b) I-V characteristics in the dark
c) External quantum efficiency (EQE)

A typical I-V curve is shown in figure 1.7a. The I-V curve measurement is the most direct technique to assess photovoltaic performance of a solar cell. The voltage where the I-V curve crosses the x-axis and the current density is zero called open circuit voltage (V_{oc}) and the current at which the voltage is zero is the short circuit current (I_{sc}).

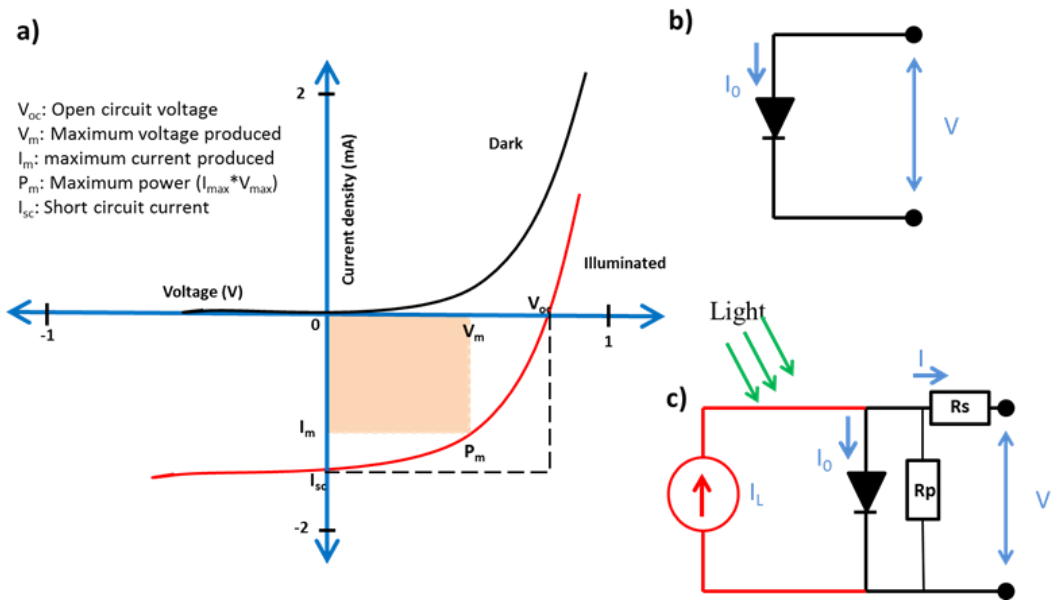

Figure 1.7: Schematic current-voltage curve representation of a BHJ solar cell (a), equivalent electrical circuit for diode (b), and illuminated solar cell (c).

Power conversion efficiency is the most important figure of merit for a solar cell. The power conversion efficiencyη can be calculated as;

$$\eta = \frac{P_{out}}{P_{in}} \tag{1.7}$$

where P_{in} is the sun's input power and P_{out} is the maximum power produced by the device. P_{out} can be calculated from the solar cell I-V curve parameters, such as short circuit current density (Jsc), open circuit voltage (Voc) and fill factor (FF) and is given by:

$$P_{out} = FF * V_{oc} * J_{sc} \tag{1.8}$$

So the efficiency can be written as,

$$\eta = \frac{FF*V_{oc}*J_{sc}}{P_{in}} \tag{1.9}$$

Supplementary vital information can be obtained from measurement of the I-V curve in the dark (figure 1.7a, black curve). The current flow is zero in the reverse direction, which corresponds to high parallel resistance R_p, as shown in the equivalent circuit (figure 1.7b). Small R_p values cause nonparallel I-V curves and in the reverse direction a dark current leakage can be measured and it is an indication of performance loss.[81] In forward direction,

we can measure the injection current, which is an indicator of losses in the current at the interface due to high series resistance R_s. Keeping R_s as low as possible is desirable for a good solar cell.[6]

External quantum efficiency (EQE) spectrum represents the response of the solar cell at certain wavelengths. By definition, it is the number of extracted charges divided by the number of photons incident per wavelength.[6] The internal quantum efficiency (IQE) is the ratio of the number of charges collected to the number of photons absorbed from the incident light. IQE considers only absorbed photons, not reflected or transmitted photons. So, IQE is always higher than EQE.

$$\mathrm{EQE} = \frac{\mathrm{electrons/sec}}{\mathrm{photons/sec}}$$

$$\mathrm{IQE} = \frac{\mathrm{electrons/sec}}{\mathrm{absorbed\ photons/sec}}$$

1.5 Degradation in organic solar cells

As mentioned in the section 1.3, OSC's have many advantages compared to inorganic solar cells. Although power conversion efficiency (PCE) of OSC's now exceeds 8%, they still suffer from limited operational stability.[32] Solar cell modules made from monocrystalline silicon have lifetime more than 25 years with more than 25% efficiency, thus contributing about 90% of current OPV market.[6,32] Organic solar cells are very sensitive and prone to attack of external agents. The stability of organic solar cells has to be investigated further and improved for commercialization.[30]A stability of 5years or more is needed for flexible while 20 years or more is needed for building-integrated applications.[6,82] Many investigations have been performed to identify the degradation mechanisms, routes, etc., and many ways have been proposed to block or minimize the degradation triggers.[3,30] However the elementary mechanisms behind electrical performance loss have so far not been fully understood or quantitatively related to the electronic and geometrical structure of the materials. To realize the market entry of OSC, much intense research work is needed in this field.

Major stress factors responsible for OSC degradation are schematically shown in figure 1.8. When solar cells are illuminated by light, degradation mechanisms such as photolytical, photochemical, and morphological changes happen in the device.[3,30] It also leads to interfacial issues between layers and facilitates growth of acceptor rich regions.[83] Physical

damages like delamination of the layers, cracking due to flexing also leads to degraded performance.[3,30] There are many other degradation triggers for OSC's such as water, oxygen, temperature etc.[33,67,68,84,85] A better understanding and improvement in the stability of organic solar cells is needed for longer lifetime and marketability.[6,30] Using encapsulation would minimize the availability of degradation triggers like oxygen, water, pollutants etc.[3,86,87] Tuning of the system properties like glass transition temperature, electronic levels, cross linking etc. would also reduce the degradation effects.[66,85,88] The use of the inverted device architecture has been shown to improve the stability against water, but not against oxygen.[67] The normal device architecture shows good stability against oxygen but dies quickly in moist atmosphere.[33] Using stable electrodes would also lead to a better performance.[89,90] The possible causes of degradation, their effects on the performance and methods for minimizing degradation effects are discussed in this section.

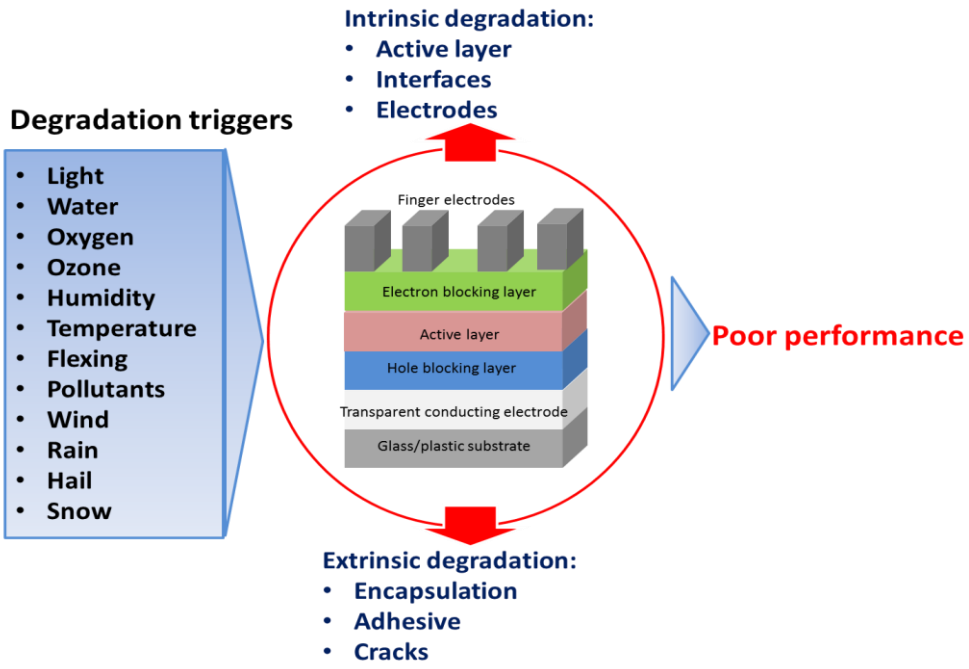

Figure 1.8: Major degradation triggers and types of degradation.

1.5.1 Physical stability

In bulk heterojunction solar cells, it has been shown that the structure is not a static one, once it has been formed after the production of the device.[30] Mechanical instability due to flexing, cracks formation and poor adhesion between layers also lead to performance losses in organic solar cells. In this subsection major physical degradation triggers affecting OSCs performance are briefed.

1.5.1.1 Morphological stability

Stability of the nanoscale morphology of the active layer is a crucial issue in BHJ organic solar cells.[86] The morphology of the active layer is optimized for minimum exciton diffusion length and maximum inner surface, but this optimum morphology will not remain stable for long term operation.[85] Several approaches are used to optimize the morphology of an organic solar cell, such as donor-acceptor blend ratio, regioregularity of polymers, molecular weights, additives, solvents, sample preparation conditions, pre and post annealing temperature, etc.[37,51,67,69,91–93]

Organic solar cells degrade quickly in the presence of oxygen, water, or elevated temperature because of their low resistance toward these degradation triggers.[30,33,69,85] There are several approaches to preserve the optimal morphology of organic solar cells against degradation. In a well encapsulated solar cell, the effect of temperature is the leading cause for performance loss.[85] In P3HT:PCBM based solar cells; thermal instability causes crystallization of P3HT, which is good for carrier transport, on the other hand PCBM groups into clusters, which reduces the interfacial area and hence the exciton dissociation.[85,94]

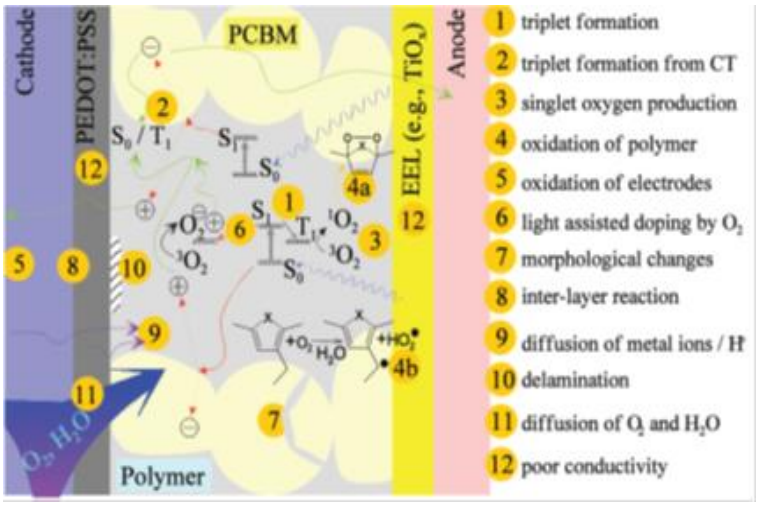

Figure 1.4: Pictorial representation of possible degradation triggers in organic solar cells.[d]

Small molecules like PCBM and even polymers like P3HT have the freedom to modify their structure, and slowly diffuse during the long operational time.[85] This makes conserving optimal morphology a difficult task. The small modifications in the microstructure eventually lead to a poor performance of the device. Different types of microscopic studies have been used to get insight of morphological modifications.[95,96] Bertho et al. have shown that use of

[d] Taken from anex1 of Establis's project proposal(http://www.project-establis.eu/)

high glass transition temperature (T_g) donor materials is a good approach.[85] Incorporating cross linkable groups to lock the optimal morphology also improve the stability.[3]

1.5.1.2 Flexibility and stability

Mechanical flexibility is one of the promising applications and major selling point of organic photovoltaics.[97] Flexibility of the substrate and all layers involved enables the bulk production of light weight OSC's in a roll to roll (R2R) process.[98] The flexibility also eases the carrying, transportation, installation of OSC's.[82,97] Use of the expensive, brittle inorganic indium tin oxide (ITO) is a major limitation to the flexibility.[3,99] ITO can be sputtered on transparent plastics like PET (poly ethylene terephthalate) but it cracks upon mechanical flexing. Cracks formation causes increase in sheet resistance and the extracted charges will not be transported to the external circuit. This can be seen mainly in the loss of fill factor in the I-V curve.[30]A detailed cost analysis of OSC revealed that ITO is one of the main cost driving factors also.[100]

These factors have motivated a search for some replacement for ITO and prepare ITO free OSC's.[93,101,102] For instance, replacement of ITO by a highly conductive poly(3,4-ethylenedioxythiophene) polystyrene sulfonate (PEDOT:PSS) layer or by a composite electrode associating PEDOT:PSS and a metal grid appears promising.[103,104] Zimmermann et al. introduced Fraunhofer type approach (Chromium/Aluminium/Chromium stack instead of ITO) and achieved efficiency 3.1% with excellent stability.[105] Manceau et al. used Kapton foil and an Aluminium/ Chromium bi-layer system as electron contact.[106] In 2014, Kaduwal et al. used the same Fraunhofer type (Cr-Al-Cr) sputtered on PET and demonstrated 2.9% efficiency of R2R produced organic solar cells.[99] Angmo et al. have demonstrated a ITO free large area (>180cm^2) organic solar cell module with power conversion efficiency 1.6%. They also tested and demonstrated that devices are stable under ISOS (International Summit on OPV Stability) conditions.[107]

1.5.1.3 Delamination

At all stacking architectures of organic solar cells, mechanical stress, chemical processes etc., can cause delamination between layers and result in formation of cracks. This is mainly due to poor adhesion between the layers, which leads to unwanted interface formation and blocks the transport of charge carriers into their respective electrodes.[3] For example, PEDOT:PSS/P3HT:PCBM interface in an inverted solar cell has very poor adhesion because P3HT:PCBM is hydrophobic and PEDOT:PSS is hydrophilic.[33] The actual fracture energy of this interface can depend on the ratio of P3HT:PCBM, the formulation of PEDOT:PSS, and

other processing conditions.[108] Angmo et al. studied P3HT:PCBM encapsulated devices for 1 year outdoor exposure and found that delamination at the interface between active layer and PEDOT is one of the primary degradation routes.[109]

1.5.2 Chemical degradation

Polymers for organic solar cells can be described as the combination of a rigid pi-conjugated backbone regularly substituted by side-chain groups ensuring their solution processability.[37,66] The relationship between chemical degradation and performance losses of organic solar cells is well explored, but the structural changes and photo-chemical stability are still largely unknown.[66] There have been many studies on the chemical stability of OSC's, it is found that oxygen diffusion and water ingress are the main reasons of chemical instability.[33,67,68,75,110] In this subsection major chemical degradation stresses which result in decrease in efficiency and reduced lifetime of an operational OPV device are introduced.

1.5.2.1 Photochemical stability

Any chemical reaction which causes the disruption of pi-conjugation in the active layer of organic solar cells leads to decrease in UV-Vis absorbance.[3] One of the main causes of organic solar cell degradation is diffusion of oxygen and water into various layers of the device.[33,110] Manceau et al. demonstrated that singlet oxygen is the main intermediate which is responsible for the degradation of P3HT in solution.[66] They list three types of degradation pathways such as formation of an α-unsaturated alcohol, formation of aromatic ketones and formation of aromatic aldehydes.[111,112] Hintz and co-workers studied the influence of environmental stresses in the degradation of P3HT, and they showed that the lower the P3HT regioregularity, the higher the degradation rate.[113] In another study, Hintz et al. reported the effects of ozonisation and photooxidation by X-ray photoelectron spectroscopy (XPS) on P3HT films and found that pathways are different for both degradation mechanisms. The authors concluded that the photo-oxidation effect is an order of magnitude higher than that of ozone attack and it degrades the alkyl side chains which leads to formation of reactive peroxides.[113] Manceau et al. found that keeping optimum amount of side chains of the pi-conjugated polymer backbone would improve stability.[66]

It has been shown that mixing of fullerene derivatives reduce the degradation rate considerably due to radical scavenging property of fullerene derivatives and their capability to quench the singlet excitons.[111,114,115] Norrmann et al. investigated water and oxygen influence on inverted P3HT:PCBM solar cell stability by using XPS and time-of-flight secondary ion mass spectrometry (TOF-SIMS) in conjunction with isotopic labelling using

$H_2{}^{18}O$ and $^{18}O_2$. They found that reactions taking place at the interface between the active layer and the PEDOT:PSS are the major causes of device failure in the case of these inverted devices and concluded that water has little influence on the degradation of inverted devices compared to oxygen.[33] Hermenau et al. followed the same technique to study water and oxygen effects on small molecule based solar cells having normal geometry. They found that water is playing a major role in the degradation mechanism for these kinds of devices.[84]

Even in the absence of oxygen and moisture, impurities present in the material affect photochemical stability of conjugated polymers.[116,117] Developments in polymer/small molecule synthesis and purification have improved the photochemical stability against impurities.[118,119] It has been shown that oxygen uptake also lowers the conductivity of fullerenes, because intercalated oxygen acts as an electron trap.[120] These effects can be partially reversed by annealing at 160-180ºC.[121] Dimerization of PCBM is another issue to be solved for better performance and stability. Recently Distler et al. reported that, by replacing PCBM with bis-PCBM leads to stable performance of OSCs against PCBM dimerization.[29] Norrman and co-workers have shown oxygen diffusion through pinholes of cathode causes expansion of C_{60} which leads to protrusion around the pinholes of cathode. This leads to increased pinhole size which amplifies the oxygen ingress into the layer.[122]

To improve stability, the photoactive layer (PAL) should be well encapsulated against all degradation stresses. Processing of PAL in oxygen poor atmosphere, at low temperature, using good encapsulation barriers, use of components which are less prone to degradation, etc., are some of the many choices that can be made to extend OPV lifetime.[3,31]

1.5.2.2 Barrier effects of layers

In organic photovoltaics, some layers show a special ability to block degradation stresses. As mentioned earlier, the inverted structure shows good barrier properties against water.[33,67] Madsen et al. reported that in dry oxygen atmosphere all layers have distinct barrier properties, and an accumulated degradation effect can be seen.[123] In the oxygen free humid atmosphere, the active layer (P3HT:PCBM) is observed to have good barrier property.[123] They found that the active layer is protecting the subsequent layers from water diffusion in inverted solar cells and damage is mainly caused by oxygen ingress. Although adding layers (or additives) may increase the barrier effects, increasing the lifetime of organic solar cells, care must be taken that the electrical properties are not deteriorated.

1.5.3 Electrode degradation

Electrodes without proper encapsulation are prone to degradation. In normal or conventional architecture organic solar cells indium tin oxide (ITO) or some other transparent conducting electrode (TCE) serve as cathode and low work function metals like aluminium (Al) act as anode.[33] In the inverted architecture ITO or TCE forms the anode, for collecting electrons and a high work function metal, usually silver (Ag) works as cathode.[67] In ITO free architectures metals form both electrodes.[99]

The low work function of aluminium (4.1eV) in conventional architecture devices is a stability-limiting factor. Since aluminium has an oxidation state of +3, upon oxygen diffusion it converts to aluminium oxide (Al_2O_3), which is an insulator.[33] In a study, Norrman et al. found that water diffusion through the pinholes of aluminium leads to degradation of all interfaces, while oxygen ingress causes localized or inhomogeneous degradation of the aluminium interface, and it propagates the degradation agents throughout the photo-active layer.[33] Furthermore, aluminium species could diffuse in the device and form organo-metallic complexes with active materials.[90] Thus, even when the photo-active layer is resistant against oxidation, aluminium degradation causes deterioration of OSC performance.[33,90]

So, one method to address this problem is avoiding the use of aluminium. This is good, not only in the point of view of stability, but in the processing point of view also. In inverted devices silver (Ag) or gold (Au) replaces Al and electron and hole transporting layers swap their positions.[67] Since Au and Ag are noble metals they present good resistance against oxidation. Studies have been undertaken to investigate the degradation of interfacial layers. Interfacial layers are used in OSCs to facilitate the electron and hole transport to respective electrodes. PEDOT:PSS is used as a interfacial layer in normal and inverted device architecture. It has been shown that PEDOT:PSS is susceptible to oxidation because of its hygroscopic nature.[33] Replacement of PEDOT:PSS with more stable materials like molybdenum trioxide (MoO_3) can lower the water diffusion. Due to its high conductivity and transparency, ITO remains the most commonly used transparent conducting electrode in OSC.[33] Schäfer et al.have shown that degradation causes a decrease in the V_{oc} of the device, and they claimed that this is due to changes in the ITO work function.[124] Good encapsulation impedes the amount of diffusion of water, oxygen and other degradation agents to the device but the currently available materials do not stop the process.[30] In the current situation, good barrier materials make organic solar cells expensive, so a compromise has to be found between cost of encapsulation and lifetime of the device.[6]

1.6 Aim of the thesis

A critical issue to be improved in organic solar cells is their operational lifetime. Current-voltage characterization is the most direct method to monitor degradation-induced performance loss in organic solar cells. But an I-V curve gives at most a hint of the degradation mechanism. The external quantum efficiency (EQE) of an OSC is dependent on efficiency of absorption (φ_{abs}), efficiency of exciton dissociation (φ_{diss}), efficiency of polaron pair separation (φ_{sep}) and efficiency of charge extraction (φ_{extr}).

$$EQE = \varphi_{abs} \cdot \varphi_{diss} \cdot \varphi_{sep} \cdot \varphi_{extr} \tag{1.10}$$

The short circuit current (I_{sc}) loss can be due to absorption loss, exciton dissociation loss, charge carrier extraction loss, recombination losses etc. Fill factor loss could be due to mobility reduction, interfacial issues, Langevin factor, background carriers etc. Knowledge of the exact degradation mechanism is needed for improving the materials, architecture and processing conditions. It is hard to pin point which causes a greater influence on the performance from simple I-V curves. Studying the causes of degradation of incomplete cells (single layers, combination of few layers) and of complete devices by using other characterization techniques, in addition to I-V curves, is necessary for getting complete knowledge about degradation mechanisms.

The effects of chemical degradation and thermal stress on the active layer of OSCs are still poorly understood. Therefore this thesis attempts to shed more light on the effects of light-induced photooxidation and thermal annealing on a model polymer system, P3HT and a series of new low band gap materials blended with fullerene, including devices made from them. Transient opto-electrical measurements are excellent tools for identifying the degradation routes. Transient absorption spectroscopy (TAS) studies gives access to time-resolved population of excitons and charged species in a complete/incomplete solar cell. It is the only technique which is capable of addressing all relevant time scales in which loss processes can occur, from femtoseconds to milliseconds.This helps to identify the reasons for performance loss of organic solar cells. In addition to TAS, complementary transient electrical techniques like transient photo-voltage (TPV), transient photo-current (TPC), charge extraction by linearly increasing voltage (CELIV) are also used to monitor degradation-induced performance losses in organic solar cells.

Chapter 2

Materials and methods

2.1 Materials

The following section briefly describes the characteristics of the materials investigated in this thesis. All the films and devices were received from Belectric OPV GmbH, except the BDT-DPP:PCBM solar cells, which were delivered by Merck Chemicals Ltd. Materials selected in this thesis for investigations have different optical absorption properties due to differences in their optical band gap. A wide range of low band gap polymer based solar cells were also investigated in this thesis. They exhibit better efficiency compared to medium bandgap polymers because of their improved spectral matching with solar irradiation.

2.1.1 P3HT

Regioregular poly (3-hexyl thiophene) [RR-P3HT] used in this work was supplied by Merck chemicals. The molecular weight (M_w) and polydispersity index (PDI) of P3HT used in this thesis are 59.5 kg mol^{-1} and 1.49, respectively. The chemical structure of RR-P3HT and the absorption spectrum of P3HT:PCBM (1:0.8) are given in figure 2.1a and b, respectively.

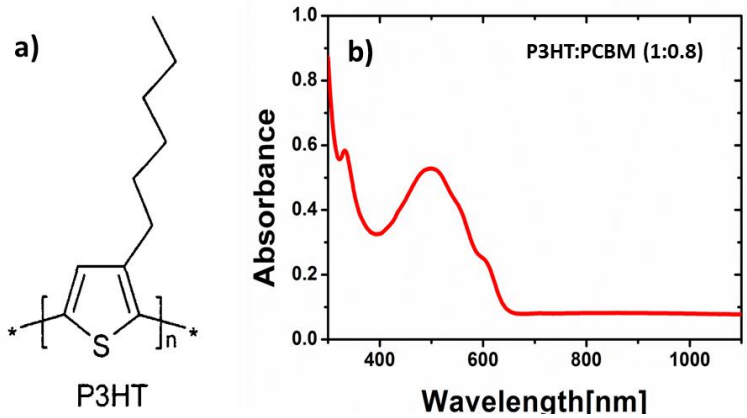

Figure 2.1: a) Chemical structure of P3HT and b) UV-Vis absorption spectrum of P3HT:PCBM film.

2.1.2 Si-PCPDTBT

The poly [(4,4 0-bis(2-ethylhexyl) dithieno [3,2-b:2 0,3 0-d]silole)-2,6-diyl-alt-(4,7-bis(2-thienyl)-2,1,3-benzothiadiazole)-5,5 0-diyl] (Si-PCPDTBT) has been provided by Konarka Technologies Inc. The molecular weight (M_w) and polydispersity index(PDI) of Si-

PCPDTBT used in this thesis is 52.8 kg mol^{-1} and 2.85, respectively. The chemical structure of Si-PCPDTBT and the absorption spectrum of Si-PCPDTBT:PCBM (1:2) are given in figure 2.2a and b respectively.

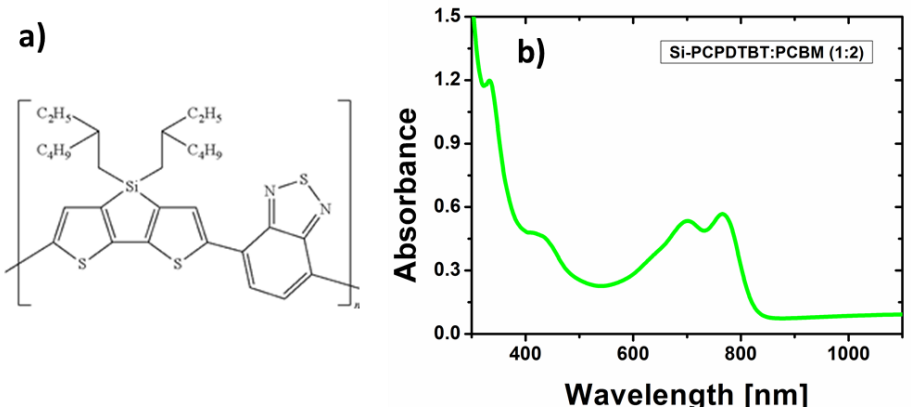

Figure 2.2: a) Chemical structure of Si-PCPDTBT and b) UV-Vis absorption spectrum of Si-PCPDTBT:PCBM film.

2.1.3 PDTSTzTz (KP115)

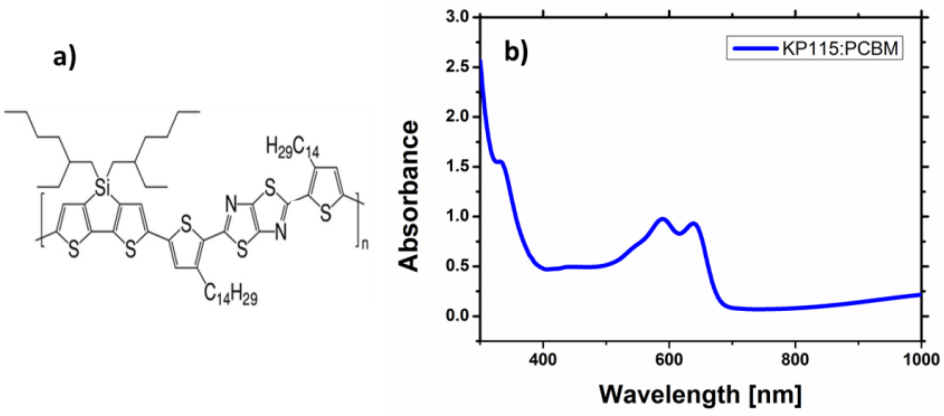

Figure 2.3: a) Chemical structures of KP115 and b) UV-Vis absorption spectrum of KP115:PCBM film.

The poly [(4,4′-bis (2-ethylhexyl) dithieno [3,2-b:2′,3′-d] silole)-2,6-diyl-alt-(2,5-bis 3-tetradecylthiophen-2-yl thiazolo 5,4-d thiazole)-2,5diyl] (PDTZTzTz or KP115)used in this work was provided by Merck chemicals. The molecular weight (M_w) and polydispersity index (PDI) of KP115 used in this thesis is 156.27 kg/mol and 3.48 respectively. The chemical structure of KP115 and the absorption spectrum of KP115:PCBM (1:2) are given in figure 2.3a and b respectively.

2.1.4 BDT-DPP polymers

The solar cells made from poly(benzodithiophene–diketopyrrolopyrrole) (BDT-DPP) incorporating $PC_{60}BM$ as an acceptor were received from Merck chemicals. Figure 2.4a

shows the detailed chemical structure and synthetic routes of the PBDTDPP (or EP) and the side chains used for solubility namely P1, P2, P4 and P6. The corresponding UV-Vis absorption spectra is shown is figure 2.4b.[37] The characteristic values of EP polymers are given in the table 2.1.

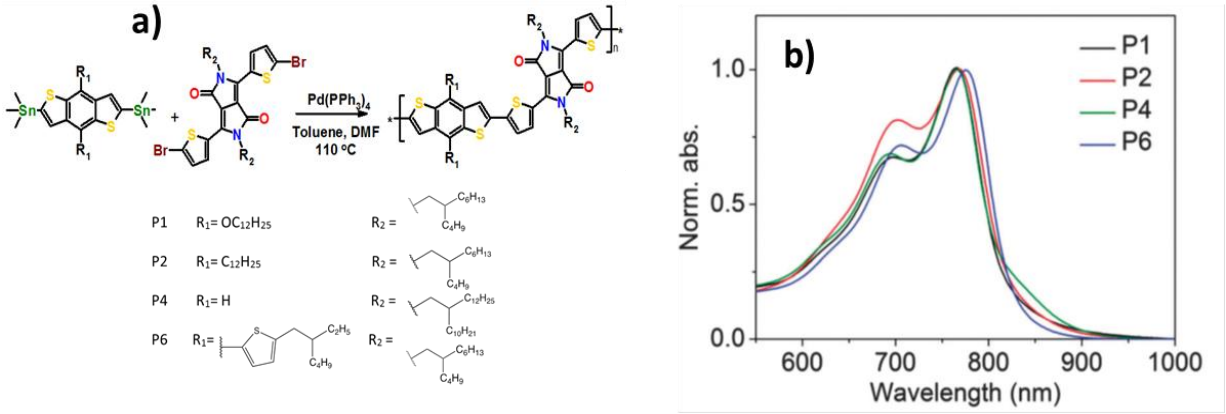

Figure 2.4: Chemical structures of BDTDPP polymers and b) UV-Vis absorption spectrum of PBDTDPP:PCBM (1:2) film with different side chains

Polymer	Molecular weight, Mw(kg/mol)	Poly dispersity index (PDI)
P1	130	3.4
P2	320	3.5
P4	72	2.2
P6	730	5.5

Table 2.1: Characteristic values of the EP polymers.

2.1.5 $PC_{60}BM$

The [6,6]-phenyl-C61-butyric acid methyl ester (PCBM) used for the Belectric solar cells has purity ~99% and was purchased from Solenne BV. PCBM used for Merck solar cells was purchased from Nano-C Inc. and used as supplied.[37] The chemical structure of PCBM is given in figure 2.5.

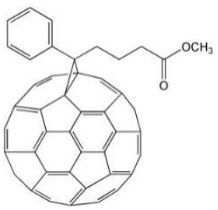

Figure 2.5: Chemical structure of $PC_{60}BM$.

2.1.6 Intermediate layers

Solar cells investigated in this thesis used poly (3,4-ethylenedioxythiophene) polystyrene sulfonate (PEDOT:PSS) as electron blocking layer (EBL) and either poly ethylene imine (PEI) or Zinc oxide used as hole blocking layer. The cells received from Belectric used a highly conductive PEDOT:PSS (Clevios^{TM}) on top of PEDOT:PSS (HTL Solar) as EBL and both were obtained from Heraeus. All were used as received. Poly ethylene imine was employed as HBL in these solar cells.

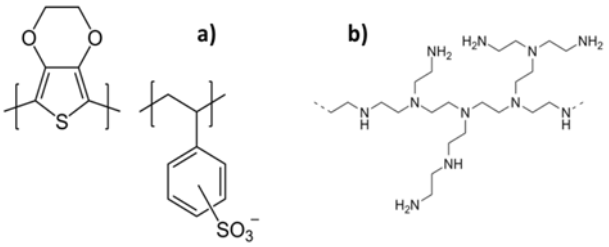

Figure 2.6: Chemical structures of (a) PEDOT:PSS and (b) PEI.

The cells received from Merck Chemicals have zinc oxide as electron transport layer. The layer was formed by spin-coating a solution of zinc acetate dihydrate (Aldrich) in DMSO at 160 g L^{-1} at 4000 rpm for 10 seconds followed by a 5 minutes thermal anneal process at 300^{o}C. The Clevios HTL Solar SCA 246-9 (Heraeus) PEDOT:PSS is used as the ETL in these devices.

2.2 Device preparation and degradation

Solutions of P3HT:PCBM (1:0.8), Si-PCPDTBT:PCBM (1:2) and PDTSTzTz (KP115):PCBM (1:2) were prepared in o-Xylene by stirring at 80 °C, 120°C and 100°C respectively, over night. These solutions were used for making both solar cell devices in an inverted stack and neat films on glass substrates. The ITO coated glass substrates were cleaned by ultrasonic bath for 10 minutes with acetone and isopropyl alcohol, respectively. The solar cells were made by applying a hole-blocking layer on an ITO-glass-substrate, followed by the photo-active layer and the electron-blocking layer (EBL) with a transparent electrode. The top electrode was realized by using the commercially available highly conductive PEDOT PHCV6 combined with an evaporated silver grid electrode on top. This architecture ensures that the degradation of the active layer in the solar cell is the same as the degradation of the neat film, since the electrodes are gas-diffusion-open.[67] The architecture also insures that transient absorption spectroscopy is sensitive across the device thickness,

because TA can be measured in transmission, avoiding destructive interference of the probe light close to the reflecting electrodes.[125] All organic layers were applied by doctor blading which is explained in the next section. Care was taken that doctor blading of the polymer:fullerene layers occurred under the same conditions for solar cells and neat films. This led to a thickness of 250 nm for P3HT:PCBM layers, 150 nm for Si-PCPDTBT:PCBM layers and 200nm for KP115:PCBM layers in order to achieve reasonable absorption.

Prior to degradation, all devices were annealed at 140°C for P3HT, at130°C for Si-PCPDTBT and KP115 for 5 minutes in a glovebox to achieve optimum morphologies of the films and active layers of the solar cells. Afterwards all devices were exposed to AM1.5 irradiation in dry synthetic air (80% N_2, 20% O_2 and 0% H_2O) for different time periods until the desired degradation was achieved. Subsequently, the degraded devices were returned into the glovebox and annealed at 130°C for 5 minutes to remove the residual oxygen doping.[32,67] The progress of degradation was monitored by UV-Vis absorption spectroscopy and the loss of optical density was then correlated with the loss in J_{sc} of the solar cells. All films, and solar cells were again annealed under vacuum at 140°C and 130°C, respectively, for 5 minutes in a cryostat (Oxford OPTISTAT), equipped with a heater, before each experiment, in order to make sure the reversible oxygen doping is removed and only irreversible degradation effects are measured.[32]

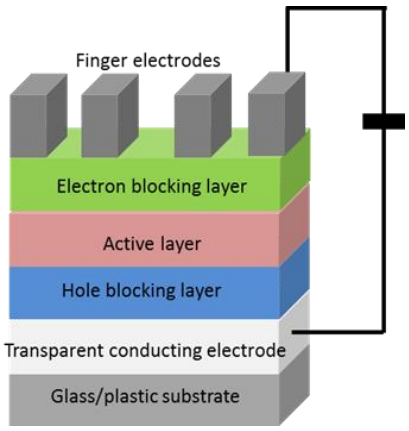

Figure 2.7: Structure of investigated organic solar cells.

The BDT-DPP (EP) solar cells were made from diketopyrrolopyrrole (DPP) and benzodithiophene (BDT) with a variety of side chains. Detailed molecular structures and names are given in section 2.1. Devices were fabricated on 13Ω/□ photo-lithography structured ITO. The zinc oxide transport layer was formed by spin-coating a solution of zinc acetate dihydrate (Aldrich) in DMSO at 160 g/L at 4000 rpm for 10 seconds followed by a 5

minutes thermal anneal process at 300˚C. The active layer was deposited by doctor blade coating. On top of the active layer 0.9 mL of PEDOT:PSS Clevios HTL Solar SCA 246-9 (Heraeus) was spread and uniformly coated by spin-coating at 1100 rpm for 130 seconds. The silver top (grid) electrode was applied by vacuum deposition at 2×10^{-6}mbar at 1-5Å/s. The devices were subsequently encapsulated with a top glass cover slide containing a 120µm cavity in the center of the slide. The outer edge of the cover slide was sealed using UV curing epoxy. The thermal degradation was done by heating at 55°C on a hot plate under ambient air for different time scales. Current- voltage characteristics were measured to monitor the changes in device parameters at each stage of degradation.

2.2.1 Coating method: Doctor blading

The doctor blading technique allows to fabricate solar cells with well-defined thickness. In contrast to the spin coating technique the material loss in the doctor blading process is as small as 5%.[93] This technique works as follows: A sharp blade is placed at a fixed distance from the substrate to be coated (usually 10-500nm). Then the coating solution put in front of the blade and the blade is moved linearly with the help of a motor across the substrate leaving a thin wedge of film after the blade. The final wet thickness of the film is ideally half of the gap between substrate and blade. The thickness of the film formed may also depend on the surface energy of the substrate, surface tension of the coating solution, viscosity of the coating solution and the speed blade movement.[93] The final dry thickness of the coated film, d, can be calculated by;

$$d = \frac{1}{2}\left(g\ \frac{c}{\rho}\right) \tag{2.1}$$

where g is the gap distance between blade and substrate, c is the concentration of the solid material in the ink in $g\ cm^{-3}$ and ρ is the density of material in the final film in $g\ cm^{-3}$.

2.3 Experimental setups

Understanding the energy-harvesting mechanisms in OSCs requires the ability to characterize the fundamental charge generation and extraction processes as a function of materials choice. In this subsection, experimental setups used to study the fundamental processes in a wide range of OSCs at both pristine and degraded conditions are explained.

2.3.1 Transient absorption spectroscopy (TAS)

Transient absorption spectroscopy (TAS, also called pump-probe spectroscopy) is a powerful technique for probing and characterizing the electronic and structural properties of short and long lived (from femtosecond to few milliseconds) excited state species of materials.[126] A schematic of a transient absorption experiment is shown in figure 2.8. The combination of a pulsed laser system and high speed data acquisition methods allows generation and probing of transient species. In general, transient absorption spectroscopy provides information on electronic and optical properties and decay kinetics of various excited states of the materials.

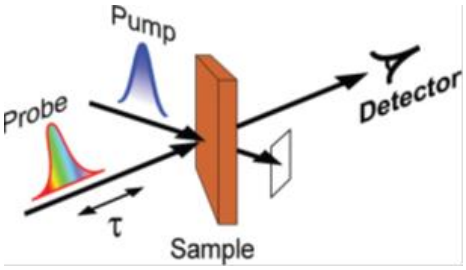

Figure 2.8: Scheme of transient absorption (pump-probe) experiment.[126]

Depending on the probing time scale one can divide TAS as follows:

1. Femtosecond-picosecond transient absorption spectroscopy;
2. Nanosecond transient absorption spectroscopy;
3. Microsecond-millisecond transient absorption spectroscopy.

Desired	Undesired	Timescale
Light absorption	Light transmission	fs
Exciton diffusion	Exciton trapping/deactivation	ps
Charge transfer	Geminate recombination	fs-ps
Charge collection	Non-geminate recombination	ns-µs

Table2.2: Elementary processes in an organic solar cell and their approximate lifetimes.

In solar cells, elementary processes like light absorption, exciton diffusion, charge carrier collection etc., happen at different time scales.[32] Details of the elementary processes and their approximate lifetimes are given in table 2.2. In this thesis, femtosecond and microsecond transient absorption spectroscopy together with transient electrical methods were used to monitor the excited state dynamics of solar cells materials.

2.3.1.1 Femtosecond pump-probe spectroscopy

Ultrafast spectroscopy (typically 10^{-14}-10^{-12}s) enables us to understand functional, structural and electronic properties of materials. Femtosecond transient absorption spectra yield important device parameters like yield of immediate charge carrier formation (from interfacial charge transfer states), yield of delayed charge carrier formation (due to exciton diffusion to interface), picosecond recombination losses and the reason for them (CT states, triplet states, etc). A detailed schematic of femtosecond pump-probe spectroscopy setup used to investigate organic solar cells in this thesis is shown in figure 2. 9.

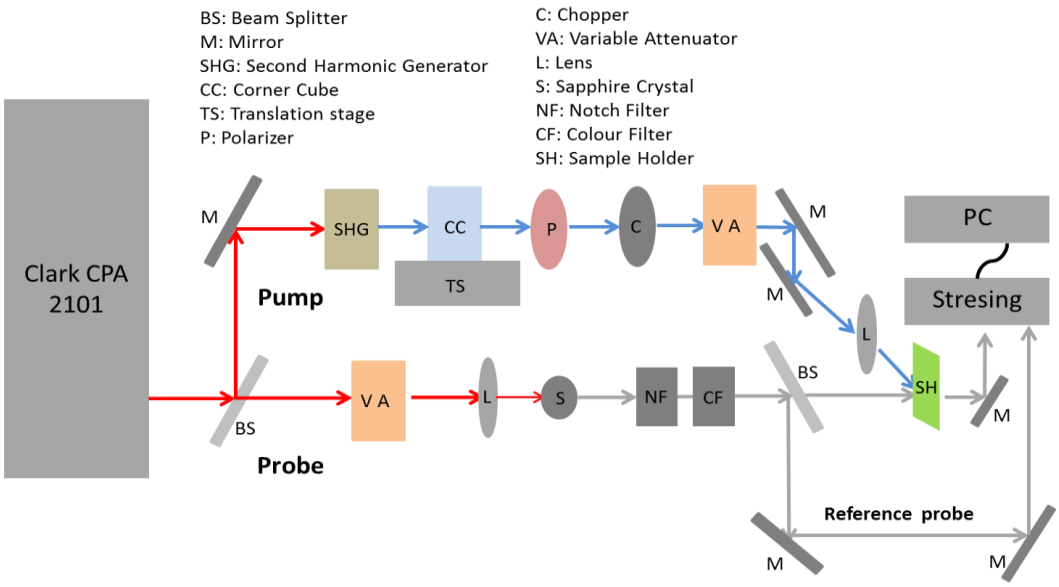

Figure 2.9: Schematics of femtosecond pump probe spectroscopy experimental setup.

A regeneratively amplified laser system was used for producing femtosecond pulses (150fs) at 1 kHz repetition rate (Clark-MXR CPA2101). The 775 nm pulses were split into two parts: one part was frequency doubled using an LBO crystal (pump pulses), the other part was focused onto a 2 mm Sapphire plate, producing a femtosecond white light super continuum from 420-1600 nm (probe pulses). The probe pulses were focused onto the sample (about 150 µm diameter), and overlapped with the pump pulse (about 300 µm diameter), the delay time of which was controlled via a mechanical translation stage and a corner cube reflector. After transmission through the sample the probe pulses were sent to a prism spectrometer (Entwicklungsbüro Stresing GmbH) with a CCD array (256 pixels, VIS-enhanced InGaAs, Hamamatsu Photonics Inc.). Data acquisition and modelling was done by custom built Python software, using open source packages *Matplotlib*, *PyQt4*, *SciPy*, *Pyserial*, among others.

In organic photovoltaics, exciton dissociation and geminate recombination (a prominent loss process that reduces the generation yield), have been shown to occur on this time scale. In contrast to microsecond TA, where essentially only one type of photoexcitation (positive polarons in the donor phase) is visible, in femtosecond TA additionally neutral singlet excitons can be observed. The TA spectra of singlets and polarons generally overlap, so matrix decomposition techniques need to be used to obtain the time-resolved population of singlet excitons and polarons separately. This thesis follows a procedure called target analysis described by van Stokkum et al.[127]

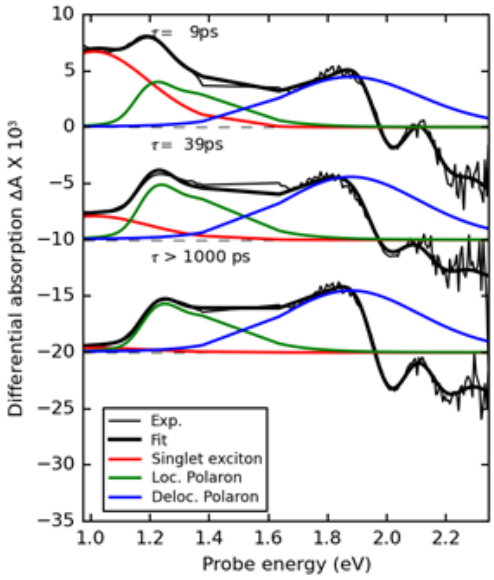

Figure 2.10: Typical evolution associated differential spectra (EADS) obtained from a global fit for P3HT:PCBM film (black thin solid line). Thick black lines represent the spectral fits to corresponding EADS, red lines indicate singlet contribution, green and blue curves represent localized and delocalized polaron states, respectively. A gap between 1.4 and 1.7 eV is due to spectral overlap with scattered light from the pump pulse.

To this end, the TA spectrum was reproduced by a superposition of 3 spectra, each with an associated lifetime following a first order sequential reaction of type $0 \rightarrow A \rightarrow B \rightarrow C \rightarrow 0$. Please note that this procedure is purely mathematical and does not involve any photophysical assumptions. Therefore, the spectra of A, B, and C do not correspond to real photophysical states (singlet excitons and charged states) but to a superposition of these, and therefore are called evolution-associated differential spectra (EADS 0, 1, and 2, respectively, thin black curves in figure 2.10). The contribution of singlets and charged states to each EADS can be obtained by spectral modelling. Only at this point, photophysical knowledge enters the procedure, essentially by requiring (i) that different states have different PA bands, (ii) that there are only 2 distinct photo-excited states in our spectral window, namely singlets and charged states of the donor polymer, and finally (iii) that both singlets and charged states

share the same transient photo-bleach. For example, P3HT:PCBM has amorphous and ordered donor phases, each with distinct optical probes for singlets, polarons and the corresponding bleach.[51] The procedure results in individual spectra for singlets and charged states (for both localized and delocalized species, if any), the spectral weights of which correspond to their concentrations.

2.3.1.2 Microsecond transient absorption spectroscopy

In OSCs, extraction of separated charge carriers and non-geminate recombination occur on sub-nanosecond to microsecond time scales.[128] A schematic representation of microsecond TAS is shown in figure 2.11. The microsecond transient absorption measurements were performed by exciting the samples at room temperature at different excitation wavelengths (depending on the sample's absorption maxima). On the sample, the pump laser had a spot size bigger than that of the probe light in order to provide homogeneous excitation conditions in the region of probing. A 970 nm (2 mm spot size) 120 mW LED was used for probing the photo-excitation dynamics of polarons in P3HT:PCBM, Si-PCPDTBT:PCBM and KP115:PCBM and a 1300 nm (2 mm spot size) 2 mW LED was used for detecting polaron dynamics in BDT-DPP:PCBM solar cells.

The pump intensity was varied by using a circular attenuator. Specifications of the pump and probe beams employed for each sample are detailed in the following chapters. The transient absorption signal was detected by an amplified Si-photodiode (Thorlabs PDA 10A EC) or an InGaAs photodiode (Thorlabs PDA 20CS ES - for BDT-DPP:PCBM) equipped with an 850 nm long pass filter in order to reject scattered pump light and fluorescence. The electrical signal from the photodiode was then sampled by an oscilloscope (Picoscope 6424) connected to a PC using custom built Python software. Data evaluation was done via custom built Python software.

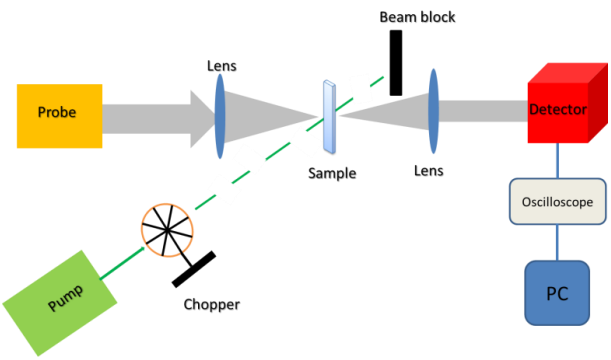

Figure 2.11: Schematics of microsecond transient absorption spectroscopy.

A simplified kinetic model for the charge carrier density in the active layer of a device of thickness d, applying idealized assumptions such as homogeneous medium, second-order recombination, and constant built-in field E_{bi} is given by,

$$\frac{dn}{dt} = G - k_L nn - \mu n \frac{E_{bi}}{d} \tag{2.2}$$

where μ is the effective charge carrier mobility, G is the photo-induced generation of extractable charge carriers, and k_L is the bimolecular charge recombination coefficient, assuming Langevin recombination.

$$k_L = 2e\mu_{eff} f_{LV}/(\varepsilon\varepsilon_0) \tag{2.3}$$

Herein, $\mu_{eff} = \mu_e + \mu_h$ is the sum of the mobilities for positive and negative charges, respectively, ε is the relative dielectric constant, ε_0 is the dielectric constant in vacuum, and f_{LV} accounts for sub-Langevin recombination, as often observed in BHJ active layers.

2.3.2 Transient electrical measurements

Electrical and photo-electrical transient measurements rely on an analysis of the features of current (or photo-current, respectively) dynamics. Transient electrical measurement such as transient photo current (TPC), transient photo voltage (TPV), photo-induced charge extraction by linearly increasing voltage (photo-CELIV) provides a wealth of insights into the charge carrier dynamics.[65,71,125,129] In this subsection, the experimental methods used for transient electrical measurements of the investigated solar cells are briefly explained. Before each experiment, all films and solar cells were again annealed under vacuum at 140°C and 130°C, respectively, for 5 minutes in a cryostat (Oxford OPTISTAT for TPV and TPC and Oxford ICE for CELIV), equipped with a heater, before each experiment, in order to make sure that the reversible oxygen doping is removed and only irreversible degradation effects are measured.[32]

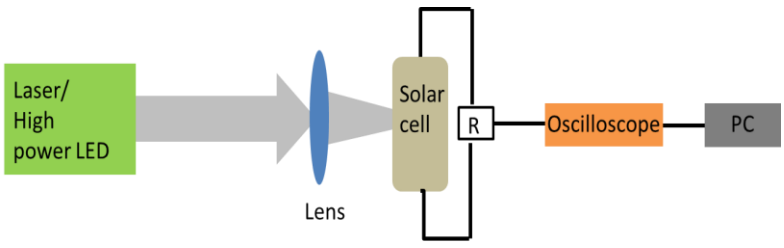

Figure 2.12: Simplified experimental setup for transient photo voltage and transient photo current measurements. For TPV the termination resistance (R) is 1MΩ and for TPC it is 50Ω.

2.3.2.1 Transient photovoltage (TPV)

Transient photovoltage (TPV) measures the changes in the open circuit voltage with time. TPV is caused by the excess carrier density of macroscopically separated electrons and holes. Unlike in TAS where one can observe all charge carriers, including the trapped (immobile) ones, transient photo voltage only monitors the mobile charge carriers. Transient photo voltage yields important information on charge carrier dynamics and charge carrier density.[125,129,130]

In the TPV measurements investigated in this thesis, the solar cell devices were connected to the 1MΩ impedance input terminal of the oscilloscope (Picoscope6424) and voltage traces were recorded. A simple schematic representation is shown in figure 2.12. Depending on the sample's absorption maxima, different excitation wavelengths and sources were used. P3HT, Si-PCPDTBT and EP10 solar cells were excited with a Nd:YAG, 532nm externally modulated CW laser. For all BDT-DPP polymer devices, a 780 nm high power light emitting diode (LED 780E) was used for excitation. No background illumination (light biasing) was used in TPV measurements for the samples investigated in this thesis except for P3HT:PCBM. The electrical signal from the solar cell was then sampled by an oscilloscope connected to a PC using custom-built Python software. One limitation of TPV is the RC time, one cannot measure anything faster than this RC time.

2.3.2.2 Transient photocurrent (TPC)

Transient photocurrent (TPC) probes the dynamics of time-resolved charge carrier extraction. Like transient photovoltage, TPC also counts only the mobile charge carriers and is blind to the immobile charge carriers. Transient photo current also provides good understanding of the charge carrier dynamics. Integrating the area under the TPC traces yields the extracted charge carrier density.

In the TPC studies performed here, the solar cells were connected to the input terminal of the oscilloscope with a termination resistance of 50Ω and the extraction current from the solar cells were recorded. All TPC measurements were done with the same experimental settings of transient photo voltage except the termination resistance. Typical photocurrent value obtained from TPC for P3HT:PCBM solar cell is about 1 mA.

2.3.2.3 Charge extraction by linearly increasing voltage (CELIV)

Charge extraction by linearly increasing voltage (CELIV) and photo-induced CELIV (photo-CELIV) are used to measure the charge carrier mobility and the concentration of

P3HT:PCBM solar cells under the absence and presence of light, respectively. The experimental arrangement for dark and photo-CELIV is given in figure 2.13

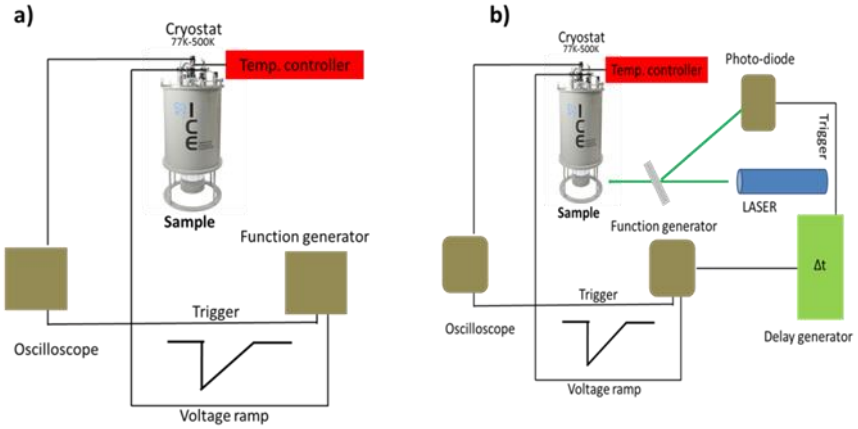

Figure 2.13: Experimental arrangements for CELIV (a) and photo-CELIV (b).

For the CELIV measurements, samples were kept in dark (in the cryostat) and equilibrium charge carriers were extracted by a linearly increasing voltage ramp generated by a digital function generator (Tektronix AFG 3011). The function generator itself acts as voltage source for the sample and trigger source for the oscilloscope. The CELIV transients were sampled and recorded by using a digital oscilloscope (50 Ohms termination, Tektronix DPO 4054B) for different photo-oxidized organic solar cells.[131]

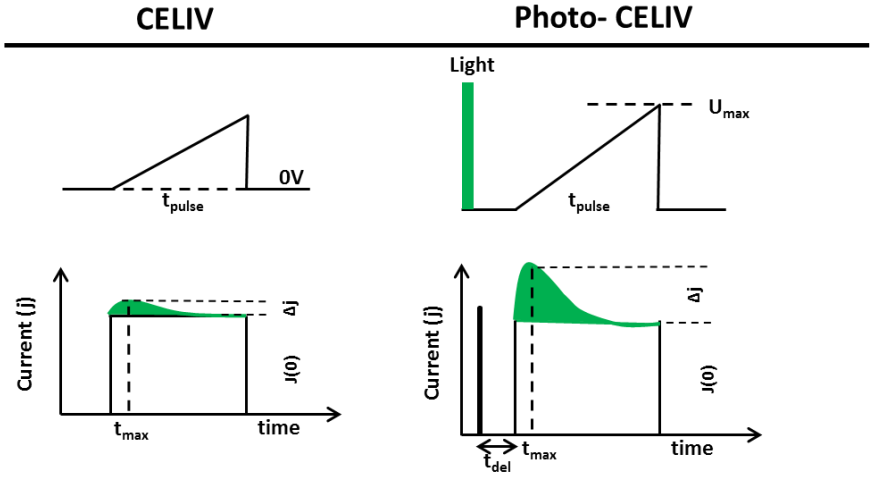

Figure 2.14: The pulse sequence and schematic response of CELIV and photo-CELIV transients. Where J(0) is the capacitive current of the cell and Δj is the photogenerated current

In the photo-CELIV experiments the solar cells were excited with short pulses from a 532nm, 5ns laser source (EKSPLA-NT 340). The exact time of the light pulse was detected by a photo-diode which triggered the delay generator. A function generator (Tektronix AFG 3011)

was used as the voltage source which was triggered by the delay generator (Tektronix AFG 3022). The delay time between voltage pulse and light pulse was controlled by using a digital function generator as delay generator .The current transients are then measured and sampled by using a digital oscilloscope (Tektronix DPO 4054B) for different delay times and at different degradation stages of the device. A home-made electrical switch was used to avoid the charge extraction during the delay time due to the built-in field. This arrangement insures that the charge loss during this period is solely due to recombination.[131]

In the CELIV experiments, the equilibrium charge carriers are extracted from the solar cells with a linear reverse bias voltage ramp (slope $A = \frac{dU}{dt} = U_{max}/\Delta t_{pulse}$).[71] The charge carrier mobility can be estimated from the time at which maximum current can be extracted (t_{max}). Under conditions when $\Delta j \leq j(0) = C \cdot A$ (C = capacitance of the cell, j_0 = capacitive current of the cell), the mobility μ is obtained as:

$$\mu = \frac{2d^2}{3At_{max}{}^2} \tag{2.4}$$

where d = thickness of sample, A = applied voltage ramp and t_{max} = time of maximum carrier extraction. Integrating the area under the CELIV traces provides the photo-generated carrier density (from photo-CELIV) and equilibrium carrier density (from dark-CELIV). The extracted charge, Q_e can be calculated by;

$$Q_e = S \int_0^{t_{pulse}} \Delta j \, dt \tag{2.5}$$

where S is the electrode area, Δj is the Faradaic current density obtained as the difference between the total current j and the capacitive current j(0), which is assumed to be constant over the whole pulse duration (see figure 2.14).[65,67] The charge carrier density (p) information can be obtained from;

$$p = \frac{Q_e}{eSd} \tag{2.6}$$

where d is the thickness of the sample and e is the elementary charge.[65,71]

Chapter 3

Photo-physics of P3HT:PCBM solar cells

Remarkable progress has been made in the field of organic solar cells in the last decade. The polymer based solar cells have achieved power conversion efficiency of more than 10% already and 15% is within reach. Polymer chemistry has played a significant part in this achievement and will be the key to further developments. On the other hand, the underlying mechanisms in the photovoltaic conversion processes are still under debate in polymer solar cells. Simple J-V curves summarize all elementary contributions to charge collection and therefore cannot be used to selectively address elementary mechanisms and loss processes. This chapter uses transient absorption spectroscopy and transient photovoltage to unravel the fundamental mechanisms occurring in the P3HT:PCBM solar cells and films. P3HT:PCBM shows many interesting properties like intensity dependent polaron generation and singlet quenching, different decay mechanisms in the films and complete devices, lateral diffusion of polarons due to the influence of highly conductive PEDOT:PSS layer etc.

3.1 Introduction

Charge generation is one of the key steps in photovoltaic devices in the conversion of light into electrical energy. In all organic solar cells, charge generation occurs via photo-induced electron transfer.[132] In this electron transfer mechanism an electron is transferred from an electron donor (D), a *p*-type semiconductor, to an electron acceptor (A), an *n*-type semiconductor, with the assistance of the additional input energy of an absorbed photon ($h\nu$). A charge-separated state is created after this photo-induced electron transfer consisting of the radical cation of the donor ($D^{\bullet+}$) and the radical anion of the acceptor ($A^{\bullet-}$). A simple schematic is given in figure 3.1.

$$D + A + h\nu \rightarrow (D^{*} + A) \text{ or } (D + A^{*}) \rightarrow D^{\bullet+} + A^{\bullet-}$$

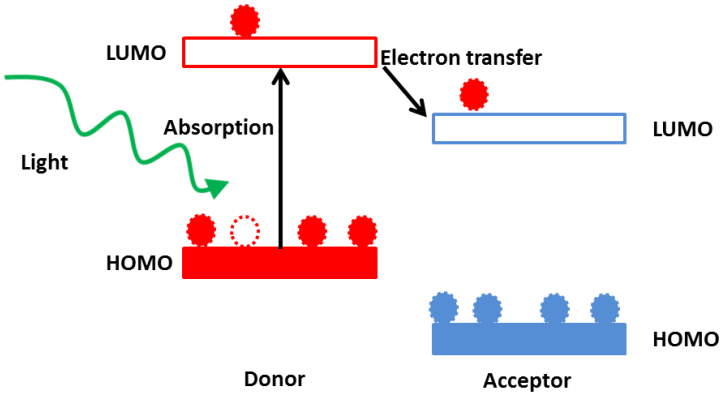

Figure 3.1: Schematic diagram of the working principle of organic solar cells.

After the absorption of photons and subsequent excitation of electrons from the HOMO to the LUMO of the organic semiconductor, the charge carriers are generated according to the following key processes: exciton generation, exciton migration and charge separation, charge transport and charge extraction. All these processes are detailed in Chapter 1. The power conversion efficiency of a solar cell depends on how efficient these processes are after the photon absorption. These events occur over highly disparate timescales ranging from femtoseconds to milliseconds and it is necessary to observe the processes over nine orders of magnitude in time and each event needs to be distinguished and analysed separately.[32,128] The external quantum efficiency can be given as;

$$EQE = \varphi_{abs}\, \varphi_{diss}\, \varphi_{sep}\, \varphi_{extr} \qquad (3.1)$$

where φ_{abs} is the efficiency of photon absorption, φ_{diss} is the efficiency of exciton dissociation, φ_{sep} the efficiency of charge pair separation and φ_{extr} is the efficiency of charge carrier extraction.

Transient absorption spectroscopy is a useful and powerful tool to clarify the underlying mechanisms in organic solar cells.[132] Many attempts have been done to improve the quantum efficiency (product of all the above cascade processes as given in equation 3.1) by altering the morphology of the active layer but many facets of the structure-function relationship are still debated.[128,133,134] Recently time-resolved studies and microscopic studies have started to unravel the structure-property relationships.[51,128,132] Howard et al. observed ultrafast charge generation in annealed P3HT:PCBM solar cells, Ohkita et al. demonstrated annealing effects on charge separation and it reduce the loss during charge collection.[51,62,129] For improving the performance of organic solar cells, molecular understanding of the series of fundamental processes after absorption of photons is necessary.

Regioregular poly (3-hexyl thiophene):phenylC_{61}-butyric acid methyl ester (RR-P3HT:PCBM) has been one of the extensively studied materials for photovoltaic applications. They have shown consistent efficiency approaching 5% and relatively high external quantum efficiency.[135,136] In this chapter, charge carrier dynamics of P3HT:PCBM based films and solar cells are investigated in order to understand the photophysics happening in these materials upon the absorption of photons. Transient absorption spectroscopy (TAS) and transient photovoltage (TPV) techniques are used to study the photo-physics of P3HT:PCBM films and solar cells.

3.2 Experimental

Experimental details for femtosecond transient absorption spectroscopy are explained in Chapter 2. The TPV measurements investigated here used the 1MΩ impedance input terminal of an oscilloscope (Picoscope6424) and a white light high power LED (MCWHL5 Thorlabs) for background illumination. The intensity of this illumination controls the V_{oc} of the device and was controlled by a DC power supply (0-30V, 0-10A). A small optical perturbation was applied by using a532nm CW Nd:YAG laser modulate by an acousto-optic modulator (AOM), which produced a voltage transient with an amplitude ΔV_0<Voc. At this open circuit condition, the generated charge carriers are restricted to the device and forced to recombine, since there are no external electrodes for current flow. By observing the decay of these carriers, one can gather important information of loss kinetics in organic solar cells. Transient absorption (TA) is an all optical measurement which probes the changes in the optical density upon photo-excitation. TA was measured in transmission mode and the same excitation

source at 532 nm was used for photo excitation for TPV and a 970 nm LED was used as probe for $P3HT^{+}$ polarons.

Photo-induced absorption (PIA) spectra were performed by using a chopped (220Hz, 1:1 duty cycle) 532 nm CW Nd:YAG laser of power P = 200 mW as an excitation source and probed by a tungsten lamp. The collimated and focused beams were guided to the sample with the aid of proper optics. All measurements were performed in the cryostat under dynamic vacuum (~10^{-4}mbar) at room temperature. The transmitted probe light through the sample is detected by an amplified photo diode [Thorlabs PDA 10A-EC] and the values are displayed on a Lock-in amplifier (Stanford Research System SR830). To check the effect of the PEDOT:PSS layer in organic solar cells, the PIA measurements were performed on films having only the active layer (P3HT:PCBM) and on the device having a highly conductive PEDOT:PSS layer as HTL by changing the pump probe overlap (Scheme 1).

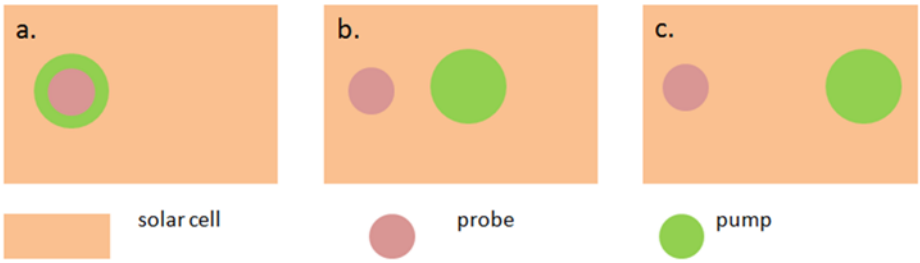

Scheme 3.1: Schematic representation of changing pump probe overlaps. a) Full overlap, d) 1st displacement from pump probe overlap, c) 2nd displacement from pump probe overlap.

In transient absorption spectroscopy (TAS) studies, annealed samples under high vacuum at room temperature were excited at 532 nm with a continuous wave Nd:YAG laser of power P = 200mW. The laser beam was modulated by using an acousto-optic modulator (AOM) with a repetition rate of 143 Hz, which corresponds to the decay dynamics of the P3HT:PCBM. A 970 nm 120 mW LED, having 2 mm spot size was used for probing the photo-excitation dynamics in the region of the P3HT hole polaron absorption. After passing through the sample, the probe beam was focused onto an amplified silicon photodiode (Thorlabs PDA 10A-EC) with a rise time of about 3 ns. An 850 nm long pass filter was mounted in front of the photodiode in order to reject scattered pump light. The electrical signal from the photodiode was then averaged on a LeCroyWaveMaster 8Zi Digital Oscilloscope, triggered by the pulse and delay generator, for typically 10^{5} excitation pulses. To confirm the lateral diffusion effect of the charge carriers by PEDOT:PSS layer (see below), the kinetics of the transmission at 970 nm is recorded for different pump probe overlap (Scheme 3.1).

3.3 Results and discussion: Photoexcitation dynamics in pristine films and solar cells

3.3.1 Femtosecond transient absorption spectroscopy

Femtosecond transient absorption (TA) spectroscopy is used to trace photophysics that occur on a time scale of femtosecond to picoseconds. TA spectroscopy can be deployed to trace the time-resolved concentration of several photoexcitations, like singlet/triplet excitons and charged states, by virtue of their specific photo induced absorption (PA) bands. Moreover, the total amount of excited states in a certain phase of the sample can be deducted from the characteristic reduction of ground state absorption, leading to a transient photo-bleach (PB). The TA spectra of singlets and polarons generally overlap, so matrix decomposition techniques need to be used to obtain the time-resolved population of singlet excitons and polarons separately. This thesis follows a procedure called target analysis described by van Stokkum et al.[127] and details of analysis are given Chapter 2.

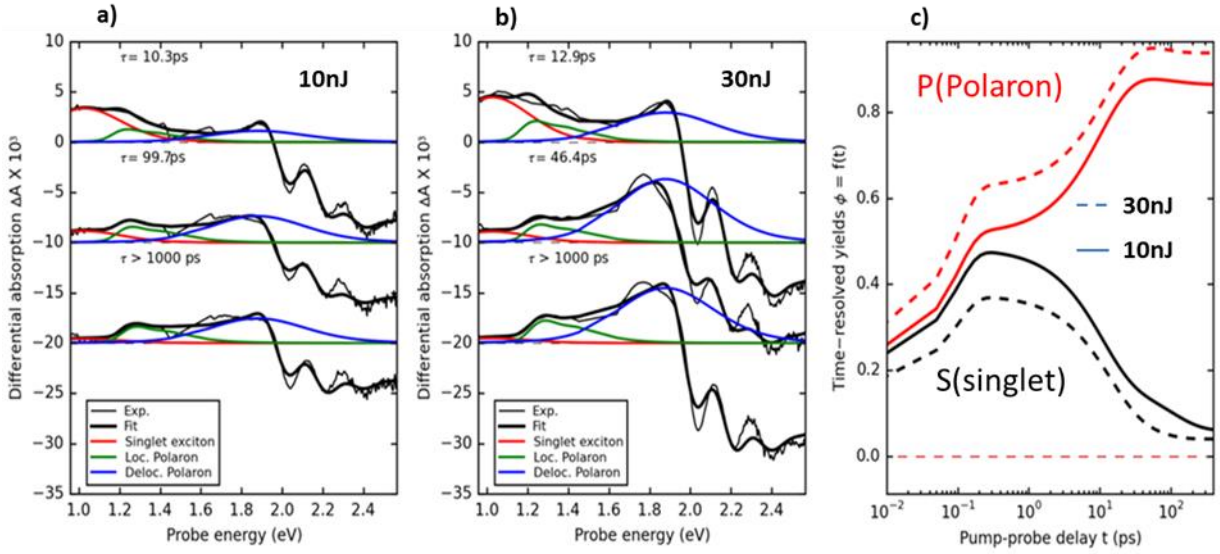

Figure 3.2: a) Evolution associated differential spectra (EADS) at 10nJ per pulse pump energy for pristine P3HT:PCBM, as obtained from a global analysis of using a 3 sequential step model (thin solid curves, fitted lifetimes are given in the legend), spectral fits to the EADS (thick solid curves) and contributions to fits from singlet (red curves) and polaron states (blue curve corresponds to polarons in the ordered phase, green curve to polarons in the amorphous phase, respectively). Note that for clarity of presentation, the contributions to the PB bands are not given. b) Same as (a), but at 30nJ. c) Time-resolved yield of polarons and singlet at both intensities (dashed lines 30nJ, solid lines 10nJ).

The figure 3.2 shows the characteristic spectra (EADS) of pristine P3HT:PCBM. Here, the simplified treatment of Guo et al. was followed, who obtained specific kinetics for singlet and charged states by subtracting the singlet contribution to the charge transient at 1.24 eV, which they found to be about one third of the maximum of the singlet absorption band at 1.0 eV,

which is solely due to exciton TA, because there is no oscillator strength for the charge absorption band at that probe energy.[51] Applying this procedure to the EADS yields spectral weights of the singlet and polaron bands, however with unknown relative cross-sections, because the optical probes for P3HT polarons and singlets are not locked via the common PB signal. Therefore, applying Guo's treatment cannot yield the absolute polaron yield, as target analysis can, but only a quantity which is proportional to it. The target analysis clearly distinguishes the polaron contributions from the ordered phase (blue line) and from the amorphous phase (green line) of RR-P3HT (figure 3.2). Singlet excitons have decayed after 100ps, most of the decay occurring on a 10 ps time scale, and both polaron bands are growing as time proceeds. Howard et al. observed efficient ultrafast charge generation in the absence of field in annealed RR-P3HT:PCBM blends, whereas this ultrafast process is much reduced in unannealed and amorphous regiorandom blends because of the favorable morphology in annealed RR-P3HT:PCBM blends.[128]

Comparison between figure 3.2a and b shows no changes in the spectral shape with increase in the pump intensity. Figure 3.2c shows the yield of singlet (black) and polarons (red) states at both intensities (dotted lines 30 nJ and solid lines 10 nJ). The polaron generation increased from 50% to 62% and the singlet yield went down from 45% to 35% at 1ps when the intensity of pump pulses increased from 10nJ to 30nJ. The same results also were observed by Ohkita et al.[62] This could be due to the fact that polaron formation is much more efficient from higher excitonic states produced by the singlet exciton-exciton annihilation.[132] Similar improvements in the immediate polaron generation were also observed. This could be due to a nonlinear increase in the absorption of photons by the material. The loss in the singlet yield is reflected in the gain of polaron states at all the delay times. This indicates at higher levels of intensities the singlet to polaron formation is more efficient and therefore also the efficiency of the solar cell under high light intensities. Care was taken to keep the time-averaged intensity low enough, so that only processes are observed that also occur under CW solar irradiation. Also note that there is no indication of triplet formation in RR-P3HT:PCBM unlike RRa-P3HT:PCBM.[128] This remarkable difference suggests that film morphology rules the primary photophysics in P3HT:PCBM organic solar cells. This difference could be due to the fact that polaron formation efficiency from polaron pairs is much higher in P3HT:PCBM than singlet fission efficiency because of large inter-chain interactions in highly ordered P3HT crystalline regions as Ito proposed.[132] To know how these polaron states are behaving at longer time scales, microsecond transient measurements were performed.

3.3.2 Microsecond transient absorption spectroscopy

In Figure 3.3, decay traces of the polaron absorption band at 970 nm are shown on a micro- to millisecond time scale after the end of the excitation pulse, long enough to reach stationary charge carrier concentrations. The decay curves allow to specifically obtain information on recombination, since both extraction and generation are absent, due to the absence of electrodes and irradiation, respectively. In order to visualize details of the decay at various times and signal levels in a single graph, a double logarithmic representation of the data was chosen. In pristine P3HT:PCBM (figure 3.3a), a strong intensity dependence of the decay curves is found: while the starting concentrations at t=1µs cover nearly an order of magnitude, after 1 ms decay time all curves are within a factor of 2. This behaviour is indicative of a pure bimolecular reaction with equal concentrations of positive and negative carriers, as expected if only photo-induced carriers are present.

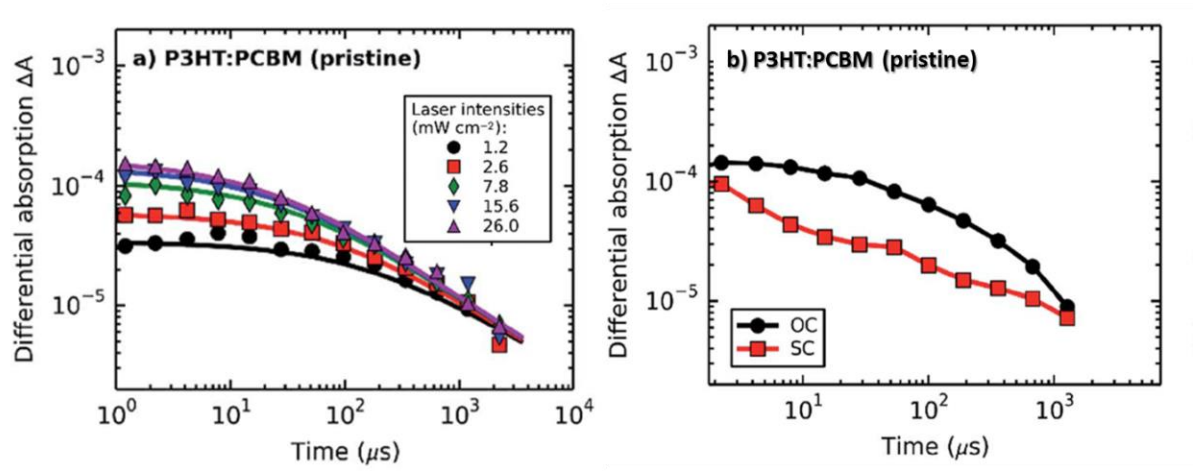

Figure 3.3: Charge carrier recombination traces in P3HT:PCBM films at different light intensities and at 970 nm probing wavelength, upon termination of illumination. Panel (a) show transients of P3HT:PCBM at different intensities and panel (b) shows the transients at open circuit and short circuit conditions.

The rate equation describing charge carrier dynamics in the absence of electrodes and other layers becomes,

$$\frac{dn}{dt} = G - k_L(t) \cdot [n(t) + c_b] \cdot n(t) \qquad (3.2)$$

Herein, G is the generation rate of polarons; k_L is the bimolecular recombination coefficient, $n(t)$ is the charge carrier density and c_b is the background carrier density. The decay traces at different intensities were fitted using global fitting with equation 3.2. The solid lines in the figure 3.3a are the fits for the respective decay transients. The fits delivered a bimolecular recombination coefficient for pristine P3HT:PCBM ~10^{-12}cm^3/s with negligible background carrier density.[32]

Figure 3.3b examines separately the open circuit (black curves) and short circuit (red curves) microsecond TAS of P3HT:PCBM. In the case of open circuit TAS all charge carriers have to undergo recombination, because there is no electrodes connected to external circuit. For the short circuit TAS, the generated charge carriers have two decay pathways. They can go for recombination and extraction. The polarons probed in the short circuit TAS are the carriers which are not extracted by the external circuit. The comparison studies shows that in pristine P3HT:PCBM solar cells the extraction is way more faster than recombination which reflects the good performance of pristine P3HT:PCBM solar cells. And also note that the starting concentration in short circuit TAS is less than that of open circuit TAS. This is because; part of the generated charge carries are extracted before this observed time window. A detailed study of degradation effects on recombination and extraction on P3HT:PCBM solar cells is presented in Chapter 4.

3.3.3 Determining recombination dynamics in an operating P3HT:PCBM solar cell

Transient lifetime measurements depend on the decay of the charge carriers over time. Transient electrical measurements such as transient photocurrent (TPC)[129], transient photovoltage (TPV)[130], providessignificant insight into charge carrier dynamics and one can compare these results with transient absorption results. Many methods have been employed to determine the lifetime and density of the charge carriers such as photo-CELIV and time of flight.[65,76] Although they measure relatively accurate values, one cannot directly relate such measurements under real device operating conditions under continuous irradiation.[130] Shuttle et al. introduced a method to study the dynamics of steady state charge carriers in organic solar cells under operating conditions.[125] They used transient photo-voltage (TPV) in complement with transient absorption spectroscopy (TAS) under continuously illuminated background irradiation in open circuit conditions to investigate the charge carrier dynamics.[125] In this section TPV and TAS measurements on P3HT:PCBM solar cell are reported under different white light background illumination intensities.

Figure 3.4 shows the TPV (red) and TAS (black) traces of P3HT:PCBM solar cell at different background illumination intensities varying from ~0.15 to 0.9suns. In figure 3.4a the applied background intensity was about 0.15 suns and the decay of TAS is slightly faster than TPV. Upon the increase of background light intensity both traces shows excellent agreement in the shape of transients. One can expect that, in the small perturbation medium the decay could be

mono-exponential, which is consistent with pseudo first order rate equation as observed by Shuttle et al.[130]

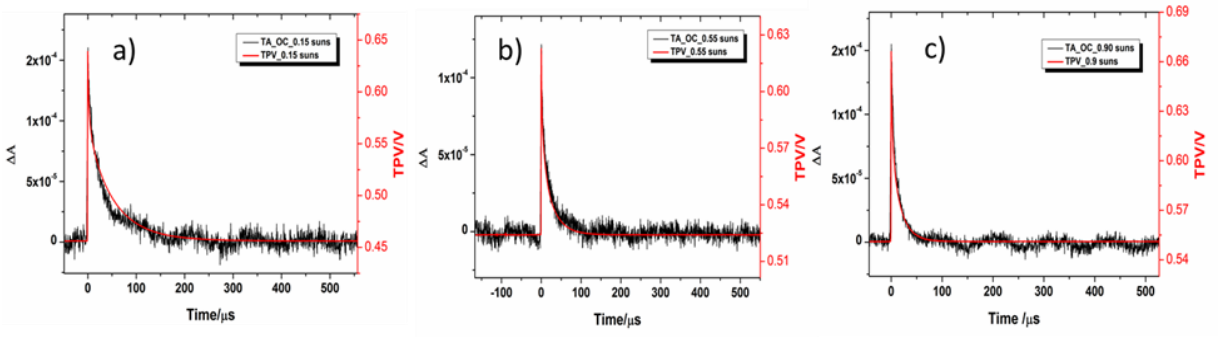

Figure 3.4: Transient absorption (black) and transient photo-voltage (red) traces at different background intensities. Approximate background intensities are given in the legends. Upon increase in the background intensity the shapes of both TAS and TPV curves become identical.

According to Shuttle et al. the mono-exponential decay of excited state can be written as;

$$\frac{d\Delta V}{dt} \propto \frac{d\Delta n}{dt} = -k_{eff}\Delta n = -\frac{\Delta n}{t_{\Delta n}} \tag{3.3}$$

where ΔV is the photovoltage, t is the time, k_{eff} is the pseudo-first-order recombination rate constant, Δn is change in the density of photogenerated carriers due to the laser pulse, and $t_{\Delta n}$ is the corresponding carrier lifetime. The recombination rate coefficient k_{eff} depends on the effective mobility of the charge carriers and Langevin recombination factor.

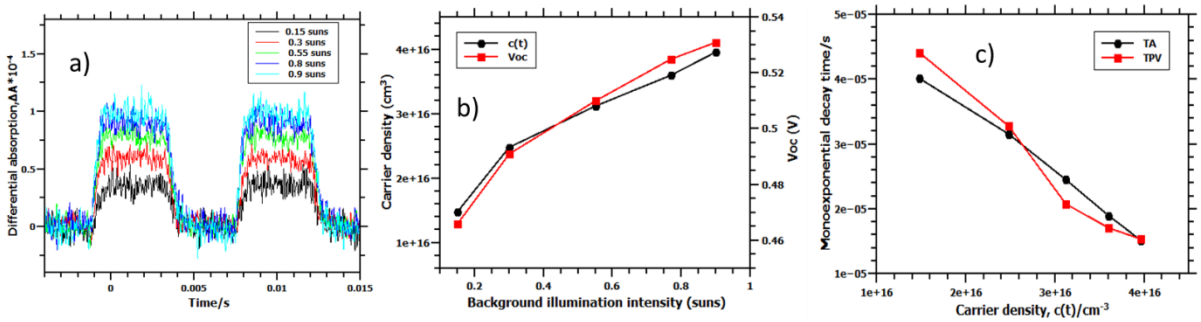

Figure 3.5: (a) TAS traces measured only with chopper background illumination to measure the background carrier density.(b) The variation of charge carrier density obtained from TAS and increase in the open circuit voltage obtained from TPV upon incease in the background light intensity.(c) Changes in the dacay time ($t_{\Delta n}$) of charge carriers with increase in the background carrier density obtained by applying mono exponential fits to TA and TPV.

Figure 3.5a represents the TAS traces measured with chopped background white light in order to obtain the information of background carrier density. Figure 3.5b shows that both the carrier density *c(t)* and open circuit voltage are monotonously increasing with background illumination. Please note that the *c(t)* is the background carrier density and was calculated from TAS with only chopped background illumination as excitation source and a 970nm LED as probe as shown in figure 3.5a. In the figure 3.5c, changes in the carrier lifetime ($t_{\Delta n}$)

are plotted for both TPV and TA measurements with carrier density changes. In agreement with equation 3.3, it is found that the carrier lifetime is strongly dependent on background carrier density and shows a psuedo first order decay(seefigure 3.4).Shuttle et al. relate this strong density dependent dynamics of P3HT:PCBM to a bimolecular recombaintion dynamics in which the bimolecular rcombination coefficient is a carrier density depenedent parameter.[130] Recent studies on the recomibiation mechanism of P3HT:PCBM shows that the recombination coeficient does not depend only on carrier density, it is more complex and depends on the energetics of the material, degradation, mobility etc,.[32] This is also in agreement with figure 3.3, which is obatined from TAS without any background illumination, where the recombination rate clearly depends on the charge carriers produced, effective mobility and energetics of active layer.[32] Nelson et al. also reported TAS studies on P3HT:PCBM where the observed bimolecular recombination was attributed to an exponential tail of sub-band-gap localized ('trap') states.[77]

In summary, the simple TPV traces can be used for calculating polaron dynamics rather than complicated TAS as previously demonstrated by Shuttle et al. In P3HT:PCBM solar cells the carrier lifetime is strongly governed by the charge carrier density.

3.3.4 Recombination dynamics in P3HT:PCBM devices and films: A comparison

There have been detailed and intensive studies on P3HT:PCBM films and solar cells in order to understand the bimolecular recombination mechanism.[32,130] It has been already reported that the bimolecular recombination coefficient is several orders of magnitude less than that predicted by Langevin formula for P3HT:PCBM.[71] This indicates that for such solar cells, the bimolecular recombination is not efficient under solar conditions.[125] Most of these studies are done in complete devices and the behavior of such studies on selected layers might show different results. Durrant and coworkers tried to understand the difference in the recombination dynamics of P3HT:PCBM only on active layer and on the complete device by using TAS in the reflectance mode for devices.[125] They found that transient follows same dynamics for both films and devices.

The TAS measurements reported herein, used a 532 nm CW Nd:YAG laser externally modulated by AOM for films and 532 nm pulsed (300 ps) Nd:YAG laser for the devices and photoinduced signals were detected by using a 970 nm LED. The samples were annealed at

140^{o}C before each measurements for 5 minutes to remove residual oxygen under dynamic vacuum (3.5x10^{-4} mbar) in a cryostat (Oxford OPTISTAT^{TM}).

Figure 3.6a shows a comparison of film (black) and device (red) TAS data collected against time under open circuit conditions. The initial ΔOD value for device is slightly higher than that of films and this in agreement with Shuttle et al. findings.[125] Shuttle et al. reported a higher ΔOD for device and they assocaite this difference in signal amplitude to optical interference effects influencing the device data.[125] But, in figure 3.6a it is clear that the difference is not as high as Shuttle et al. observed, this could be due to fast diffussion of polarons into high conductive PEDOT:PSS side and they cannot be probed at this wavelength. Figure 3.6b shows normalized traces of figure 3.6a. It is clear form the figure 3.6 that the recombination in the film is faster than that of device after 10µs which is in contradiction with Shuttle et al. observation. They found that both film and device follow same kinetics.[125] The calculated bimolecular rate constant (k_b) for film and device are ~2*10^{-12} and ~0.8*10^{-12} cm^3/s respectvely.

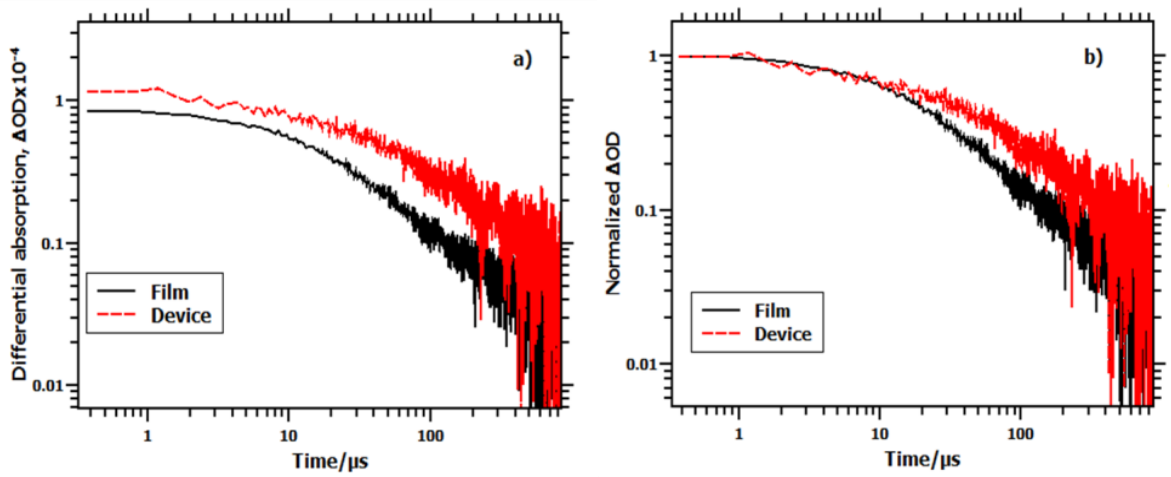

Figure 3.6: (a) Transient absorption decay traces for film (balck) and for complete device (red) and (b) normlalized transient absorption traces.

The rate equation for bimolecular recombination is given by;

$$\frac{dn}{dt} = -k_b(n\,p) \tag{3.4}$$

where k_b is the bimolecular rate constant, and n and p are time dependent concentrations of negative and positive polarons. In the case of films this equation holds well, since the distribution of carriers in the active layer is not influenced by a built in field (no electrodes, no drift).

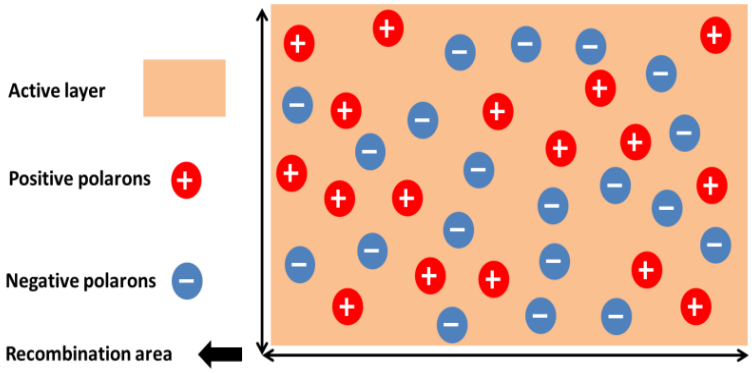

Figure 3.7: Schematic representation of charge carrier distribution in film.

Figure 3.7 is a schematic representation of charge carriers distribution in P3HT:PCBM active layer. In the case of films having ideal morphology one can expect about equal number of holes and electrons in the active layer as depicted in figure 3.7. So, in films it is easy to find the partner and to get recombined. This explains fast bimolecular recombination in P3HT:PCBM films.

$$\frac{dn}{dt} = -k_b n^2 \tag{3.5}$$

In the solar cell, the equation 3.5 is valid with a slight modification.

$$\frac{dn}{dt} = -k_b n_{eff}^2 \tag{3.6}$$

where n_{eff} = r.n, r<1

$$\frac{dn}{dt} = -k_b r^2 n^2 \tag{3.7}$$

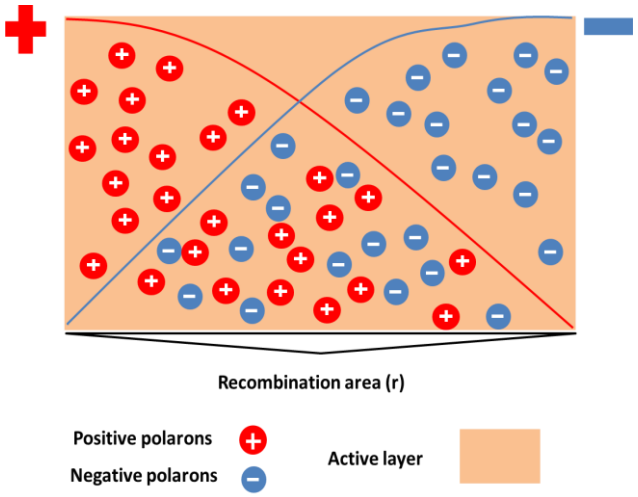

Figure 3.8: Schematic representation of the charge carrier distribution in solar cells.

Equation 3.7 represents the recombination rate equation for solar cell devices. The effective area available for recombination is less compared to that available in films. Because of the

presence of electrodes, both diffusion and drift come into play. This reduces the total number of electrons and holes available for recombination and hence affects the recombination rate k_b. This could explain why the carriers in the solar cell recombine slower than those in the films. An additional influence should come from the charge generation capacity of the electron transport layers (ETL) and hole transport layers (HTL). Holes in the HTL and electrons in the ETL are definitely not available for recombination. The slower recombination after 10µs could be also due to fast lateral movements of positive polarons within the highly conductive (h.c.) PEDOT:PSS layer, whereupon they are not available for recombination. The conductivity difference of PEDOT:PSS layer used in the solar cell and structure of their (normal architecture) device might be the reasons why Shuttle et al. observed a comparable decay dynamics for both film and device. The effects of h.c.-PEDOT:PSS on charge carrier dynamics are discussed in the following session.

3.3.5 Lateral diffusion of polarons in P3HT:PCBM solar cells induced by high-conductivity PEDOT

In building integrated photovoltaics (BIPV), device transparency is a must, so the metallic back contact has been substituted by thin silver stripes. To enable efficient extraction by the silver stripes, special high conductivity PEDOTs (h.c.-PEDOTs) are used.[32,67] Since parallel to the layer planes in the device structure (shown in figure 2.7), there is no electric field available, the last step of carrier extraction inside the h.c.-PEDOT phase towards the silver contacts must proceed by diffusion.

For the sake of optimizing device architectures towards low recombination losses, it is necessary to understand the consequences of lateral diffusion in h.c.-PEDOT on the processes occurring in the active layer. Here, a comparative study of photovoltaic devices comprised of P3HT:PCBM, a well-studied active layer, and a hole selective contact made of several h.c.-PEDOTs is presented. Transient absorption (TA) spectroscopy is used as probing technique, because it is selectively sensitive to charges in the P3HT phase.[130] Using pulsed and focused irradiation of solar cells with small active areas, it is possible to follow the lateral diffusion of holes in PEDOT – and their back equilibration into P3HT – in real time. The results might pave the way to reduce recombination losses of OPV in BIPV.

If PEDOT is present, then the decay traces are dominated by a fast initial phase of around 10 µs lifetime which is independent of intensity, followed by an intensity dependent part which has similar decay times as the decay observed without PEDOT present. It is therefore clear

that PEDOT can influence the recombination behaviour of charges in P3HT. Since figure 3.9 shows that the PEDOT-induced process is intensity independent, it cannot be recombination-related; one can therefore exclude a different morphology in the active layer, induced by PEDOT and leading to fast recombination. Rather, a non-recombinative loss path for P3HT polarons was assumed, removing them from the spectral (probing at 970 nm) or geometrical (1mm probe spot) observation window on a 10 µs time scale. The former process could be caused by vertical diffusion into the PEDOT, the latter one by lateral diffusion out towards the edges of the active device area, where the intensity of the Gaussian probe pulse is near zero. To distinguish between these two effects, the pump-probe kinetics of P3HT polarons varying the geometrical overlap of pump and probe beams were recorded (Scheme 1). The result is shown in Fig.3.10 on a linear time scale.

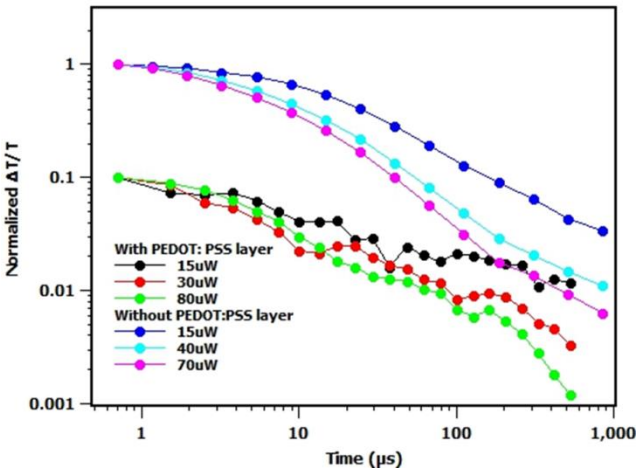

Figure 3.9: Normalized transient absorption traces for P3HT:PCBM film without PEDOT:PSS layer and for the whole device having PEDOT:PSS layer. Note that layer traces referring to samples 'with PEDOT:PSS' are normalized to 0.1 for the sake of clarity, corresponding to an arbitrary shift in the logarithmic ordinate by one decade..

When pump and probe pulses overlap perfectly, then a sharp initial polaron decay was observed, followed by a slower decay, both observation being in agreement with figure 3.9. If the pump pulse overlaps only partially (pump and probe are separated by a distance of 0.5 times the probe diameter) with the probe pulse (blue curve in figure 3.10), the same qualitative behaviour was observed, however the fast initial decay starts from a lower value. If there is no overlap (green curve), then the situation changes drastically: instead of a fast decay, a fast rise observed. The second important observation is that after 50 µs, all curves collapse into one unitary decay trace. Hence the intensity dependent slow part of the polaron decay, which is caused by bimolecular polaron recombination in the active phase, does not depend on the geometrical position of the pump pulse. So, the bimolecular recombination at

the position of the probe pulse does not depend on where the charges have been created. This notion supports the picture of fast lateral diffusion mediated by PEDOT, allowing the polarons to spread over the whole active area at their disposal. On a qualitative level, this picture is confirmed by figure 3.10b, showing that the dynamics of the fast polaron decay at full pump-probe overlap matches the dynamics of polaron build up when pump and probe are distant.

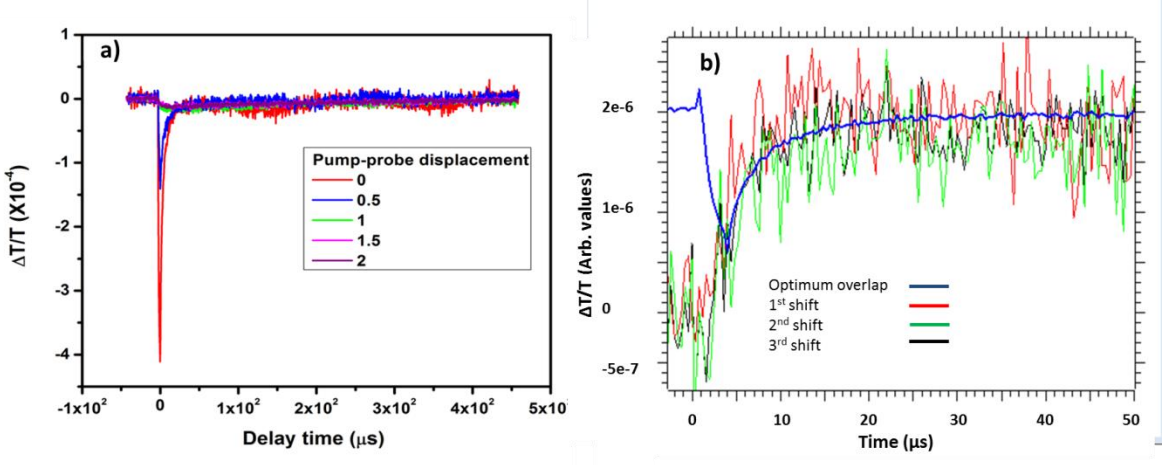

Figure 3.10: Detecting lateral diffusion of charge carriers: a) Microsecond transient absorption decay traces obtained by varying pump probe overlap; legend represents the pump and probe displacements measured in probe beam diameters. b) Comparing the dynamics observed with zero displacement between pump and probe beams to polaron build up when pump and probe are displaced relative to each other.

Observing a TA signal without pump and probe overlap, it is necessary to prove the nature of the absorbing states, because measurements at one single probe wavelength of 970 nm do not permit to demonstrate that P3HT polarons cause the TA transient when pump and probe do not overlap. To this end, transient absorption spectra under modulated CW irradiation at 220 Hz for samples with and without PEDOT were recorded (figure 3.11).

In the presence of PEDOT, the typical P3HT polaron spectrum, peaking at around 1000 nm is obtained both with and without pump-probe overlap, while in the absence of PEDOT, the TA spectrum is virtually zero, even after extensive y-stretching not showing any band that can be associated with the P3HT polaron. And also note that the ΔOD value at 1000nm is more than 2 times higher without PEDOT. This also indicates that part of the generated polarons are immediately transferred to the PEDOT phase and are then not absorbing at around 1000 nm. This set of measurements confirms the picture of PEDOT mediating the lateral diffusion of polarons in P3HT.

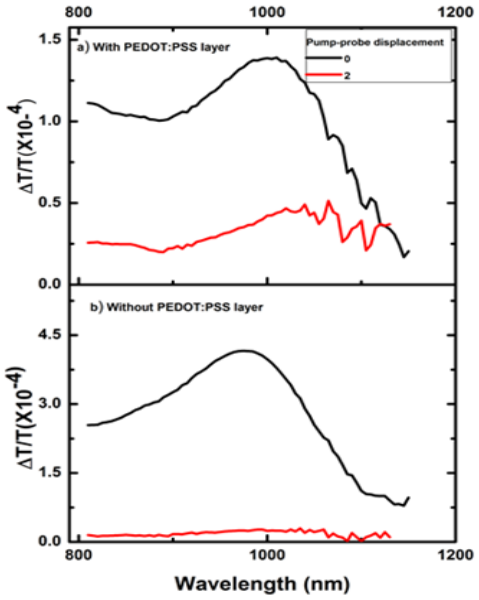

Figure 3.11: Photo induced absorption (PIA) spectra with full overlap between pump and probe (black, represented as 0) and pump and probe are separated by a distance of 2 times the probe diameter (red curves, represented as 2) of (a)P3HT:PCBM solar cell having h.c PEDOT:PSS layer and of (b) P3HT:PCBM film.

The main processes involved to justify lateral polaron diffusion, in agreement with all experimental observations, are summarized as follows: the pump pulse generates charge pairs at the donor-acceptor interface which in the case of a bulk heterojunction (BHJ) is not a sharp 2D interface parallel to the substrate, but distributed throughout the active layer; hence, charge generation is usually modelled by a "virtual semiconductor", substituting the 2-phase BHJ by a homogeneous single active material with effective band energies. Charge generation in this model is then governed by Lambert-Beer's law, generating most of the carrier pairs within a 50 nm distance from the PEDOT layer (under the illumination conditions of the experiment, that is, 532 nm). Under the built-in field, the holes drift towards the PEDOT layer but the resulting concentration gradient counteracts this drift. Assuming typical P3HT hole mobilities, the stationary state between drift and diffusion is installed in less than a microsecond, and hence on a time scale shorter than our experimental resolution. Due to the high doping concentration in h.c.-PEDOT, there will be no electrical fields inside PEDOT even in the presence of excess holes from pulsed photo-generation. It is therefore possible using standard drift-diffusion software like PC1D, to calculate the expected equilibrium distribution between h.c.-PEDOT and P3HT, which will depend on the effective field that P3HT holes experience close to the PEDOT interface, and on the difference of the respective polaron energies inside PEDOT and P3HT, respectively.

3.4 Summary

Transient absorption and transient photovoltage studies were performed on pristine P3HT:PCBM films and solar cells in order to understand the photo-induced processes. An intensity dependent polaron yield and singlet yield is observed from picosecond TAS on films. The polaron generation yield increased from 50% to 62% and the singlet yield went down from 45% to 35% at 1ps when the intensity of pump pulses increased from 10nJ to 30nJ. Microsecond TAS on films shows a bimolecular recombination dynamics of charge carriers. Open circuit and short circuit TAS reveal that the extraction is two orders of magnitude faster than recombination in pristine P3HT:PCBM solar cells. TPV and TAS comparison studies under solar cells operating conditions with background illumination show the same kinetics for both traces suggesting that a simple TPV trace can be used for calculating polaron dynamics rather than complicated TAS as previously demonstrated by Shuttle et al. The same study also demonstrated that in P3HT:PCBM solar cells the carrier lifetime is strongly governed by the charge carrier density and the open circuit voltage.

The comparison between the recombination dynamics of P3HT:PCBM films and solar cells shows that the film exhibits a faster decay than device. This can be due to reduced recombination area because of the presence of electrodes in the case of devices. The influence of highly conductive PEDOT:PSS layer on the charge carrier dynamics was also studied. The presence of h.c. PEDOT facilitates lateral movements of charge carriers along with vertical diffusion. This causes a fast intensity-independent initial decay and slow intensity dependent final decay of the charge carriers, as shown in figure 3.9. It is also observed that all traces decay into one unitary trace, which suggests that the bimolecular recombination at the position of the probe pulse does not depend on where the charges have been created. This notion supports the picture of fast lateral diffusion mediated by PEDOT, allowing the polarons to spread over the whole active area at their disposal.

Chapter 4

The effect of oxygen induced degradation in P3HT and Si-PCPDTBT solar cells[e]

Due to light weight, transparency and flexibility, organic photovoltaics (OPV) are ideal for building integration. As this application requires solar cell lifetime of more than twenty years and oxygen ingress cannot be avoided at competitive cost on this time scale, OPV modules must be intrinsically stabilized against photo-oxidation. To this end, the mechanism of rapid performance loss of OSC due to oxygen-induced degradation must be understood. In this chapter, transient absorption experiments and electrical studies in P3HT:PCBM and Si-PCPDTBT:PCBM thin films and solar cells after controlled photo-oxidation are explained, studying charge carrier dynamics on the femtosecond to millisecond time scale. Before any appreciable changes in absorption occurs, photo-oxidation leads to a strong reduction in the recombination and extraction of charge carriers due to a decrease of charge carrier mobility and an increase in the background carrier concentration, whereas the generation of charge carriers is not affected. Extraction is shown to be retarded even more strongly than recombination, possibly by a reduction of the extraction field by the background carriers. Overall, the recombination yield is increased with degradation, explaining the strong performance loss already at low degradation levels.

[e]*Parts of this chapter are published in* ***S. Karuthedath****, T. Sauermann, H.-J. Egelhaaf, R. Wannemacher, C. J. Brabec, L. Lüer,* ***Jour. Mater. Chem. A****,* ***3****, 3399, 2015 and in M. Stephen,* ***S. Karuthedath****, T. Sauermann, K. Genevičius, G. Juška,* ***Proc. of SPIE Vol. 9184,*** *918424, 2014.*

4.1 Introduction

In poly-3-hexylthiophene (P3HT) films, it has been shown that irradiation in oxygen atmosphere causes irreversible bleaching of the ground state absorption, attributed to oxygen induced chain scission and formation of stable photoproducts, probably in a radical chain reaction.[113] In OSCs based on P3HT and[6,6]-phenylC_{61}-butyric acid methyl ester (PCBM), oxygen-induced degradation causing 2% ground state absorption loss leads to a 70% reduction in the short circuit current.[67] Therefore, the observed strong effect on J_{SC} cannot be attributed to a mere loss of initially excited states due to absorption loss. Considering photoelectric conversion as a sequence of the elementary steps (i) absorption, (ii) exciton diffusion to the bulk heterojunction, (iii) charge formation by exciton dissociation, and (iv) charge extraction, oxygen-induced degradation is therefore expected to cause a strong reduction in at least one of the latter three processes.

With respect to the second step, it has been shown recently that at elevated levels of degradation (5-20% of optical density loss), an ultrafast exciton quenching channel is active that might explain at least partially the reduction of the overall photovoltaic yield.[68] However, the extent of exciton quenching is by far not strong enough to account for the drastic loss of short circuit current; moreover, it is not clear whether this process plays any role at lower levels of degradation.

In order to shed more light on the effect of photo-oxidation on the two elementary steps involving charge carriers, in this chapter transient absorption (TA) study of photo-induced charges in thin films and OSCs, comprising two prominent active materials, namely the blends of P3HT:PCBM and blends of low-band gap copolymer poly[(4,4 0-bis (2-ethylhexyl) dithieno[3,2-b:2 0 ,3 0-d]silole)-2,6-diyl-alt-(4,7-bis(2-thienyl)-2,1,3benzothiadiazole)-5,5 0 -diyl] (Si-PCPDTBT) with PCBM are studied. Transient photo-induced charge extraction by linearly increasing voltage (photo-CELIV) was also used to measure the electrical parameters of the devices and to confirm the transient absorption results.

4.2 Experimental Section

Inverted organic solar cells were made in nitrogen atmosphere and films of active layer were realized by doctor blading. The details of the sample preparation and degradation steps are described in Chapter 2. UV-vis spectra of films and current-voltage characteristics were measured at each stage of degradation to monitor the optical density (OD) loss and current

density (J_{sc}) loss respectively. Femtosecond and microsecond to millisecond transient absorption (TAS) were performed in a cryostat (Oxford OPTISTAT) under dynamic vacuum (~10^{-5}mbar). All solar cells and films were again annealed under vacuum at 140°C and 130°C, respectively, for 5 minutes in cryostat equipped with a heater, before each TAS experiment, in order to make sure the reversible oxygen doping is removed and only irreversible degradation effects are measured. The details of experimental arrangements are given in Chapter 2.

The absorption maxima of positive polarons in P3HT, and Si-PCPDTBT are at 980 nm and1300 nm, respectively.[51,137] A high power 970 nm LED was used as probe source where both materials show sufficiently large polaron absorption cross-sections with negligible superposition of other long-lived photo-excited states. On a microsecond time scale, the contribution of singlet exciton absorption, which is known to overlap strongly with polaron absorption at 970 nm can be safely neglected because excitons, even if they do not reach an interface, are quenched intrinsically by radiative and non-radiative processes on a few nanosecond time scale.[51] This notion holds also for delayed exciton regeneration due to charge recombination: due to the short lifetime of excitons, the stationary exciton concentration caused by microsecond charge recombination will be negligible. Therefore, one can consider the ΔA (970 nm) time traces that will be discussed in the remainder of this thesis, as proportional to the concentration of polarons (positive or negative) in the P3HT, Si-PCPDTBT phases, respectively.

For photo-CELIV measurements of P3HT:PCBM solar cells, the devices were excited at absorption maxima with a 0.1mJ laser pulsed at 3-5 ns (EKSPLA -NT 340). The sample was negatively biased by applying a triangle voltage pulse from function generator (Tektronix AFG 3011) and corresponding current transients were sampled and recorded using an oscilloscope (Tektronix DPO 4054B). The RC time was determined to be approximately 50ns calculated from the geometrical capacitance. An electrical setup is used to maintain open circuit condition before the application of triangle pulse and hence to avoid carrier extraction during the delay time. The photo-CELIV transients were recorded for a range of delay times from 2-100μs for each sample and the mobility is observed to be more or less constant within this time range and the delay time was internally controlled by the function generator.[131] All experimental details are illustrated in Chapter 2.

4.3 Results

Figure 4.1a and c shows the J-V characteristics of studied solar cells after specified times of irradiation by a sun simulator under dry synthetic air. To relate the electrical performance to the optical absorption of the devices, UV-Vis spectra of films were measured (figures 4.1b, and d). After 240 minutes of irradiation, the J_{SC} is irreversibly reduced to 35% (25%) of the original value, while the loss in OD is only around 2% (3.5%) for P3HT:PCBM and Si-PCPDTBT:PCBM, respectively.

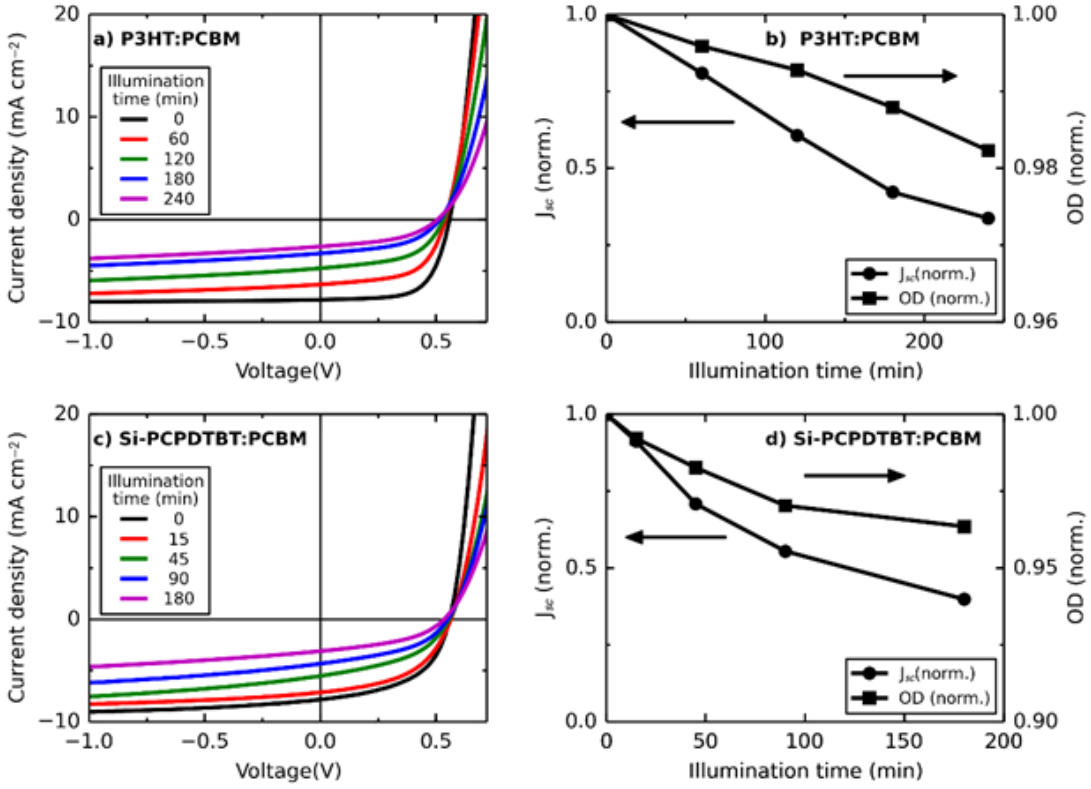

Figure 4.1: Current density–voltage (J–V) characteristics (1st column) and a comparison of optical density (OD) losses and electrical losses (second column) for P3HT:PCBM (panels a and b) and for Si-PCPDTBT:PCBM (panels c and d), during degradation of the devices by irradiation with the light of a sun simulator under synthetic air.

The vast majority of the electrical performance loss of the solar cells can therefore not be ascribed to a loss in optical absorption, in agreement with earlier findings.[67,113] Oxygen induced photo-degradation obviously affects mainly the internal quantum efficiency (IQE) of the solar cells. Transient absorption spectroscopy in films and OSCs was performed to single out the factors that contribute to the loss of IQE. This chapter first analyses picosecond transient spectra to evaluate the effect of degradation on charge carrier formation and then turn to microsecond transients to elucidate the effect of degradation on charge carrier

recombination and extraction followed by photo-induced charge extraction by linearly increasing voltage (photo-CELIV) studies to measure the charge carrier mobilities.

4.3.1 Transient absorption spectroscopy

In OPV, charge carrier generation involves exciton diffusion and dissociation at the D/A interface, a process known to occur on a femtosecond to hundreds of picoseconds time scale.[51] Depending on the material and morphology, charge carrier separation, occurring on a picosecond time scale, can be opposed by geminate recombination.[128]In order to study whether photo-oxidation has an influence on exciton diffusion and/or geminate recombination, femtosecond transient absorption (TA) spectroscopy was performed. Figures 4.2a and 4.2d, shows TA spectra of a pristine P3HT:PCBM and Si-PCPDTBT:PCBM film, taken at low enough pump intensity so that only those processes are observed that also occur under CW solar irradiation. In agreement with previous reports, a photo-induced absorption (PA) band of polarons at ~1.25 eV (~1.0 eV), a very short lived band at ~1eV (~0.85 eV), assigned to singlet excitons, and a transient photo-bleaching (PB) band around ~2.3 eV (~1.7 eV) were found for P3HT:PCBM and Si-PCPDTBT:PCBM respectively.[51,128,137]

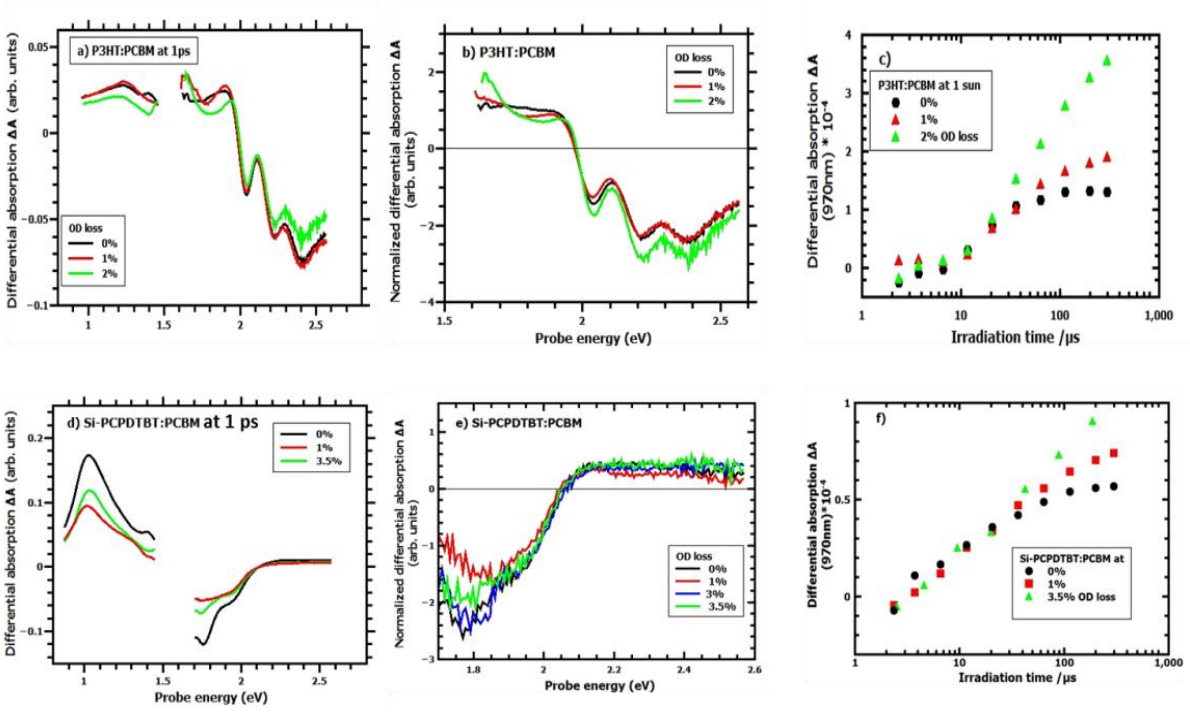

Figure 4.2: Charge generation in P3HT:PCBM and Si-PCPDTBT:PCBM as a function of photo-oxidation. (a,d) Femtosecond transient absorption spectra upon pumping with 150fs pump pulses at 387nm. (b,e) Ground state bleach part after 400ps normalized to polaron band of corresponding materials. (c,f) Charge density increase (measured at 970nm) upon switching on irradiation at ~1 sun and ~0.1suns for P3HT and Si-PCPDTBT, respectively at different degradation levels.

Figure 4.2a and d, shows the picosecond TA spectra and figure 4.2b and e shows the PB regions at 400ps at different degradation levels, representative of the amount of charge

carriers that survive geminate recombination for P3HT and Si-PCPDTBT respectively. It is important to note that the presence of PB in figure 4.2 is insensitive to the type of excitation: a conjugated segment of polymer which is excited cannot contribute to ground state absorption, irrespective of whether the excitation is neutral or charged. Since both, singlets and polarons share the same PB, it is possible to quantitatively obtain the time-resolved exciton and polaron yields. The ground state bleach does not seem to have changed much after 400ps which is an indication of unchanged charge generation yield. Hence, at degradation levels relevant for device operation, neither exciton diffusion nor geminate recombination is significantly influenced by photooxidation. This finding, obtained by femtosecond spectroscopy, is confirmed by charge dynamics during illumination with very weak microsecond pulses at 1 absorbed sun for P3HT:PCBM and 0.1 absorbed suns for Si-PCPDTBT:PCBM, which are displayed in figure 4.2c and f respectively. It is found that the rise of polaron absorption during the first microseconds of irradiation is independent of degradation.

A simplified kinetic model for charge carrier density in the active layer of a device of thickness *d*, applying idealized assumptions such as homogeneous medium, second order recombination, and constant built-in field $E_b$is given by,

$$\frac{dn}{dt} = G - k_L \cdot n \cdot n - \mu \cdot n \cdot \frac{E_{bi}}{d} \tag{4.1}$$

where μ is the effective charge carrier mobility, *G* is the photo-induced generation of extractable charge carriers, and k_L is the bimolecular charge recombination coefficient, assuming Langevin recombination.

$$k_L = 2 \cdot e \cdot \mu_{eff} \cdot f_{LV}/(\varepsilon \cdot \varepsilon_0) \tag{4.2}$$

Herein, $\mu_{eff} = \mu_e + \mu_h$is the sum of the mobilities for positive and negative charges, respectively, ε is the relative dielectric constant, ε_0 is the dielectric constant in vacuum, and f_{LV} accounts for sub-Langevin recombination, as often observed in BHJ active layers.

According to equation4.1, we can neglect the recombination term at early times while charge concentration is still low, so the initial rise of charge density is a measure of the generation of extractable carriers for both P3HT:PCBM and Si-PCPDTBT:PCBM solar cells.

In figure 4.3, decay traces of the polaron absorption bands are shown on a micro- to millisecond time scale for the same films as in figure 4.2 upon light off, after a long enough irradiation period to reach stationary charge carrier concentrations at the respective degradation levels (between 5 and 83 ms). According to equation 4.1, these decay curves allow to specifically obtain recombination information, since both extraction and generation are absent, due to the absence of electrodes and irradiation, respectively. In order to visualize details of the decay at various times and signal levels in a single graph, a double logarithmic representation of the data was chosen. In pristine P3HT:PCBM (figure 4.3a), a strong intensity dependence of the decay curves is found: while the starting concentrations at t=1µs cover nearly an order of magnitude, after 1 ms decay time all curves are within a factor of 2. This behaviour is indicative of a pure bimolecular reaction with equal concentrations of positive and negative carriers, as expected if only photo-induced carriers are present. When this condition is met, equation 4.1 holds, and the time integral evaluates to intensity independent, hyperbolic dependence of concentration on time for long times. This behaviour is experimentally confirmed in figure 4.3a, in agreement with previous reports on pristine P3HT:PCBM.[125,130]

Photo-degradation of the P3HT:PCBM films causes a drastic change of the charge recombination dynamics, compare figures 4.3a and 4.3b. First, note an overall reduction of the recombination rate: at 1 sun, it takes 200 µs for the 2% degraded sample to lose half of the initial carrier concentration while in the pristine case, as much as 5/6 of the initial carriers are lost at the same time. Second, the long-term behaviour is entirely different for degraded P3HT:PCBM: there is no asymptotic straight line as in the case of the pristine sample, the curves rather tend towards infinite slope, which is typical for the double logarithmic representation of an (stretched) exponential function. Moreover, the curves in figure 4.3b do not collapse into a unitary, intensity independent long-time behaviour as in figure 4.3a. Both observations are in agreement with a reduction of the reaction order towards pseudo-first order, which is usually caused by excess concentrations of either positive or negative carriers. Irreversible degradation in Si-PCPDTBT:PCBM films leads to a similar behaviour as in P3HT:PCBM, namely, an overall reduction of the recombination rate and a transition towards a lower recombination order. However, note that even in the pristine case, Si-PCPDTBT:PCBM does not exhibit perfect second order behaviour, that is, the single decay curves at different intensities do not collapse into a unitary, intensity-independent straight line for long times.

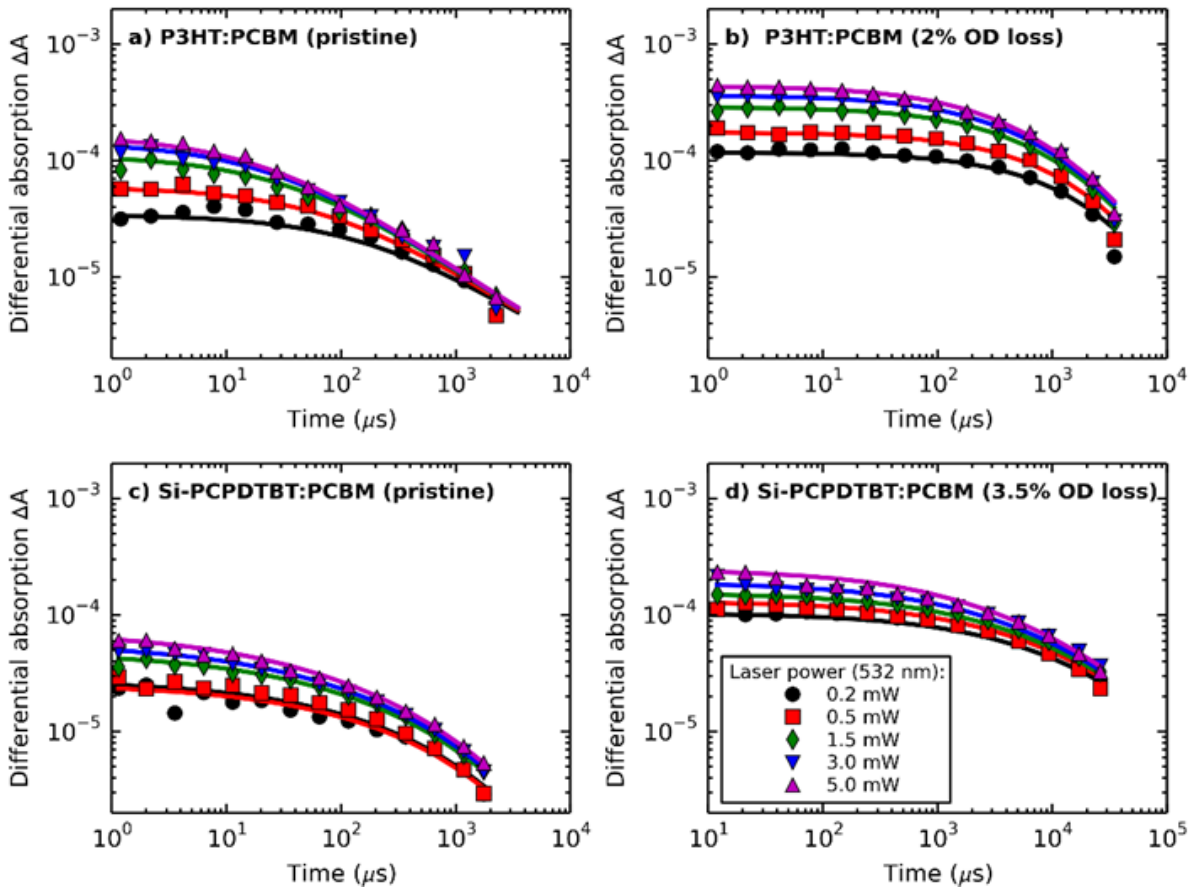

Figure 4.3: Charge transients in polymer:PCBM films at different light intensities at 970 nm probing wavelength, upon termination of illumination. Panels (a) and (b) show transients of P3HT:PCBM at degradation levels of 0% and 2%, respectively. Panels (c) and (d) are transients of Si- PCPDTBT:PCBM at degradation levels of 0% and 3.5%, respectively. For panels (a–c), the samples were illuminated for 5.5 ms before light-off, at a repetition rate of 91 Hz; for panel (d), the illumination period was 83.3 ms at 6 Hz repetition rate. The intensity of the laser (532 nm) during light-on is given in the legend.

4.3.2 Photo-CELIV

Photo-induced charge carrier extraction by linearly increasing voltage (photo-CELIV) has been widely used to study charge transport in organic semi-conductors following pioneering work by Juška et al.[65,71,138] CELIV is one of the most direct methods to measure the dispersive charge carrier transport in organic semiconductors.[65] The charge carrier mobility can be estimated by the time at which maximum current can be extracted (t_{max}). Under conditions when $\Delta j \leq j_0$, the mobility μ is obtained as:

$$\mu = \frac{2d^2}{3At_{max}^2} \tag{4.3}$$

where, d - thickness of sample, A - applied voltage ramp and t_{max}-time of maximum carrier extraction.

Figure 4.4a shows the variation of CELIV transients in the dark with respect to degradation time with a ramp rate of 10^5V/s. CELIV measurements in the dark reveal an increasing concentration of equilibrium carriers and an increase in the t_{max}as degradation proceeds. Figure 4.4b represents the corresponding transients of photo-induced carriers with a ramp rate of 10^4V/s. As in the dark CELIV, here also the t_{max} is increasing, which is a representative of decrease in the mobility according to equation 4.3. The dynamics become more dispersive upon degradation which also supports the picture of reduced mobility. The mobility obtained from photo-CELIV could be claimed to be the effective mobility of both charge carriers, however, the characteristic t_{max} is said to be mainly influenced by faster carrier. This becomes more significant when the carrier mobilities extremely differ from each other. The main advantage of CELIV is that one can measure the carrier mobility and carrier density independently. Figure 4.4c shows the extractable equilibrium and photo-generated carriers with respect to delay times with a ramp rate of $5*10^3$ V/s for the pristine cell. The charge carrier density can be obtained from integrating the CELIV transients in dark and under illumination, respectively.

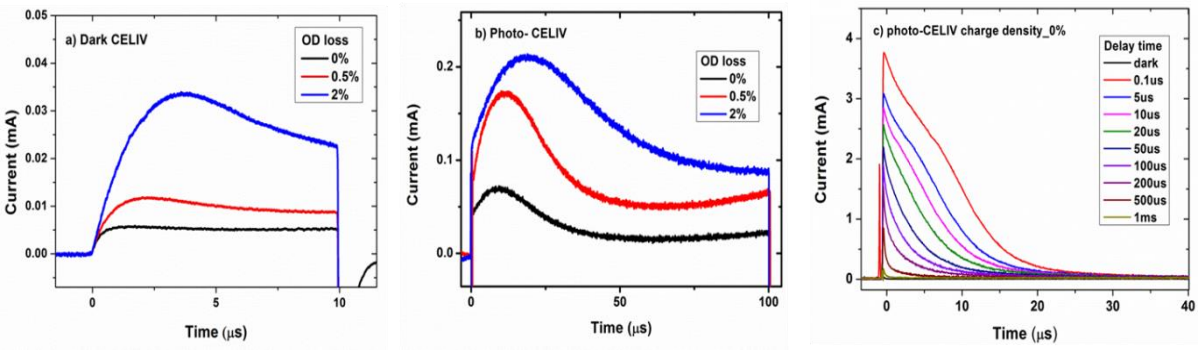

Figure 4.4: a) Dark CELIV transients at different levels of degradation at 1V applied voltage with a ramp rate 10^5V/s. b) Corresponding photo-CELIV transients with a ramp rate 10^4V/s for mobility measurements and carrier density measurements. c) Photo-CELIV transients with respect to delay time without any offset for the pristine sample with 1V pulse and ramp rate of $5*10^3$ V/s for pristine sample.

In conclusion, the main effects of oxygen-induced degradation on both, P3HT:PCBM and Si-PCPDTBT:PCBM films, are a strong retardation of charge recombination and a concomitant transition from reaction orders close to two towards reaction orders close to unity. The electrical characterization reveals an increase in the extraction time upon degradation. These results are in accordance with the results presented by Deibel et al.[139] They are clearly in contradiction to any defect enhanced recombination rate as the reason for the degradation of device performance.[140]

4.4 Discussion

4.4.1 Transient absorption spectroscopy

In the following section, the qualitative observations of the previous section by a quantitative kinetic model are described for TAS. Since the measurements in figures 4.2 and 4.3 have been performed in films without charge extraction layers and electrodes, recombination via device related shunt resistances and charge extraction need not be considered. The rate equation describing charge carrier dynamics thus becomes;

$$\frac{dn}{dt} = G - k_L(t) \cdot [n(t) + c_b] \cdot n(t) \tag{4.4}$$

Equation 4.4 refines the simple model as represented in equation4.1 in two aspects. First, it allow for a population of mobile background carriers of concentration c_b, which arises from degradation and might result from degradation-induced trap states, most likely for electrons. Second, we consider the fact that charge carrier mobility in P3HT:PCBM depends on the occupied density of states and therefore, in time-resolved experiments, implicitly also on time.[130,141] This causes the bimolecular recombination coefficient to be time-dependent, which is usually taken into account by defining

$$k_L(t) = k_L^0 \cdot (t/1\mu s)^{\gamma} \tag{4.5}$$

where k_L^0 is the value of the bimolecular recombination coefficient (in cm^3/s) at t = 1 µs, and γ is the dispersive parameter.[77,125,142]Note that generally, care must be taken when extracting device relevant information from decay curves: once the carrier population has decayed far below the steady state value at 1 sun, n_{ss}(1 sun), mobilities and hence the observed recombination times will be different from those under 1 sun CW illumination. For this reason, the value for k_r^0 at t = 1µs is reported and discussed, when the remaining carrier population is still close to n_{ss}. Inserting the Beer-Lambert law, $A = \sigma cd$, into equation 4.4, yields;

$$\frac{d\Delta A}{dt} = \tilde{G} - \tilde{k}_L(t) \cdot (\Delta A + A_b) \cdot \Delta A \tag{4.6}$$

where $\tilde{G} = \sigma dG$, $\tilde{k}_L(t) = k_L(t)/(\sigma d)$. Herein, $\sigma \approx 1\text{x}10^{-16}\text{cm}^2$ ($\sigma \approx 3\text{x}10^{-17}\text{cm}^2$) are the absorption cross-sections of polarons in the P3HT (Si-PCPDTBT) phase at 970 nm, d=250 nm is the film thickness, and A_b is the absorption of the background carriers of concentration c_b. Equation4.6 can be directly used to fit the transient absorption traces in figures 4.3 and 4.4.

Fitting equation 4.6 to the rising curves after switching on the illumination in figure 4.3, degradation-dependent generation parameter $\tilde{G}$ was obtained.Dividing this parameter by the incident photon flux give the polaron yield before non-geminate recombination (per absorbed photon). For P3HT:PCBM, a polaron yield between 0.6 and 0.7 was found, not significantly depending on the degradation level (black symbols in figure 4.5a). An analogous analysis for Si-PCPDTBT (figure 4.3f) was not possible because of the time resolution limit of our microsecond TA spectrometer. However, picosecond TA data, available for both P3HT:PCBM and Si-PCPDTBT, confirm that there is no significant change of the polaron yield with degradation (see red and green symbols in figure 4.5a).

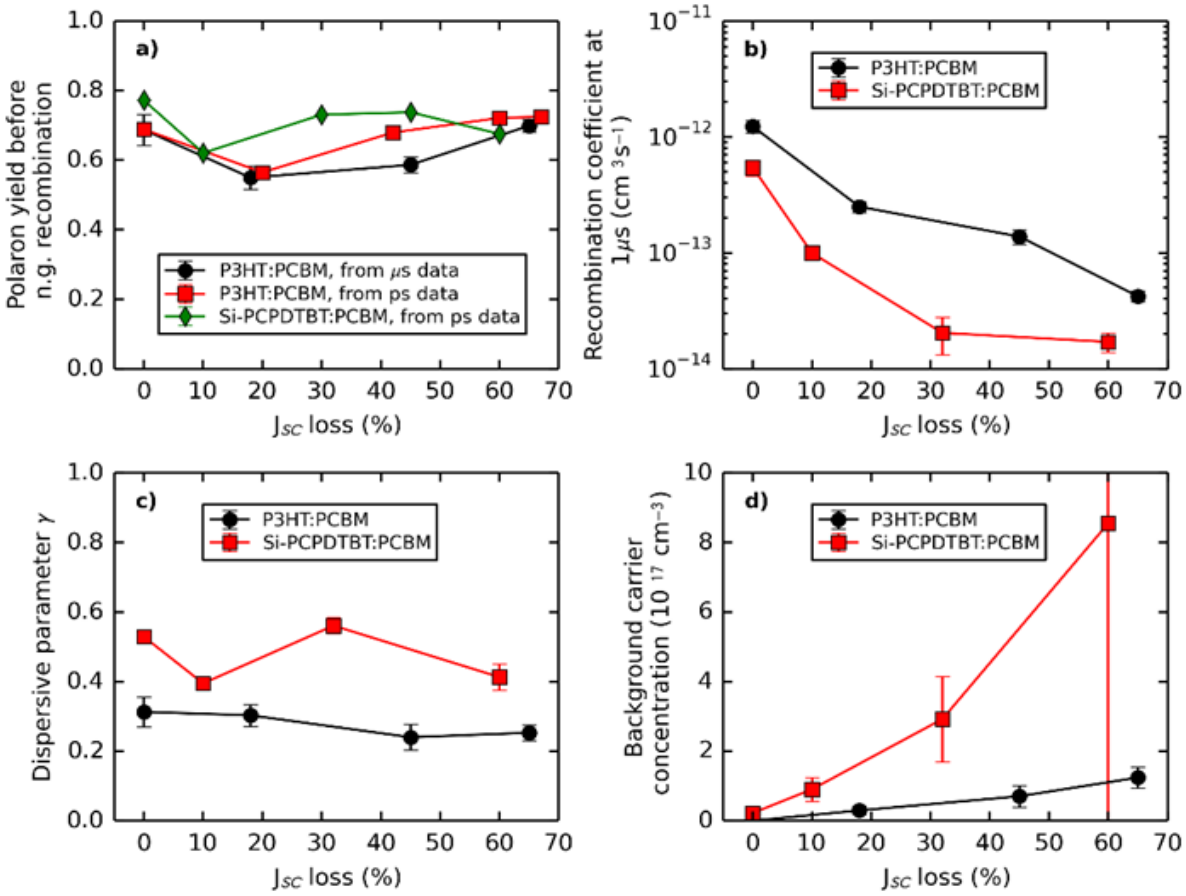

Figure 4.5: Fitting parameters from fitting of the curves in Fig. 4.3 (panel a) and Fig. 4.4 (panels b–d) using eqn (5). (a) Polaron yield per absorbed photon before non-geminate recombination. Black symbols: absolute data for P3HT:PCBM from microsecond transients ; red symbols: relative data for P3HT:PCBM from femtosecond TA spectra, scaled such that pristine values coincide; blue symbols: absolute data for Si-PCPDTBT from a global analysis of the femtosecond spectra (see figure 4.4). (b) Bimolecular recombination coefficient at time t =1 µs, assuming a charge absorption cross-section of $1*10^{-16}$ cm^2 in P3HT and $3*10^{-17}$ cm^2 in Si-PCPDTBT. (c) The exponent of the time-dependent reaction coefficient in equation 4.5 (d) Background carrier concentration, assuming the same charge absorption cross-sections as in (b). Panel (d) has been obtained by fitting decay traces after pulsed irradiation under the conditions of figure 4.3.

Fitting the decay traces after termination of illumination (figure 4.3) one can set G = 0 in equation 4.6. As can be seen by inspecting the solid curves in figure 4.3, equation 4.6

describes very well the charge recombination in both P3HT:PCBM and Si-PCPDTBT:PCBM, at all degradation levels including the pristine case, with one single parameter set valid for all irradiation intensities (i.e., all fits given in figure 4.3 are *global* fits). Figure 4.5b displays the evolution of the recombination coefficient k_L^0 (given at t = 1µs), of the exponent γ, and of the background concentration c_b as a function of degradation, as obtained from the fits (panels b, c, and d, respectively). We find that photo-degradation strongly reduces k_L^0 for both, P3HT:PCBM and Si-PCPDTBT:PCBM. At a J_{sc} loss of around 60%, k_L^0 is reduced by more than an order of magnitude. According to Langevin's formula, this suggests a drastic reduction of charge carrier mobility µ already at early stages of degradation.[71]

Figure 4.5c displays the dispersiveness parameter γ. A value of γ = 0 would correspond to a time-independent mobility as implicitly assumed in equation 4.1, leading to a slope of -1 as asymptotic long-time behaviour in the double logarithmic graphs in figure 4.3. For γ > 0, the charge carrier mobility is reduced over time, and the asymptotic slope is between 0 and -1. The γ values displayed in figure 4.5c are around 0.25 and 0.5 for P3HT and Si-PCPDTBT, respectively. They do not show a clear evolution with degradation. Figure 4.5d shows the background carrier density, as obtained from the global fits after pulsed irradiation, which is more sensitive to background carriers than CW illumination. With increasing photo-degradation, a monotonous and strong increase of the background carrier concentration is obtained for both blends. The background carrier concentration in Si-PCPDTBT:PCBM is generally higher than in P3HT:PCBM, and is nonzero even in the pristine case.

For high background carrier densities and long times, $n << c_b$ and hence the square bracket in equation 4.4 becomes constant, reducing the effective recombination order to one. The long-time asymptote is therefore no longer a straight line as in the case of a bimolecular reaction, but a stretched exponential, the slope of which bends towards -∞ in a double logarithmic graph. This behaviour can be clearly observed in all panels of figure 4.3, except figure 4.4a, which reports the only experiment with negligible background carrier density.

Figure 4.6 presents TA decay curves of photo-induced charges in P3HT:PCBM solar cells of different degrees of degradation under open circuit (OC) and short circuit (SC) conditions, after pulsed irradiation. While under OC conditions, the charge decay is only governed by recombination, under SC conditions both recombination and extraction occur simultaneously. The comparison between OC and SC transients at different degradation levels yields

therefore information about the efficiency and the time scale of charge extraction. In the undegraded sample, the difference between the charge carrier transients at OC and SC conditions is significant, which is in accordance with the short circuit current density of J_{sc} = 7.5 mA/cm^2 observed in this device. When comparing the differently degraded samples, it is readily noticed that the charge carrier concentrations at about 1µs are approximately the same for all samples, irrespective of the extent of degradation, thus confirming that charge carrier formation is not significantly affected by degradation of the active layer.

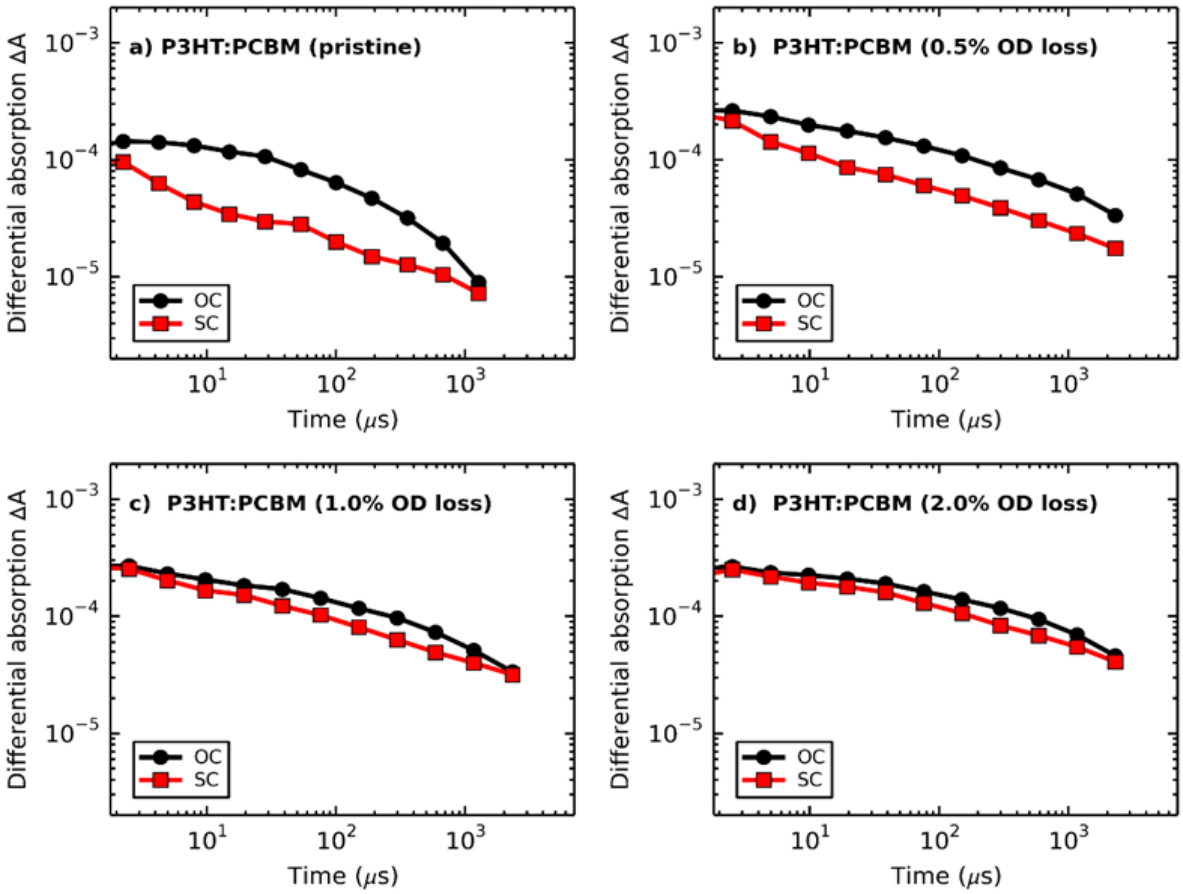

Figure 4.6: TA traces in P3HT:PCBM solar cells under open circuit (OC) and short circuit (SC) conditions, at various stages of photo-degradation, as given in the legends. Charge carriers were created by 300 ps pulses at 1.83 mJ pulse energy in order to achieve initial carrier densities similar to those in Fig. 3a and b; repetition rates were 91 Hz for panel a and 41 Hz for all other panels.

The TA traces measured at OC conditions clearly show that charge carrier recombination slows down considerably upon degradation of the devices and thus confirm the trend observed for the light modulation experiments in figure 4.4 in films. While in pristine samples half of the photo-induced charge carriers have recombined after about 60 µs, it takes several hundred µs to reach the same extent of charge carrier loss in the 2% degraded devices. Also charge carrier extraction becomes slower upon degradation, as obvious from

the traces measured at SC conditions. Actually, charge carrier extraction is even more affected than recombination. While 80% of the charge carriers have disappeared after less than 100 µs in the pristine sample, more than 50% of the charge carriers are still present after this time in the 2% degraded device. With increasing degradation, the difference between SC and OC measurements, which is significant in pristine cells, becomes very small after 2% of OD loss (figure 4.6): the maximum ratio of the transient absorption signals at OC and SC conditions is reached after 10 µs, 100 µs, and 300 µs for 0.5, 1, and 2% OD loss, respectively, thus covering about 2 orders of magnitude.

In summary, photo-oxidation of the active layer hardly affects the charge carrier generation rate, whereas both recombination and extraction are slowed down considerably. The difference between recombination and extraction rates disappears almost completely in heavily degraded devices, which explains the loss of J_{sc} with progressing degradation. In order to gain some more understanding whether this drastic reduction in extraction efficiency can be explained by the reduction of charge carrier mobility (figure 4.5b) or by the increase of background carrier concentration (figure 4.5d), calculations of the IQE as function of µ, c_b and the non-Langevin factor $f_{LV}$is presented in figure 4.7. The curves have been obtained by inserting equations 3 and 4 into equation 1 for dn/dt=0 (steady state) and then relating the rate of extraction to the rate of generation. Since equation 4 refers to Langevin (i.e., exclusively drift driven) recombination in homogeneous three-dimensional space, while, e.g., carrier transport in P3HT:PCBM has been proposed to be quasi - 2D, the results in figure 4.7 are to be considered as instructive approximations.[143] It is also important to highlight that the effective charge mobility μ_{eff} in equation 1b is microscopic, while typically charge carrier mobilities are measured macroscopically using techniques like, CELIV.[65] In BHJ materials, the presence of grain boundaries and limited percolation paths might reduce the macroscopic mobility against the microscopic one.

Consequently, extraction might be penalized against recombination. Therefore the curves in Figure 4.7 should be understood as upper limits for IQE at the given parameters. Solid curves refer to zero background carrier density and thus reflect the dependence of IQE on µ for a reaction order of two. Assuming a reasonable built-in field, it is found that the IQE for c_b= 0 drastically depends on the non-Langevin factor: for f_{LV} = 1, a mobility reduction from 10^{-3} to 10^{-4} cm^2/Vs suffices to bring down IQE from 23% to only 8%. On the other hand, if f_{LV} is 0.001 (recombination rate is 1/1000 of the one expected from Langevin kinetics), then IQE remains at 56% even for mobilities as low as 10^{-5} cm^2/Vs. We conclude that a mobility

reduction of more than an order of magnitude, as conjectured from figure 4.5b, significantly reduces IQE, as long as non-Langevin factors are close to unity. The presence of background carriers further reduces IQE, compare solid, dashed, and dotted curves of same colour, respectively.

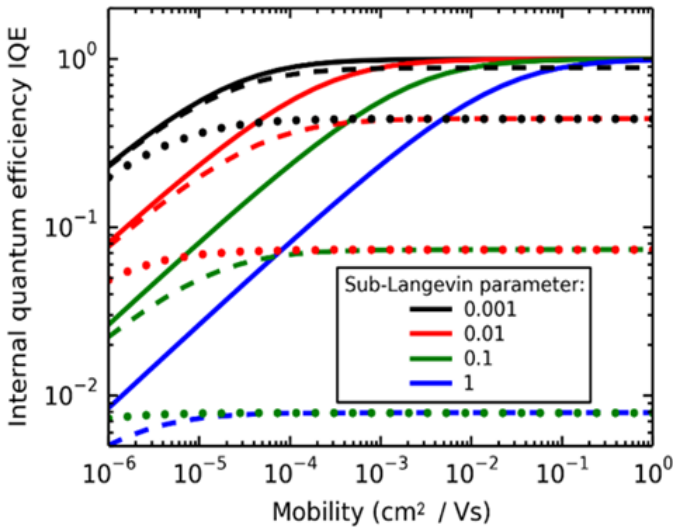

Figure 4.7: Simulation of internal quantum efficiency (IQE) as a function of effective charge carrier mobility for various values of the sub-Langevin parameter fLV, according to eqn (1a) and (4). The background carrier concentration c_b was set to 0, 10^{17} and 10^{18} cm^{-3} (solid, dashed and dotted curves, respectively). The fixed parameters were: 1 absorbed sun, built-in voltage 0.6 V, electrode spacing d =250 nm.

For P3HT with its low non-Langevin factor, background carrier concentrations up to $10^{17}cm^{-3}$ (as obtained in figure 4.5c) do not cause a significant lowering of IQE. The situation is different for Si-PCPDTBT, where background carrier densities close to $10^{18}cm^{-3}$ have been found. Since also the non-Langevin factor is lower in this material (f_{LV}=0.5 has been published as lower limit), background carriers can have a strong effect on IQE in this material.[144]In summary, figure 4.7 shows that in the case of Si-PCPDTBT reduced mobility and enhanced background carrier concentration easily account for the observed loss of J_{sc} upon photo-oxidation of the active layer (see figure 4.1). The situation is different for P3HT:PCBM. Because of the low non-Langevin factor in P3HT, even the combination of both effects in figure 4.7 does not fully explain the strong J_{SC} reduction observed in figure 4.2.[65] Therefore, it might be necessary to invoke additional degradation effects to account for the J_{sc} loss, e.g., the reduction of the built-in field. Such a reduction of the built-in field is indeed expected from the presence of mobile background carriers, as they form a space charge region shielding the built-in potential, similar to the case of reversible performance degradation in P3HT:PCBM.[67]

4.4.2 Photo-CELIV

The black curve in the figure 4.8a shows the equilibrium charge carrier density or dark carrier concentration and its changes upon degradation. This is calculated from CELIV curves at constant voltages and with optimized ramps for each sample to have a complete extraction without substantial injection. The dark CELIV measurements disclose that there is an increase in the carrier concentration upon photo oxidation. This increasing background (equilibrium) carrier concentration could be an effect of doping of active layer by oxygen. A detailed mechanism of oxygen doping is reported by Hintz *et.al* who states that the increase in electron traps triggered by oxygen effectively leads to an increase in the number of mobile holes.[113] The effect of such an increase in background concentration could be expected to be detrimental in device performance owing to the screening of field of the device as concluded from the transient absorption measurements.

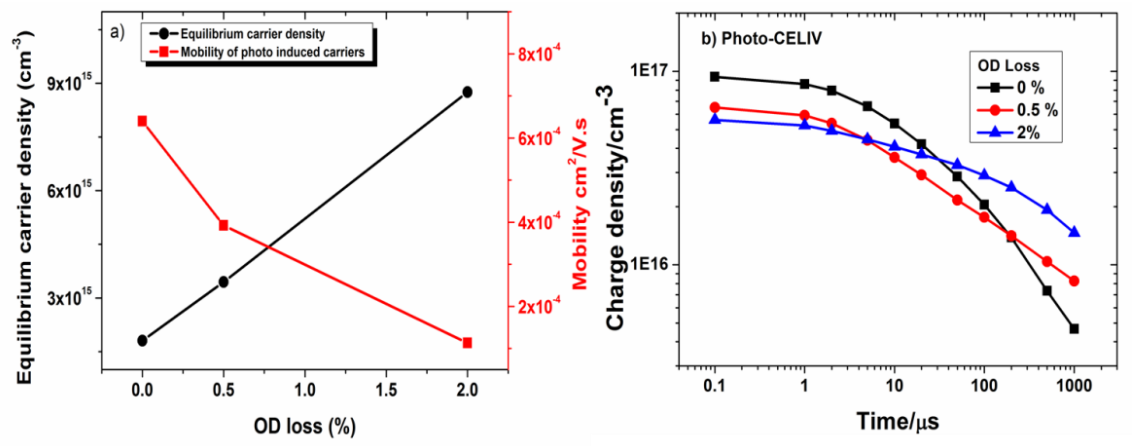

Figure 4.8: a)Equilibrium carrier density with degradation, from dark-CELIV transients with ramp rate 10^5V/S (black curves) and corresponding loss the mobility obtained from photo-CELIV with ramp rate 10^4V/S. b) Calculated extracted carriers at different delay time for different degradation levels.

The red curve in figure 4.8a shows the mobility values calculated from figure 4.4b for different degradation levels. The mobility values reduced by about 5times as the degradation proceed. This reduction of mobility could be a critical parameter for the observed deteriorating performance of the OSC device along with the influence of back ground carriers as observed from the transient absorption studies. These could be arising from a number of degradation effects including destruction of the ideal morphology and possible oxygen induced traps.

In regard to recombination studies, firstly charge carrier dynamics on a micro-second time scale was obtained from photo-CELIV measurements with long pulse times with a ramp rate of $5*10^3$V/s as shown in figure 4.4c as pristine case an example. Figure 4.8b shows the

results obtained for extracted charges with respect to delay times at different degradation levels. The plot reveals that while initial extracted charges are lesser for degraded samples they tend to be present inside the device for a longer time. The reduction in extracted carrier concentration at short delay times indicate a poorer charge transport as degradation proceeds and latter part of the curve corresponding to longer delays indicates a slower recombination in more degraded samples. The recombination being slowed down could be an effect of reduction of mobility and also a manifestation of the trapping effect.[32] With increasing degradation, more charges tend to be stuck in the device even after hundreds of microseconds. Thus the increase in number of traps can also have an influence on dynamics of interplay between these two mechanisms and at what time scale the latter one starts to predominate. These results are clearly in agreement with TAS results of P3HT:PCBM, where the extraction is severely deteriorated upon degradation as shown in figure 4.6.

4.5 Summary

The charge transients in films of P3HT:PCBM and Si-PCPDTBT:PCBM on a femtosecond to millisecond time scale and also photo-CELIV transients of the complete device as a function of photo-degradation were analysed in order to understand the reason for the electrical performance loss due to irreversible photo-oxidation which is one of the limiting factors of device lifetime in inverted OSC structures. For both polymer:PCBM blends, the charge generation rate hardly changes during photo-oxidation, suggesting that the charge separation coefficient is practically independent of the level of degradation. However, in P3HT:PCBM, oxygen induced degradation causes a strong reduction of the charge recombination coefficient, which formally corresponds to a reduction of charge carrier mobility. This is in stark contrast to inorganic semiconductors where often a defect-enhanced recombination rate is found.[140] Concomitantly, the order of charge carrier recombination is reduced from values of close to two in pristine P3HT:PCBM films to values close to unity already at degradation levels as low as 0.5% OD loss. The extraction rate of charge carriers is even more seriously reduced by photo-degradation than expected from the mobility changes calculated from the recombination term, which leads to the loss of short circuit current in degraded devices. While the rate of extraction exceeds that of recombination by two orders of magnitude in pristine samples, both rates are more or less equal in strongly degraded samples. The photo-CELIV measurements confirm the mobility reduction and the strong reduction of extractable carriers due to increase in the background carrier density.

The calculation of the IQE reduction as a function of f_{LV}, cb, and μ, shows that at reasonable values for f_{LV}, μ plays a stronger role than c_b, but both effects might not be sufficient to explain the strong J_{SC} reduction observed upon photo-oxidation. This suggest that the increased background carrier density introduced by irreversible degradation contributes to the loss of short circuit current by shielding the extraction field in the bulk of the devices, which corresponds to a decrease of E_{bi} in equation 4.1 and thus leads to an additional decrease of the extraction term. This additional decrease leads to a longer dwelling time of the photo-generated carriers in the device so that in turn their recombination is significantly enhanced in the pseudo-first order reaction observed in our TA measurements, similar to the effect that has been shown to be operative in reversibly degraded P3HT:PCBM solar cells.[67]

Chapter 5

Photo-oxidation effects in silole-based polymer:PCBM solar cell[f]

The efficiency of organic solar cells (OSCs) has crossed the 10% milestone due to the introduction of low band gap materials. The trend in the efficiency is promising in terms of commercialization of OSCs, but insufficient lifetime so far opposes widespread implementation. PDTSTzTz (or KP115) is a Silole based new low band gap polymer getting considerable attention due to its favourable structural properties like relatively semi-crystalline morphology and better matching with AM1.5 solar spectrum compared to P3HT. Oxygen induced degradation of KP115:PCBM in the presence of light for 180 minutes caused an irreversible loss of 80% short circuit current density (Jsc) with only 5% loss in the optical density. To understand the mechanism of this strong performance loss in short time, this chapter used transient absorption spectroscopy to inspect the charge carrier dynamics on a femtosecond to millisecond time scale. Reduction in the effective mobility and formation of isolated D/A regions without percolation paths are the reasons for the massive reduction in the performance of KP115:PCBM upon photooxidation. The results from opto-electrical studies also support this picture and show a delayed recombination and increased extraction time of charge carriers upon photooxidation.

[f]*This chapter is going to be submitted for publication: "Photo-oxidation effects in silole-based polymer:PCBM solar cells", **S. Karuthedath**, D. Derbew, A. Distler, H.-J. Egelhaaf and L. Lüer (2015).*

5.1 Introduction

Insufficient stability is a major issue in organic solar cells for their wide spread implementation. The present world record power conversion efficiency has recently surpassed over 10% for organic solar cells.[145] This steady growth in the power conversion efficiency promises the commercial success of this versatile technology. However, improving stability of OSCs got relatively poor attention until recently.[32,67,68] This is a major challenge to be solved in order to enter market segments concerning long – time investments, e.g. in the construction sector. In this chapter, we investigate the irreversible photooxidation effects in OSCs based on a Silole based polymer, PDTSTzTz (or KP115) (poly [(4,4′-bis (2-ethylhexyl) dithieno [3,2-b:2 ′ ,3 ′ -d] silole) -2,6-diyl-alt-(2,5-bis 3-tetradecylthiophen-2-yl thiazolo 5,4-d thiazole)-2,5diyl]) and PCBM ([6,6]-phenylC_{61}-butyric acid methyl ester). This polymer is starting to get considerable attention because of its relatively semi-crystalline morphology and better matching with AM1.5 solar spectrum compared to P3HT.[29,144–146] The chemical structure and the ground state absorption spectra of this polymer are given in Chapter 2.

A recent work addressing the effects of controlled photooxidation in P3HT:PCBM and Si-PCPDTBT:PCBM based solar cells concluded that the observed short circuit current loss (Jsc) upon degradation is due to the combined effects of reduction in the effective mobility and reduction in the extraction efficiency.[32] Inverted structure KP115:PCBM solar cells shows reproducible efficiencies around 5% with 200-250nm thick active layer. Tracey Clarke et al. studied the consequences of photodegradation in the absence of oxygen in encapsulated KP115:PCBM solar cells. They relate the initial sharp drop in Jsc to the loss in the efficiency of charge carrier transport and extraction. They observed a delayed bimolecular recombination due to enhancement of trapping of charge carriers.[146]In the following, we show that upon photooxidation of KP115:PCBM solar cells for 180 minutes, the Jsc is irreversibly reduced to about 80% of its initial value. A combination of time-resolved all optical and opto-electrical studies have been performed on controlled and systematically photooxidized non-encapsulated KP115:PCBM solar cells and films to understand the huge performance loss upon photooxidation.

5.2 Experimental

All solar cells had an inverted structure with optimised KP115: PCBM ratios of 1:2. The devices were made in nitrogen atmosphere and all films of the active layer were realized by doctor blading. The details of the sample preparation and degradation steps are described in

Chapter 2. To measure the current voltage characteristics, solar cells were illuminated with simulated solar spectrum of *SteuernagelSolartest 1200 Oriel* solar simulator at intensities of 100mW/cm^2.The current density-voltage (J-V) characteristics of the devices were recorded using Keithley 2400 SMU in combination with Keithley 7001 Multiplexer system and custom software.

UV-Vis spectra of films and current-voltage characteristics were measured at each stage of degradation to monitor the optical density (OD) loss and current density (Jsc) loss respectively. All films and solar cells were again annealed under vacuum at 130°C, for 5 minutes in a cryostat equipped with a heater (Oxford OPTISTAT), before each set of time-resolved (TAS,TPV and TPC) experiments, in order to make sure the reversible oxygen doping is removed and only irreversible degradation effects are measured. Femtosecond and microsecond to millisecond transient absorption (TAS) studies were performed in cryostat under dynamic, ~10^{-5}mbar pressure. Femtosecond pulses at 387nm, 150fs at a repetition rate of 1 kHz were used for femtosecond TAS and an externally modulated 532nm Nd:YAG CW laser was used for microsecond TAS. Transient photovoltage and photocurrent measurements were also performed under the same condition with an externally modulated 532nm CW laser as pumping source with a termination resistance of 1MΩ and 50Ω respectively. The details of experimental arrangements are given in Chapter 2.

5.3 Results and discussion

5.3.1 Current density-voltage characteristics

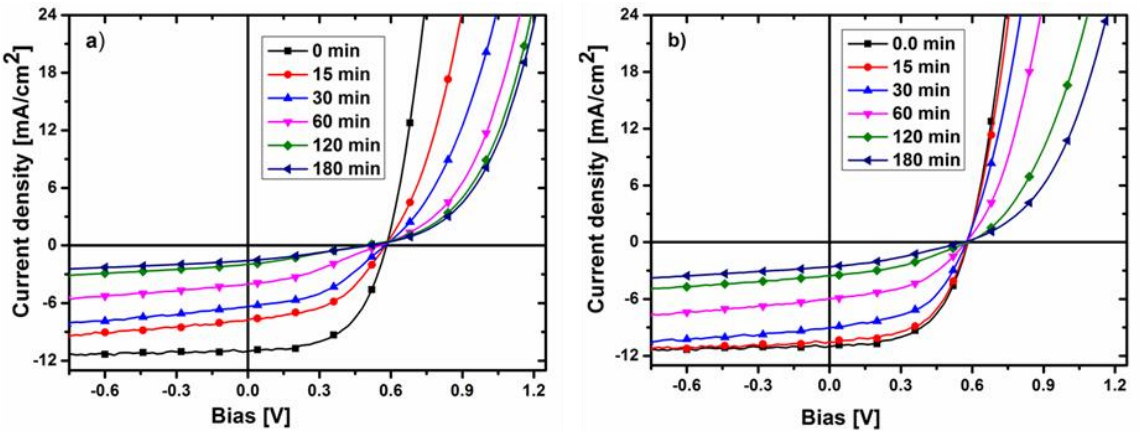

Figure 5.1: Current density-voltage curves for pristine and photo-oxidized KP115:PCBM (1:2) solar cells measured at AM1.5 sun. a) Before reannealing and b) after reannealing at 130^{o}C for 5 min in glove box.

The current density–voltage curves at different degradation times between 0hrs to 3hrs in synthetic air under AM1.5 sun is given in figure 5.1. The observed power conversion efficiency loss with photooxidation of 180 minutes is about 80%, which is mainly due to reduction in the short circuit current (Jsc). Figure 5.1a represents the J-V curves before re-annealing and figure 5.1b shows the J-V curves after re-annealing at 130^{o}C for 5 minutes in the nitrogen atmosphere to remove the reversible degradation triggers as performed for other polymer solar cells in the literature.[32,67] The reannealing partially brought back the PCE to a certain extent at the early stages of degradation, and on longer exposure to photooxidation the reversibility is progressively reduced. Another notable change upon heating is the disappearance of S-shape in the J-V curves (figure 5.1). Changes in each of the parameters and the extent of recovery due to reannealing is given in figure 5.2.

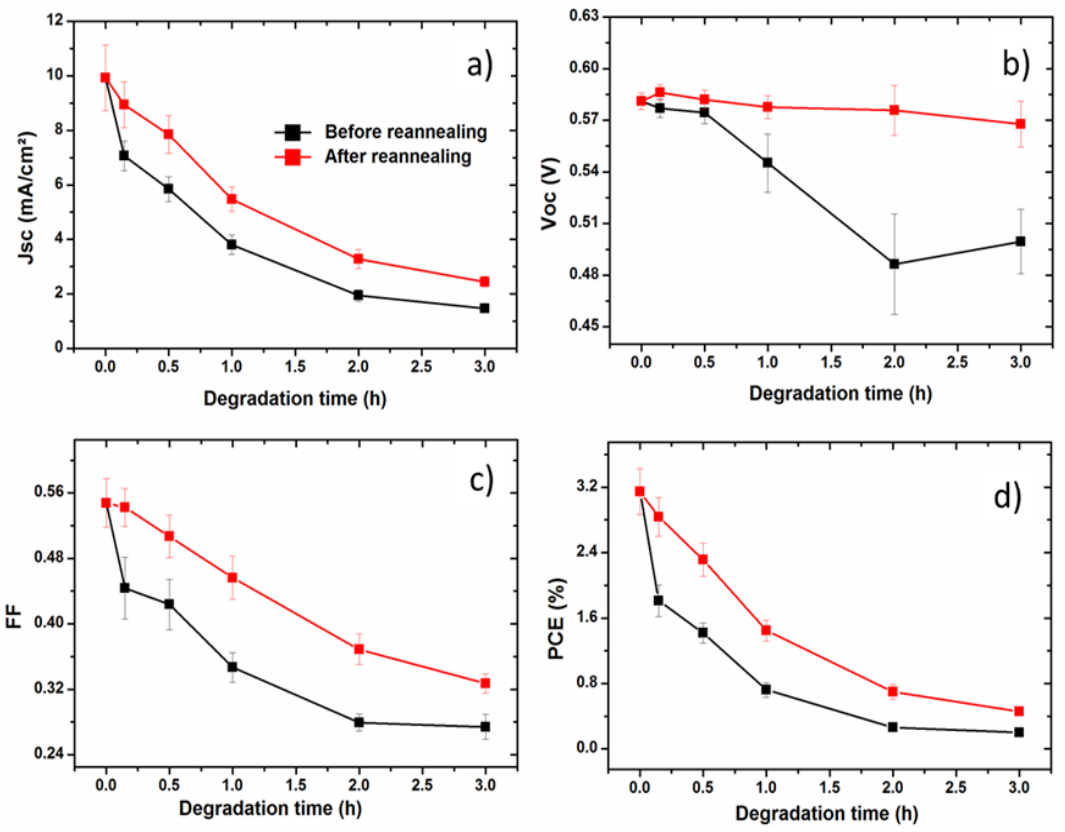

Figure 5.2: Parameters extracted from figure 5.1. a) Short circuit current density, b) open circuit voltage, c) fill factor and d) power conversion efficiency before and after reannealing (black and red curves respectively) at 130^{o}C in glovebox for all photooxidation levels.

Upon light exposure in synthetic atmosphere (~80%N_2, ~20% O_2 and ~0% H_2O) the J_{sc} drops down to more than 80% before reannealing and after reannealing the J_{sc} loss was around 75% after 3hrs (figure 5.2a). The open circuit voltage is shown to have a reduction of about 20% upon degradation and is completely reversed after the reannealing (figure 5.2b). The

observed reduction in the fill factor (FF) is about 35% after the heat treatment (figure 5.2c). As shown in figure 5.2d, the loss in PCE is about 80% after reannealing. The substantial loss in J_{sc} and the loss in fill factor are the major causes of PCE reduction. Since the S-shape has been removed by annealing and the loss in FF is not huge, V_{oc} stays constant and the major cause is J_{sc} loss, so the degradation of the electrodes is minimum.[75]

5.3.2 UV-Vis absorption spectra

Figure 5.3a represents the UV-Vis absorption spectra of pristine and photooxidized KP115:PCBM thin films. A decrease in the optical density (OD) of about 0.05 of the absorption peaks at ~650nm and ~590nm was observed and a comparable loss in the PCBM absorption maximum region (~335nm) was also detected. This means that there is no significant photon absorption loss to affect the J_{sc} of the solar cell. These spectra are measured after the reannealing; therefore the observed changes are not reversible. Moreover, the absence of substantial changes in the absorption spectra proposes that no significant concentration of photooxidation products has been formed that reduces the conjugation length of the polymer, which has been reported for other polymer systems like P3HT and Si-PCPDTBT.[32,67] Clarke et al. also found the same effects for photodegradation of KP115:PCBM solar cells.[144] Figure 5.3b compares the loss in optical density to corresponding loss in the Jsc. As in the case of previously reported materials, KP115 also has shown huge loss in the Jsc for a very small change in the optical absorption.[32,67,144]

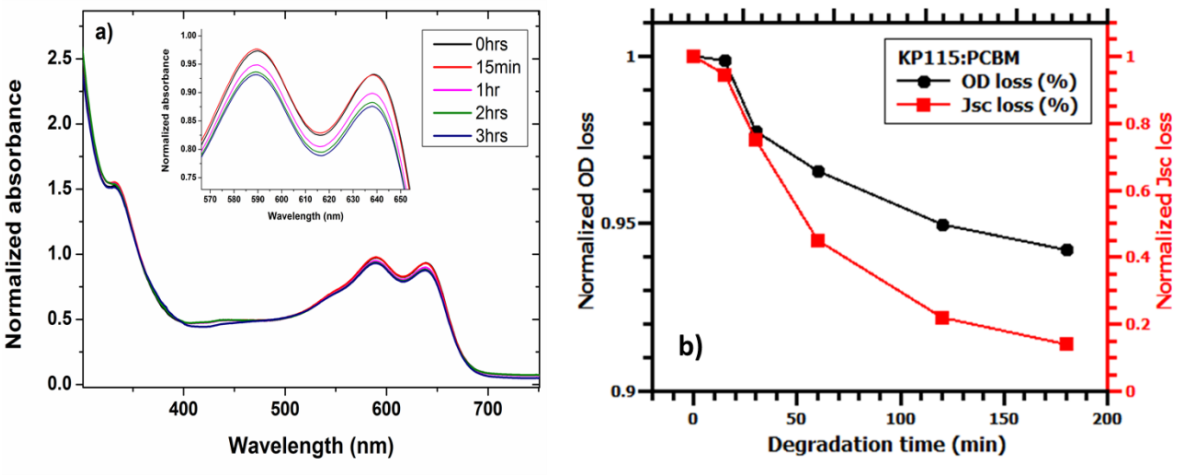

Figure 5.3: a) UV-Vis absorption spectra of KP115:PCBM for all photo-oxidation levels, inset shows the zoomed in region where the KP115 absorption peak changes. b) Comparing normalized optical density loss (black spheres) with loss in short circuit current (red squares) for all degardation levels.

It has been already reported that oxygen mainly attacks the active layer rather than the other layers in the organic solar cells, particularly in the presence of light.[32,67] To get a deeper

understanding of the effects of photo-oxygenation and to unravel the underlying mechanisms, studies on the fundamental processes in the organic solar cells are necessary. In order to shed some light on this matter, this chapter used transient absorption spectroscopy (TAS) having a time scale range from few picoseconds to milliseconds along with transient photoelectrical methods such as transient photovoltage (TPV) and transient photocurrent (TPC).

5.3.3 Picosecond transient absorption spectroscopy

Picosecond transient absorption spectroscopy is an efficient and widely used tool to detect ultrafast dynamics of photo-excited states.[132] The pristine and photooxidized KP115:PCBM thin films (thickness about 200nm) were excited at 387nm pump having ultrashort pulses (about 150fs) from a Ti-Saphire laser. The white light probe (derived from the same source by self-phase modulation) measured the excited state spectra for a wide spectral range from 400nm to 1500nm.[126] All measurements were done under dynamic vacuum (~10^{-5} mbar) and all samples were reannealed before each experiment to remove the reversible degradation stresses. All experimental details and schematics of the femtosecond TAS are explained in Chapter 2.

In organic photovoltaics, exciton dissociation and geminate recombination, the prominent loss processes that reduce the generation yield, have been shown to occur on this ultrafast time scale. TA spectroscopy can be deployed to trace the time-resolved concentration of several photoexcitations, like singlet/triplet excitons and charged states, by virtue of their specific photo induced absorption (PA) bands. The TA spectra of singlets and polarons generally overlap, so matrix decomposition techniques need to be used to obtain the time-resolved population of singlet excitons and polarons separately. The analysis of KP115:PCBM femtosecond TAS was done by a procedure called target analysis described by van Stokkum et al., and explained in Chapter 2 and 3.[127]

The left panel of figure 5.4 shows the characteristic spectra of pristine KP115:PCBM thin film at 200nJ pump energy and the obtained lifetimes of each spectrum is given in each of the panels. The thick black curves in the figure 5.4 are the fits to the EADS by a spectral model involving singlet excitons, polarons in the amorphous phase and in the ordered phases. The contribution of singlets and charged states to each EADS can be obtained by spectral modelling. The bands assignment were done by using literature knowledge from previously published works.[144,146] The left panels in figure 5.4(a-c) represents the EADS from 0 to 2 and corresponding spectral fits of pristine KP115:PCBM thin film. As T. Clarke et al. found, the

band at 1.16eV (1070nm) is assigned as contribution from localized polarons (blue curves) and band at 0.85eV (1450nm) is chosen as contribution from singlet excitons.[144,146]For the sake of clarity of representation, contributions to the PB bands are not given.

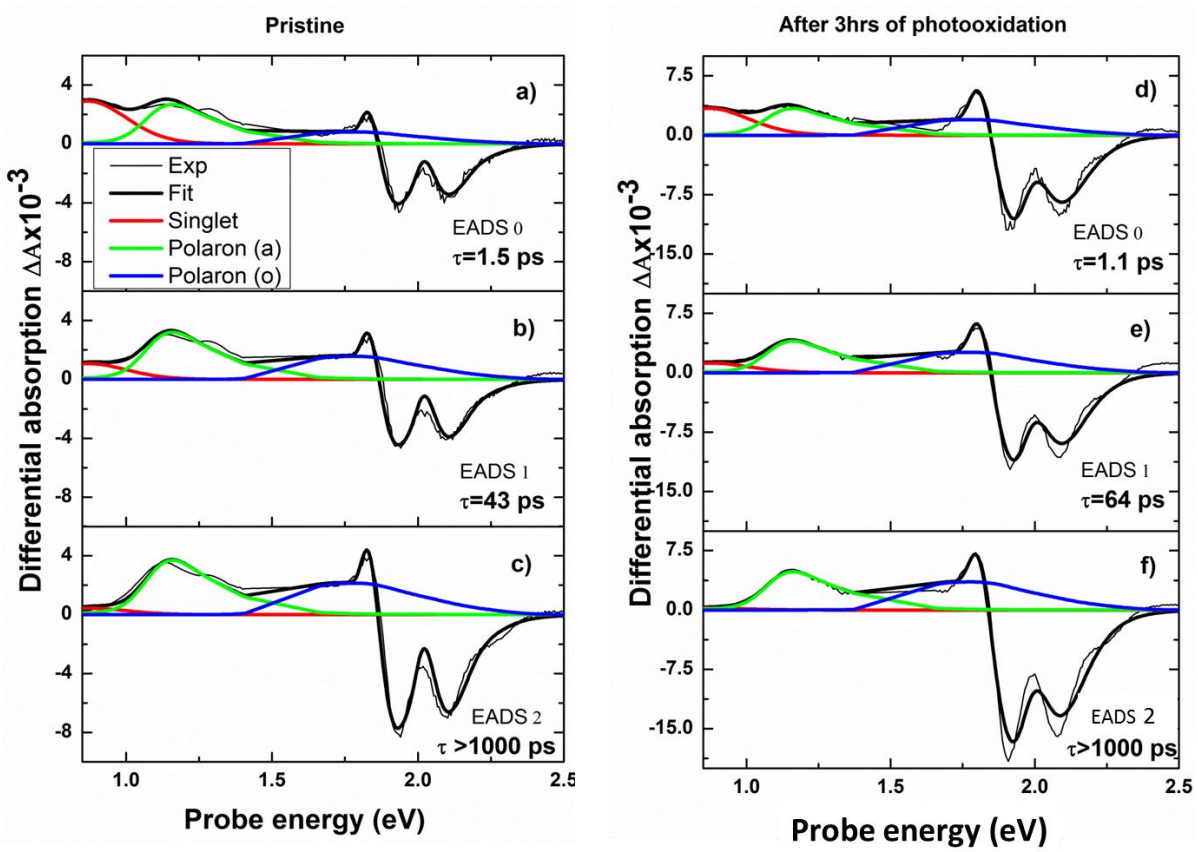

Figure 5.4: Evolution associated differential spectra (EADS) at 200nJ pump intensity for KP115:PCBM, as obtained from a global analysis of using a 3 sequential step model (thin solid curves, fitted lifetimes are given in the legend), spectral fits to the EADS (thick solid curves) and contributions to fits from singlet (red curves) and polaron states (green curves: polarons from amorphous region, blue curves: polarons from ordered region).Note that for clarity of presentation, the contributions to the PB bands are jot given. The right panel shows the EADS and respective spectral fits of pristine and left panel shows the same for photooxidized KP115:PCBM thin films.

In KP115:PCBM the localized charge carriers (green curves) are formed immediately after the photo excitation and stays constant or keep slightly increasing upon spectral evolution. For the P3HT:PCBM spectra, see figure 3.2 of Chapter 3. This striking favourable ultrafast and long lived charge carrier formation would in principle help the better performance of the device. Since the band at 1.16eV is not decaying with time, so, one can conclude the 1.16eV band contains no singlet excitons, and comprises only with (localized) polarons from the amorphous region.[144,146] As a compensating effect, an increase in the photo bleach bands was also observed, possibly making the transfer of charges onto the donor phase by charge transfer from PCBM. Note that the polarons from ordered region (blue) is mainly diffusion mediated and is building up with time as in the case of P3HT:PCBM. The right panel of figure 5.4 describes the EADS and respective spectral fits after 3hrs of photooxidation of the

KP115:PCBM film. All colour codes are same as in the left panel. Two important observations can be made by comparing both panels of figure 5.4. One, the localized charge carrier concentration is not changed upon photooxidation like in P3HT upon degradation.[32] This stable and unaffected polaron band at 1.16eV shows that photooxidation does not affect the charge carrier generation and recombination in the picosecond time range. Second, the singlet exciton quenching efficiency also slightly increased upon photooxidation, which means that the attacked oxygen acts as acceptors (traps) and quenches the singlet excitons.

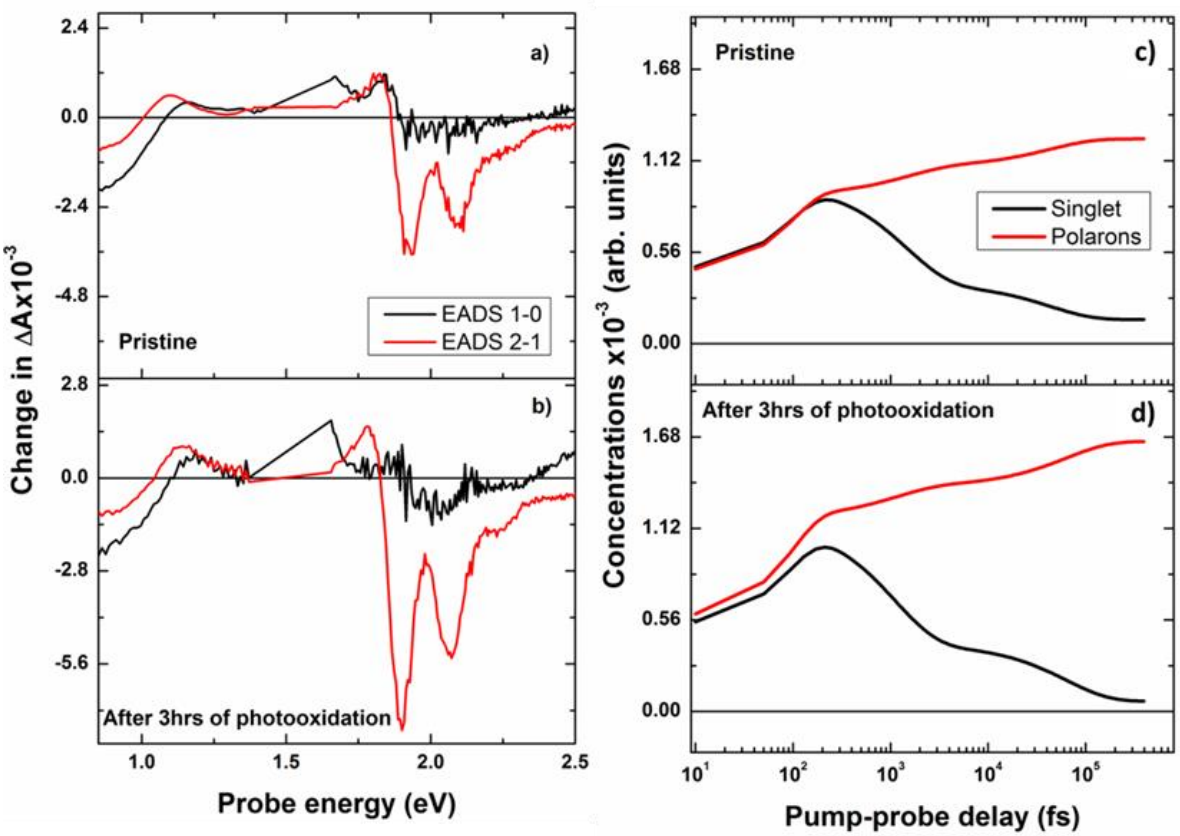

Figure 5.5: Difference in the EADS a) for pristine and b) for photooxidized KP115:PCBM thin films. Black lines show the difference between EADS 1 and EADS 0, red lines represents the difference between EADS 2 and EADS 1. Panels c and d represents the changes in the singlet (black lines) and polaron (red lines) concentrations for pristine and photooxidized KP115:PCBM films.

Figure 5.5a and b shows the changes in the EADS for pristine and photooxidized KP115:PCBM thin films, respectively. The traces were obtained simply by subtracting the one EADS from its previous EADS (for e.g. EADS 2-EADS 1gives EADS 2-1). In both cases (pristine and degraded) the changes in the spectral shapes are similar. Changes in the singlet band became half, the polaron band slightly increased and the photo bleach band enlarged. This huge change in PB band during EADS 2-1 transition is reflected in the unchanged (or slightly increased) polaron band at 1.16eV. The right panel of figure 5.5 shows evolution of singlet (back curve) and polaron (red curve) concentrations for pristine and degraded films

respectively. As observed from figure 5.4 the ultrafast polaron generation is relatively unchanged upon photooxidation (see red curves in figure 5.4c and d). Another noteworthy finding is that the singlet quenching became slightly faster and that effect is reflected in the polaron band. This means that the oxygen acts as singlet quencher (singlet reaches to oxygen traps faster than to reaching to donor/acceptor (D/A) interface) and enables polaron formation. Changes in the traces due to this quenching effect are clearly visible in figure 5.5b in the time range of 50ps to 300ps. But this effect is minor. This finding points to the remarkable properties of KP115:PCBM solar cells, since all solar cells based on other polymers shows clear degradation trends in both singlet and polaron dynamics. These findings could not explain the huge electrical losses in this material. To understand the losses, transient absorption studies at 970nm on microsecond to millisecond time scales were performed.

5.3.4 Microsecond transient absorption spectroscopy

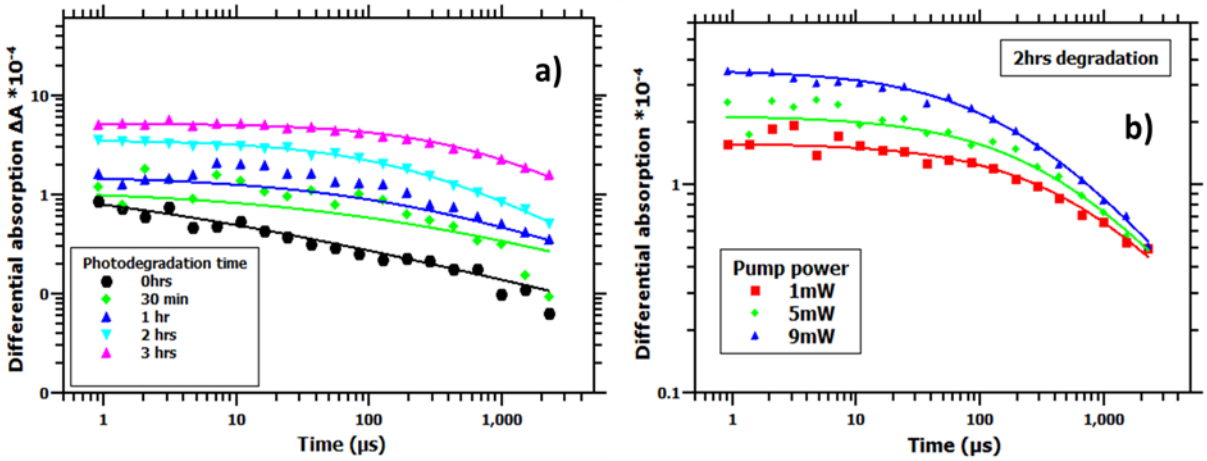

Figure 5.6: Charge transients of KP115:PCBM solar cells a) at different degradation levels and at 9mW and b) at different pumping intensities for 2h photooxidation. The symbols are measured curve and solid lines are corresponding fits with equation 5.1.

This section describes the charge carrier dynamics of KP115:PCBM solar cells upon photooxidation in the microsecond to millisecond time domain. KP115:PCBM has both crystalline and amorphous regions like P3HT:PCBM. Recently, T. Clarke et al.have applied a bimodal system to explain the charge carrier dynamics in KP115:PCBM solar cells. They assigned the feature around 750nm to the delocalized polarons originating from semi crystalline region and the band at around 1070nm to the localized polarons from amorphous region.[144,146] At the probe wavelength used in this thesis, 970 nm, KP115:PCBM has good polaron absorption with negligible super position of other long lived states. In this subdivision the charge carrier dynamics of KP115:PCBM solar cells at 970nm upon

photooxidation is described by using results obtained from microsecond transient absorption studies.

Figure 5.6 shows the charge carrier transients obtained at 970 nm for KP115:PCBM solar cells under different degradation conditions and at different intensities. Charge carrier transients after switching off the long pump pulse at 532 nm at around 1sun intensity for different photooxidation levels are shown in figure 5.6a. We used long enough irradiation periods (~12ms to 17ms) to make sure that the carriers are decaying from a stationary state where the generation and recombination of charge carriers are in equilibrium. Slopes of the transients become slower and the initial differential absorption (ΔA) values increases upon degradation. The same result has been obtained for P3HT:PCBM under the same condition and described in Chapter 4. The slowness in the decay transients and increase in the initial ΔA could be due to the reduction in the effective mobility of charge carriers. To get a quantitative picture on what is happening to the charge carriers upon photooxidation, a global fitting was performed on the obtained decay transients using the following equation.

$$\frac{dn}{dt} = G - k_L(t) \cdot [n(t) + c_b] \cdot n(t) \tag{5.1}$$

where$k_{L(t)}$ is

$$k_{L(t)} = k_L^0 \left(\frac{t}{1\mu s}\right)^{\gamma} \tag{5.2}$$

Herein, k_L^0 is bimolecular recombination coefficient in cm^3/s, γ is the dispersive parameter, *n(t)* is the time dependent photogenerated carrier concentration and c_b is the background carrier concentration. The solid lines in figure 5.6a represent the global fits with the bimolecular recombination model (equation 5.1). Interestingly there is no signature of background carriers observed unlike in P3HT and Si-PCPDTBT. This is a good indication that the effect of background carrier concentration is negligible in KP115:PCBM upon photo-oxidation and only the reduction in the effective mobility and morphological changes are the main reasons for the performance loss. Tuning and locking the nanomorphology at optimum condition would result in a stable photovoltaic performance of KP115 solar cells.

Unlike in P3HT:PCBM solar cells, the photooxidation does not alter the recombination dynamics in KP115:PCBM solar cells. Figure 5.6b shows the decay transients of 120 minutes photo-oxidized KP115:PCBM solar cells. A strong intensity dependence of the decay curves is found: while the starting concentrations at t = 1µs cover more than a factor of 3, but after

1ms decay time all curves join to a unitary point. This behaviour is indicative of a pure bimolecular reaction with equal concentrations of positive and negative carriers, as expected if only photo-induced carriers are present. When this condition is met, equation 5.1 holds, and the time integral evaluates to intensity independent, hyperbolic dependence of concentration on time for long times. It has been reported that the P3HT:PCBM solar cells follow bimolecular recombination mechanism when they are pristine, and upon photooxidation the reaction order changes to pseudo first order.[32] In the case of KP115:PCBM solar cells the recombination mechanism does not change though the recombination time is increased with photooxidation. In conclusion the photooxidation in KP115:PCBM solar cells reduces the effective mobility of the charge carriers, but no effects of background charge carriers in the recombination dynamics are observed and the recombination dynamics is not altered.

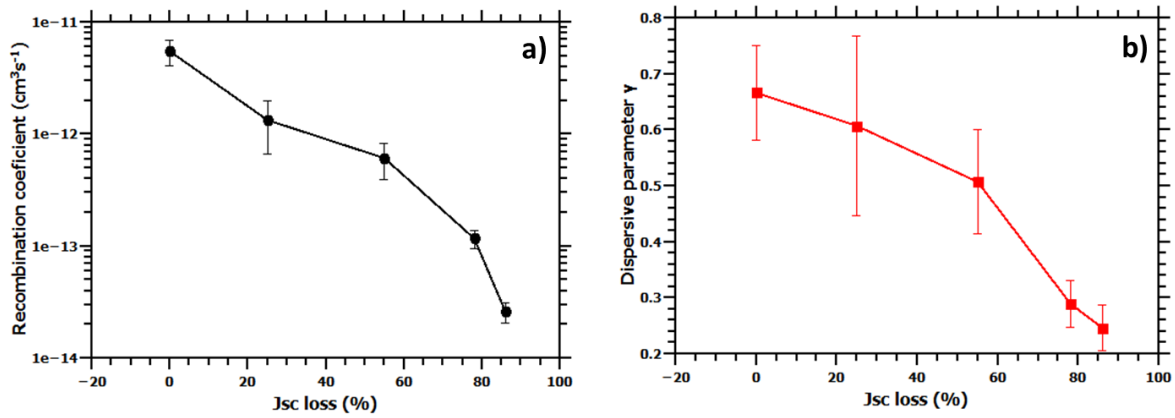

Figure5.7: Parameters obtained from the global fits of figure 5.4a using equation 5.1. a)Evolution of bimolecular recombination coefficient at 1µs, and b) dispersive parameter, γ for all degradation levels.

Figure 5.7a shows the evolution of the bimolecular recombination coefficient, k_L^0, at all levels of photooxidation. At J_{sc} loss around 60%, k_L^0 is reduced more than one order of magnitude, keeping the same pace for further degradation. This suggests a drastic reduction in the mobility already at early stages of degradation as observed for other similar systems.[32] Figure 5.7b displays how the dispersiveness parameter γ is changing with degradation. A value of γ = 0 would correspond to a time-independent mobility as implicitly assumed in equation 5.2, leading to a slope of -1 as asymptotic long-time behaviour in the double logarithmic graphs in figure 5.6. For γ> 0, the charge carrier mobility is reduced over time, and the asymptotic slope is between 0 and -1. Here the observed changes in γ cover about a factor of two with degradation and the value approaches 0 as the degradation proceeds. In general, this behaviour indicates a narrow density of states distribution, which in principal is beneficial for charge transport because the effects from deep trapping should be reduced. But, the overall performance is certainly deteriorating upon photooxidation. Why does the

mobility become a weaker function of concentration than in the pristine case? There could be electronic factors (e.g. only exposed high energy states are photooxidized, and once photooxidized they act as scatters reducing the mobility, and no longer as deep traps causing a large gamma) or morphological factors (certain low energy positions are removed by annealing effects). One cannot clearly distinguish between these possibilities. But the electronic suggestion sounds reasonable, because figure 5.7a proves the reduction in the overall mobility.

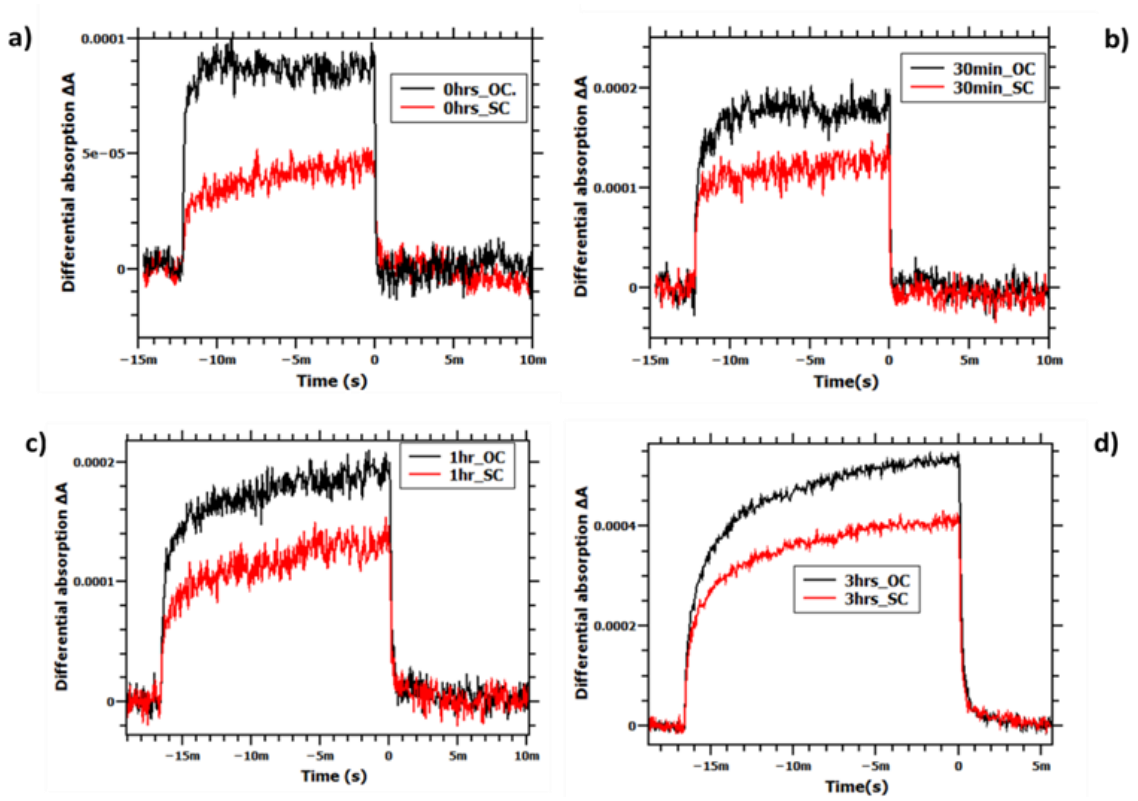

Figure5.8: TA traces in KP115:PCBM solar cells under open circuit (OC) and short circuit (SC) conditions, at various stages of photooxidation, as given in the legends. Charge carriers were created by long pulses (12 to 17ms) in order to create the stationary state by achieving equilibrium between charge generation and recombination.

Figure 5.8 presents TA traces of photo-induced charges in KP115:PCBM solar cells of different degrees of degradation under open circuit (OC) and short circuit (SC) conditions, after irradiation with long pulses. While under OC conditions, the charge decay is only governed by recombination, whereas under SC conditions both recombination and extraction occur simultaneously. The comparison between OC and SC transients at different degradation levels yields therefore information about the efficiency and the time scale of charge extraction. As the degradation precedes, the amount of non-extractable carriers are getting higher, meaning that charge generation is not affected by the degradation (as observed from picosecond transient spectroscopic studies) but the charge recombination and extraction is

reduced as in the case of P3HT:PCBM solar cells.[32] Please also note that the charge extraction is not complete even in the pristine case, indicating that morphology is not optimum even in the very pristine cells and has to be modified in order to achieve better energetics for efficient charge transport. The most probable scenarios which reduce the short circuit current and hence power conversion efficiencies are reduction of the built-in field and passivation of the active layer by forming islands. The absence of background charge carriers due to photooxidation discards the built-in field picture. The disruption of ideal morphology and hence formation of the isolated donor-acceptor (D/A) islands would explain the extraction loss in the absence of background carriers. Figure 5.9 schematically represents the island formation picture upon photooxidation of KP115:PCBM solar cells. So, together with this extraction loss due to islands formation, the reduction in the effective mobility would expound the performance loss of KP115:PCBM solar cells upon photooxidation. This findings need to be confirmed by independent complimentary methods. The following section is deals with photoelectrical measurements such as TPV and TPC on the same devices explained here.

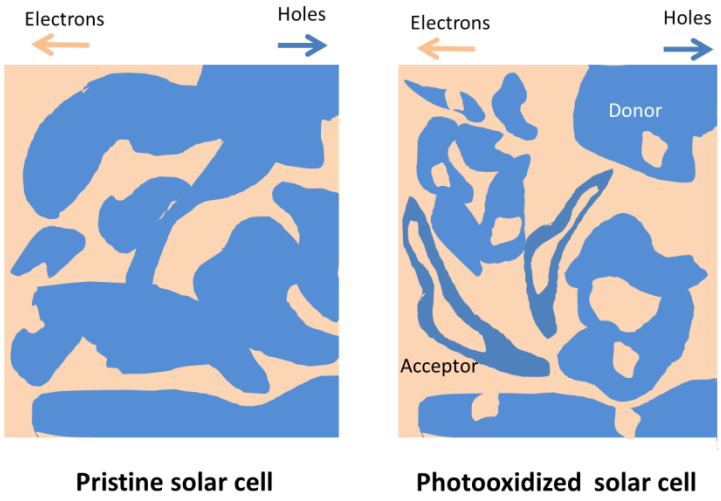

Figure 5.9: Disruption of percolation pathways in KP115:PCBM solar cells upon photooxidation. a)Sub-optimal morphology in pristine solar cell and b) islands formation upon photooxidation.

5.3.5 Transient photovoltage decay

Transient photovoltage (TPV) decay measures the decay of the open circuit voltage (V_{oc}) over the time domain. TPV measures the charge carrier lifetime upon a small perturbation in the charge carrier density.[130] Figure 5.10a shows the normalized transient photovoltage decay of KP115:PCBM solar cells at different degradation levels and at approximate 1sun illumination with a long 532nm pulse excitation. Long pulses (~12ms to 17ms) are used in the measurements to make sure that the carriers decay from a stationary state where the

generation and recombination of charge carriers are in equilibrium. The decay of mobile charge carriers upon photooxidation shows a clear decline of the recombination rate. This picture is consistent with published results on P3HT:PCBM solar cells.[32]

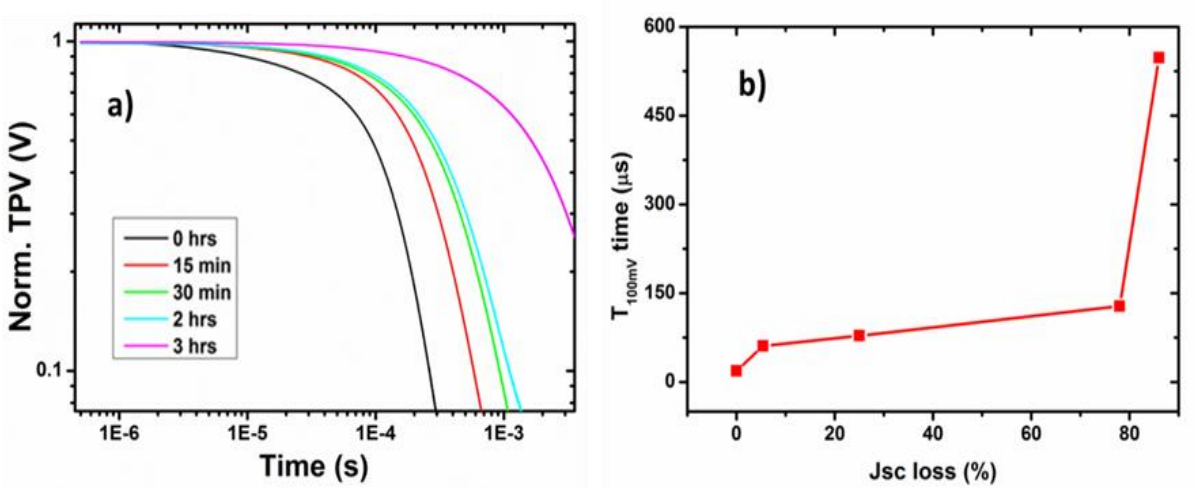

Figure 5.10: a) Normalized transient photovolatge traces of KP115:PCBM solar cells at different levels of degardation. b) Time taken to drop 100mV of initial Voc at each degradation levels

Figure 5.10b shows the time taken to drop 100mV of the initial Voc. Observing the recombination time to lose initial 100mV from pristine to most degraded ones; it covers close to 30 times compared to pristine one. This clearly indicates a fall in the recombination rate which is also confirmed by transient absorption measurements. T. Clarke et al. observed a broadening in the DOS upon photodegradation of KP115:PCBM solar cells.[144] They suggested reduction in the recombination rate would have an impact on the increase of the total charge carrier density.[144] The TAS analysis showed narrowing of the DOS (the gamma values are approaching to zero) and discards the DOS broadening picture upon photooxidation.

5.3.6 Transient photocurrent decay

In order to probe the possible changes in charge carrier extraction upon photooxidation,the transient photo-current (TPC) technique was employed. Transient photocurrent is a useful technique to understand the operation of polymer solar cells and distinguish loss mechanisms.[147] Like transient photo-voltage, TPC also counts only mobile charge carriers and is insensitive to immobile charge carriers. The transient photo current decay of KP115:PCBM solar cells were obtained after exciting with externally modulated 532nm pulses from a CW Nd:YAG laser. Details of experimental arrangements and condition can be found in Chapter 2.

Figure 5.11a shows the TPC traces of a KP115:PCBM solar cell at different levels of photo-oxidation. It is very clear from the TPC transients that the steady state current gets reduced upon photo-oxidation. The maximum extractable current decreased from ~0.6mA to ~0.05mA, more than an order of magnitude. By integrating these curves one can calculate the amount of extractable charge carriers produced after a pulsed irradiation.[147]

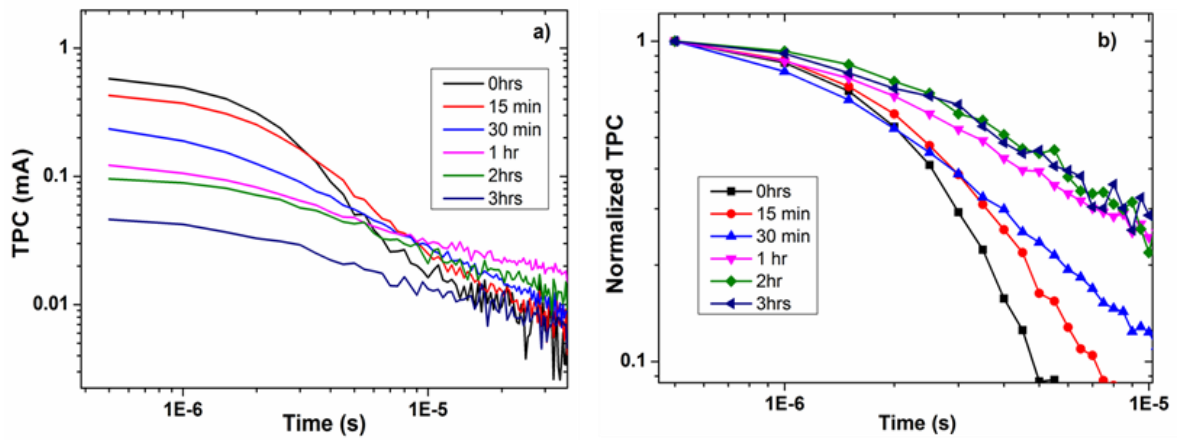

Figure5.11: a)Transient photocurrent decays of KP115:PCBM solar cells upon photooxidation and b)normalized TPC traces of a.

The extractable charge carriers $Q_e$can be calculated by;

$$Q_e = \int_0^{t_{pulse}} \Delta I \, dt \tag{5.3}$$

where, ΔI is the photocurrent measured by TPC. The charge carrier density, p can be calculated by;

$$p = \frac{Q_e}{e\,S\,d} \tag{5.4}$$

where d is the thickness of the sample, S is the device area and e is the elementary charge.[65,71] This reduction in the current could be explained by the islands formation and the building up of trapped charge carriers upon photooxidation which can be detrapped after long time and available for extraction and recombination. One can easily observe this from figure 5.11b, where the charge carriers still can be extracted after 10µs for the degraded solar cells. Figure 5.11b presents the normalized version of figure 5.11a. All decay curves are becoming slower upon degradation except for 30minutes (blue curve) which shows a faster decay for first 2µs then following the normal trend. This slowness could be due to slowness of charge carriers (reduction in mobility) with degradation. These observations are quantitatively described below.

Figure 5.12a shows the amount of extractable charge carriers. This is obtained by merely integrating the area under the curve of figure 5.11a using equation 5.3. In figure 5.12a, a quantitative picture of the huge reduction in the amount of mobile extractable charges carriers is given. The loss in carrier density could be attributed to islands formation due to morphological modifications happening upon photooxidation as presented in figure 5.8. The oxygen creates more and more deep traps with time and oxygen exposure, which attracts and traps the charge carriers in to it along with disruption of percolation pathways by forming isolated D/A phases. The mobile charge carriers generated are isolated in the bulk and cannot escape to the electrodes. Both issues are due to the breaking of sub-optimal nanomorphology due to oxygen exposure. The time taken to extract 60% of the initial charge carrier concentration is given in figure 5.12b for all levels of degradation. The extraction time increased from ~2.5 µs to ~6 µs as the degradation continues. This observation is clearly in agreement with all TAS and TPV findings. This slowness in the extraction can be explained by reduction in the effective mobility due to traps formation and due to morphological changes (islands formation). Since the mobility is carrier density dependent, the reduction in the number of extractable mobile charge carriers could also play a role in the effective mobility.

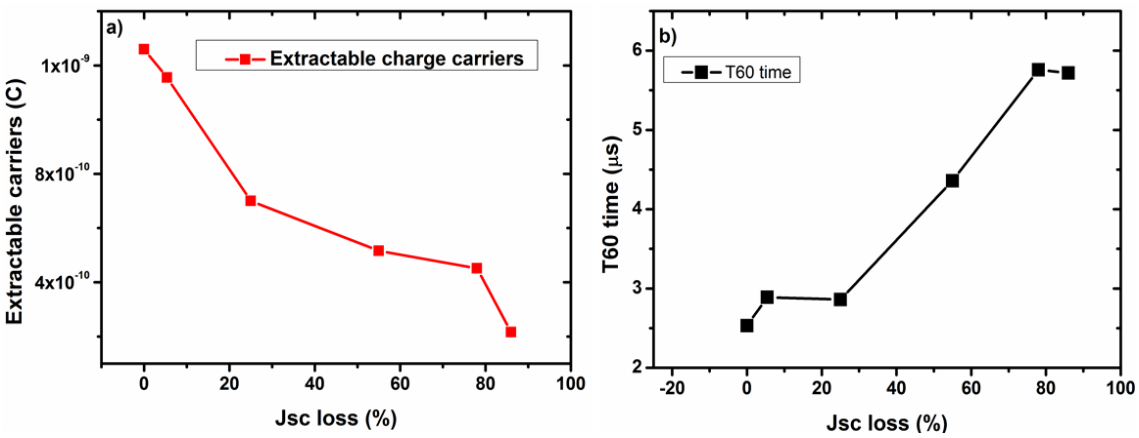

Figure 5.12: a) Amount of extrcatble charge carriers with photooxidation obtained by integarating the area under the curve of each TPC transients and b) time taken to drop 60% of initial carrier density for at each degradation level.

In conclusion, the effect of isolated D/A islands formation is more severe issue than the reduced mobility in KP115 solar cells. The reduction in the charge carrier extraction rate is factor of 2, which could not explain the drastic 80% loss in the short circuit current. So the reduction of mobility is not the main reason for the performance loss. And we did not observe any signature of reduction (or screening) of built-in field as observed for P3HT:PCBM.[32]As explained before, the generation of charge carriers is not effected by the oxidation, but the

recombination and extraction is. As it is clearly visible in figures 5.11a and 5.12a the amount of extractable carriers are reduced upon degradation. So, the photo induced charge carries does not feel the extraction field to get extracted by the electrode even though the recombination is appreciably slowed down upon photo-oxidation.

5.4 Summary

This chapter investigated the photooxidation effects in a novel Silole based polymer, KP115 with PCBM by using time-resolved transient techniques. The inverted KP115:PCBM solar cells shows a drastic reduction in the short circuit current density and hence the power conversion efficiency upon oxygen exposure in the presence of light. The charge generation, recombination and extraction strongly depends on blend morphology.[148,128] The result from picosecond transient absorption spectroscopy showed barely any changes in the spectral shape and shows very small changes in the time dependent yield of extractable charge carriers. Upon photooxidation, the oxygen acts as singlet quencher and thereby formation of polarons. But this is a minor effect. This result clearly proves the absence of generation losses due to photooxidation like in the other polymer systems like P3HT or Si-PCPDTBT.[32] This suggests that the charge separation coefficient is independent on degradation and most of the localized charge carriers are generated immediately after the excitation. So, the picosecond data could not explain the huge loss in the performance of KP115:PCBM solar cells upon photooxidation.

The studies on the recombination dynamic in the microsecond to millisecond time scales showed that, the bimolecular recombination dynamics in KP115:PCBM does not alter upon photooxidation. This is in stark contrast to the photooxidation effects in P3HT:PCBM solar cells where the recombination dynamics changed from bimolecular to pseudo-monomolecular trap assisted recombination.[32] The absence of background carriers along with unchanged recombination dynamics makes this polymer attractive. However, a strong decrease in the recombination coefficient is observed upon photooxidation of KP115:PCBM solar cells. The open circuit and short circuit TAS demonstrated that the amount of nonextractable charge carriers is getting higher upon degradation proceeds. This observation suggests a reduction in the mobility of the charge carriers and interruption of percolation paths due to the formation of D/A islands could be the reasons for the performance loss.

The transient electrical studies support and confirm the island formation picture. Transient photovoltage shows a monotonous decrease in the decay time traces with photooxidation. The time taken to lose initial 100mV is decreased more than an order of magnitude. The transient photocurrent decay showed a decrease in the extraction rate and density of extracted charge carriers upon photooxidation. The time taken to drop 60% of initial carrier density doubled after 3h of photooxidation. This loss in the extractable carrier density and extraction/recombination rate are due to reduced effective mobility and isolated percolation pathways as observed from transient absorption studies.

In conclusion, KP115 is a promising material for photovoltaic applications because of its favourable properties like semi-crystallinity and better matching with solar AM1.5 spectrum. Moreover, the photo-oxidation on these materials does not alter the recombination order and creates no background carriers, which are the major deteriorating effects of performance in the case of P3HT:PCBM solar cells upon photo-oxidation. The huge power conversion efficiency loss could be explained by the formation or D/A isolated phases and reduction in the effective mobility due to formation of oxygen traps upon photooxidation. Tuning and stabilizing the nanomorphology would yield a better stability and performance against photooxidation. Further studies need to be done on this material in order to explore and improve the stability against other degradation mechanisms such as humidity and elevated temperature.

Chapter 6

Improved thermal stability of low band gap polymer solar cells: Relating device performance to blend morphology[g]

To obtain OSC with long-term stability, it must be understood how intermolecular interactions control morphological evolution and how morphological evolution in turn influences the elementary processes in the photovoltaic event chain. Here, we present a comparative study of OSC made from PCBM blended with a series of low-bandgap polymers of the DPP class with different solubilizing side chains but identical conjugated backbone. This allows us to specifically study the effects of inter-chain interaction on thermal degradation. Combining transient absorption spectroscopy from femtoseconds to milliseconds with transient photocurrent measurements, we are able to single out the effect of thermal degradation on all relevant elementary processes. On a picosecond time scale we find that in some materials, thermal degradation reduces the yield of ultrafast polaron generation due to domain size growth, while the delayed charge generation pathway (mediated by exciton diffusion) becomes lossy. The losses are partially made up for by reduced geminate charge recombination upon degradation, observed for all samples. On a microsecond time scale, we observe a strong decrease of non-geminate recombination upon degradation, which is explained by vertical demixing of donor and acceptor rich phases, since the effective extraction mobility is found to decrease as well. Only one of the materials shows a stable charge mobility indicating that vertical demixing is not significant; this material has substituents that induce sufficient intermolecular interactions for the formation of a bicontinuous networks and does not incorporate any groups with a special affinity towards one of the selective contacts. This material matches good pristine performance with improved long-term stability.

[g]*This chapter is going to be submitted for publication: "Improved Thermal Stability of Low Band Gap Polymer Solar Cells: Relating Device Performance to Blend Morphology", **S. Karuthedath**, G.Morse, J.Cabanillas-Gonzales and L. Lüer (2015).*

6.1 Introduction

The discovery of conducting polymers in 1970s and intense research on conjugated polymers has opened possible alternatives for energy harvesting.[10] Organic solar cells (OSCs) have many advantages compared to inorganic solar cells like, high absorption yield, light weight, flexibility, colour tunablity, semi-transparency, and – depending on market volume – potentially lower costs.[5,6,97,102] These interesting properties make them apt for wearable, colour tunable, semi-transparent power generation applications.[6,79] For such applications sustained stability and maximum efficiency must be achieved and maintained throughout the entire operating period. Using low band gap materials is a promising approach to increases the efficiency as they increases the spectral overlap matching and thereby increase the photon intake.[37,92,146,148,149] Recently, the power conversion efficiencies (PCE) of OSCs reached around 9% with new types of low band gap materials.[150,151] Further improvements and understanding of the nanomorphology would yield efficiency greater than 15% with longer lifetime.

Conjugated polymers are known for their instability against environmental conditions which leads a reduced operational lifetime.[30,31] It has been already shown that many degradation triggers like, water[33,84,152] oxygen[32,67], light,[37]heat[85,153], humidity[33,122], chemical modifications [66,111], mechanical stresses[3] deteriorate the performance of organic solar cells. There have been a lot of attempts to minimize the degradation effects and improve the stability such as encapsulation[3,31,154], using inverted architecture[67,68]changing the blend ratio[83] adding extra layers[105], attaching side chains[37],etc. Using encapsulation minimizes the availability of degradation triggers like oxygen, water, pollutants etc., but do not protect from thermal and light induced effects.[3,85,146,155] Understanding the effect of such degradation triggers in the conducting polymers gives insights and keys to improve the stability of organic solar cells.

Stability of the nanoscale morphology of the active layer is a crucial issue in organic solar cells.[3,30]An optimized morphology for a bulk heterojunction consists of donor and acceptor rich domains not larger than the exciton diffusion length, in order to match maximum charge carrier generation (reduced if domains are too large) and maximum carrier transport (reduced if domains are too small). Such optimum morphology can be achieved e.g. by controlling the donor-acceptor blend ratio[156] regioregularity of polymers[51,128], molecular weights [157,158] additives[37] solvents[159], sample preparation condition[160,161], pre and post annealing temperature.[67] However, this morphology is usually not thermodynamically stable, and

therefore tends to evolve over time, especially at elevated temperatures typically reached under device operation.[85]In fact, in a well encapsulated solar cell, the effect of temperature is the dominant cause for performance loss [3,85,155] Optimum nanomorphology can be altered by thermal stress e.g. via demixing of the materials along the stack direction[162], domain growth[37], and interfacial deactivation.[163] In P3HT: PCBM based solar cells, thermal instability causes crystallization of P3HT, which on one hand enhances carrier transport, on the other hand leads to clustering of PCBM, which reduces the interfacial area and hence exciton dissociation.[85] The reason for the morphological evolution is that small rigid molecules like PCBM gradually diffuse in the bulk enabled by voids that are dynamically formed in the polymer phase close to its glass transition temperature T_g.[85] Different types of microscopic studies have been used to get insight into morphological modifications.[95,96] Bertho et al. have shown that using high T_g donor materials is a good approach.[85] Incorporating cross linkable groups to lock the optimal morphology also improve the stability.[3,111]

A novel class of low-bandgap polymers containing benzodithiophene (BDT) as a donor and electron deficient diketopyrrolopyrrole (DPP) as acceptor moiety, have recently gained much attention, showing power conversion efficiencies (PCE) greater than 6% in single junction OSC.[91,158,159] Multi-junction tandem solar cells based on DPP polymers have gained PCE more than 7% with mid bandgap polymers such as P3HT or PCDTBT.[164,165] Transient absorption studies have demonstrated the presence of ultrafast singlet fission into triplet states. A further triplet generation path was observed upon non-geminate charge recombination. Both pathways of triplet generation represent loss paths in competition with the generation of extractable charge carriers. A specific dependence of side chain substitution of the DPP polymers was shown, clearly highlighting the influence of morphology on these loss channels. The elementary mechanism controlling the yield of triplet mediated loss channels has however so far not been clearly understood. Moreover, the influence of side chain modification on operational stability has so far been investigated only by few groups.[166] J. Durrant's group proposes a model for triplet generation mediated by bound polaron states in organic solar cells.[167]

Here, we present a comprehensive study of long term performance of DPP polymers comprising different side chains during thermal treatment corresponding to device operation. By combining femtosecond spectroscopy with global and target analysis techniques, we quantify charge generation processes and the respective loss channels on a femtosecond to

picosecond time scale. As this technique is sensitive only to the active layer of the OSC, it yields insight into thermally induced morphological changes in the active layer. Relating these changes to opto-electrical studies on a microsecond to millisecond time scale, allows us to map these thermally induced morphological changes specifically on to operational performance losses. This complete picture results in specific design principles, which do not completely avoid morphology evolution, but avoid the detrimental effect of morphology evolution on device performance for a significant period. This renders the devices more stable, but brings also advantages in terms of a wider optimum process parameter range during industrial production.

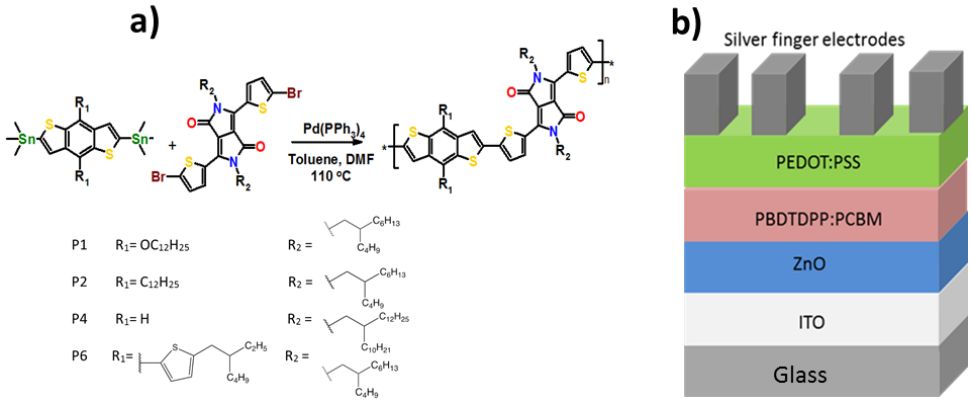

Figure 6.1: Chemical structure donor polymers studied (a) and inverted device architecture (b).

As a model system, different side chains of benzodithiophene (BDT) are synthesized and co-polymerised with diketopyrrolopyrrole (DPP) forming four low bandgap poly- BDT-*alt*-DPP (PBDTDPP) polymers namely EP2, EP4 and EP6 respectively. The chemical structures of these polymers are given in figure 1 along with a schematic of the stack used in our inverted solar cells architecture. The polymers are subsequently characterized, optimized in glass to glass encapsulated inverted PSC devices and their stability assessed under thermal degradation at 60ºC in absence of oxygen and light on a hot plate. All synthesis, XRD, AFM, UV-Vis, FTIR, current voltage investigation details on these devices are recently published.[37] Although the electronic structure of all materials is similar, initial electrical performance and response to thermal stress depend strongly on the side chains.[37]

6.2 Experimental

All synthesis, device preparation, encapsulation and current-voltage characterization details are described in a previous publication.[37] Figure 6.1 shows molecular structure of EP2, EP4 and EP6 and the inverted PBDTDPP:PCBM (1:2) solar cell architecture, which we used for

TA and TPC measurements. This architecture enables to probe TA spectra in transmission, avoiding destructive interference of the probe light close to the reflecting electrodes. [32,130]

For femtosecond transient absorption (TA) studies details are explained in Chapters 2 and 3.Microsecond transient absorption transients at selected probe wavelengths were obtained by exciting the samples at room temperature at 780nm (spot size ~4 mm) with an externally modulated high power LEDs (Thorlabs LED780E). The devices were pumped at different intensities covering more than an order of magnitude with a pulse duration of at least 8ms, such that the concentration of photoinduced carriers reached a stationary state. A probe wavelength of 1300 nm (~2 mm spot size), provided by a continuous wave LED was used for polaron detection. The transient absorption signal was detected by an amplified InGaAs photodiode (Thorlabs PDA20CS-ES) equipped with a 970nm long pass filter in order to reject scattered pump light and fluorescence. The electrical signal from the photodiode was then sampled by an oscilloscope (Picoscope 6424) connected to a PC using custom built Python software. Data evaluation was done via custom built Python software.

For transient photocurrent studies, solar cell devices were connected with an external 50Ω resistor to the input terminal of the oscilloscope (Picoscope6424) and current traces were recorded. All devices were excited by a 780nm high power LED (Thorlabs LED780E). The electrical signal from the solar cell was then sampled by the Picoscope 6424, transferred to a PC and evaluated using custom built Python software.

6.3 Results and discussion

6.3.1 Electrical performance in the pristine state and after thermal degradation

Table 6.1 summarizes the findings of Morse et al.[37] It was found that in the pristine case, EP1 and EP2 show the best PCE values while those of EP4 and EP6 hardly exceed 2%. EP1 shows a very high short circuit current, adequate for its optical bandgap of 1.6 eV, but has a relatively low fill factor. Improved matching of the solar spectrum, as compared to a higher bandgap polymer like, P3HT, comes therefore at the price of increased recombination losses, a situation often encountered in OSC comprising low-bandgap polymers. EP2 has a lower short circuit current but a better fill factor than EP1, such that the PCE value is still above 4%. Both EP4 and EP6 suffer from severe recombination losses, shown by their very low fill factors. EP4 is additionally penalized by a low short circuit current, pointing towards

significant generation losses in addition to the recombination losses. All materials show very similar V_{oc} values.

Upon thermal degradation at 55°C for 50 hours, we find a significant drop of both Jsc and FF for EP1. In contrast, EP2 is found to be very stable against thermal degradation, showing constant Jsc and only a slight drop in FF. EP4 loses both Jsc and FF, while in EP6; both Jsc and FF are reduced upon thermal treatment, but less compared to EP1.

In summary, we find that the type of substituents has a profound impact on the device performance as well as on the stability of the devices against degradation. This has been related to differences in the crystallization tendency.[37] However, growth of crystallites and the concomitant increase of the size of donor- and acceptor rich regions are not necessarily detrimental for device performance. As the example of P3HT:PCBM shows a growth of the domain size can be beneficial for charge generation because the amount of geminate recombination is reduced, as long as the domain size is not exceeding the exciton diffusion length in the donor rich domains.[128] In order to understand why in some cases, crystal growth penalizes charge generation and recombination and in others not, the isolated contributions to either processes must be quantified. In the next section, we combine femtosecond spectroscopy with global and target analysis to quantify the three elementary processes that control the amount of extractable charges, namely ultrafast charge carrier generation at the D/A interface, delayed charge generation mediated by exciton diffusion towards the D/A interface, and geminate recombination of charge pairs. In the subsequent section, we study charge recombination dynamics under solar conditions, allowing us to quantify the rate of non-geminate charge recombination and the extraction yield.

Material	**Voc(p)** (V)	**Voc(deg)** (V)	**Jsc(p)** (mA/cm^2)	**Jsc(deg)** (mA/cm^2)	**FF (p)** (%)	**FF(deg)** (%)	**PCE(p)** (%)	**PCE(deg)** (%)
EP1	640	620	13.5	11.1*	49.7	31.6	4.30	2.17
EP2	660	660	10.8	10.5	54.4	50.5	3.88	3.50
EP4	680	680	8.47	7.79	48.5	45.2	2.80	2.40
EP6	660	620	12.5	8.86*	35.9	27.3	2.96	1.50

Table 6.1: : Electrical parameters of OSC comprising materials EP1,2,4, and 6 under AM1.5 conditions, in the pristine state (p) and after 50 hrs at 50°C (deg). An asterisk marks values that have been reached after an intermediate increase of the respective parameter at short degradation times.

6.3.2 Generation of extractable carriers

Femtosecond spectroscopy, in combination with global and target analysis, is used to address photoexcitation dynamics of singlet excitons, triplet excitons and polarons (labelled as S, T and P, respectively). In figure 6.2 and 6.3, we show transient absorption (TA) spectra of all devices, both pristine and degraded conditions, at t = 0.39 ps and 335 ps. In order to disentangle the strongly superposed contributions from S, P, and T a spectral decomposition has been performed, globally fitting all TA spectra over the whole time range from 0.3 to 400 ps at all pump intensities and both degradation states with a common spectral model with a single set of spectral parameters. In short, we assume that after 100 ps, the S population is very low, allowing us to model all available TA spectra for t > 100 ps assuming only T and P. Assuming that T is at least partly created by nongeminate P recombination – which has been shown recently in a similar set of materials[159]– we assign the band that grows under high intensity pumping to T, and the rest of the TA bands to P. Justification of the assignment is obtained when one set of spectral shape parameters fits all experimental situations resulting in very different T/P ratios. Then the spectral shape parameters are fixed, and the whole dataset is fitted including the S states.

Figures 6.2 and 6.3 show that the spectral shapes and energetic positions for the S, P, and T states are rather similar for all studied materials. Singlet excitons show a rather broad absorption from 1.0 to 1.2 eV, caused by a strong vibronic progression which is typical for PA bands of first excited singlet states. The polaron absorption is characterized by two absorption bands which are not caused by vibronic coupling but refer to different electronic states, at 0.8 and 1.4 eV. Triplet-triplet absorption, finally, is characterized by a single and relatively sharp band at 1.1 eV. The absence of vibronic coupling is typical for triplet states.[168]

The inspection of the TA spectra, together with their decomposition into contributions for S, P, and T, yield valuable qualitative insight into the reason for the observed electrical performance of the materials in solar cells, and their susceptibility to thermal degradation. In EP1 at 0.39 ps, we find that the amount of P is clearly decreased after 50 hours of thermal treatment, showing that the yield of ultrafast carrier generation is decreased. This behaviour has been found before in P3HT:PCBM and attributed to a growth of polymer rich domains, such that a significant amount of excitons can only dissociate upon diffusion towards the D/A interface, a picosecond process.[128] We show however below that in EP1, exciton diffusion

does not create many additional polarons, which may be caused by impurities of the donor rich phase like, molecularly dissolved PCBM. Thus, since thermal degradation in EP1 replaces highly efficient ultrafast charge generation by less efficient diffusion mediated charge generation, we can expect a drop of J_{sc} resulting from thermal degradation, in agreement with Table 6.1.

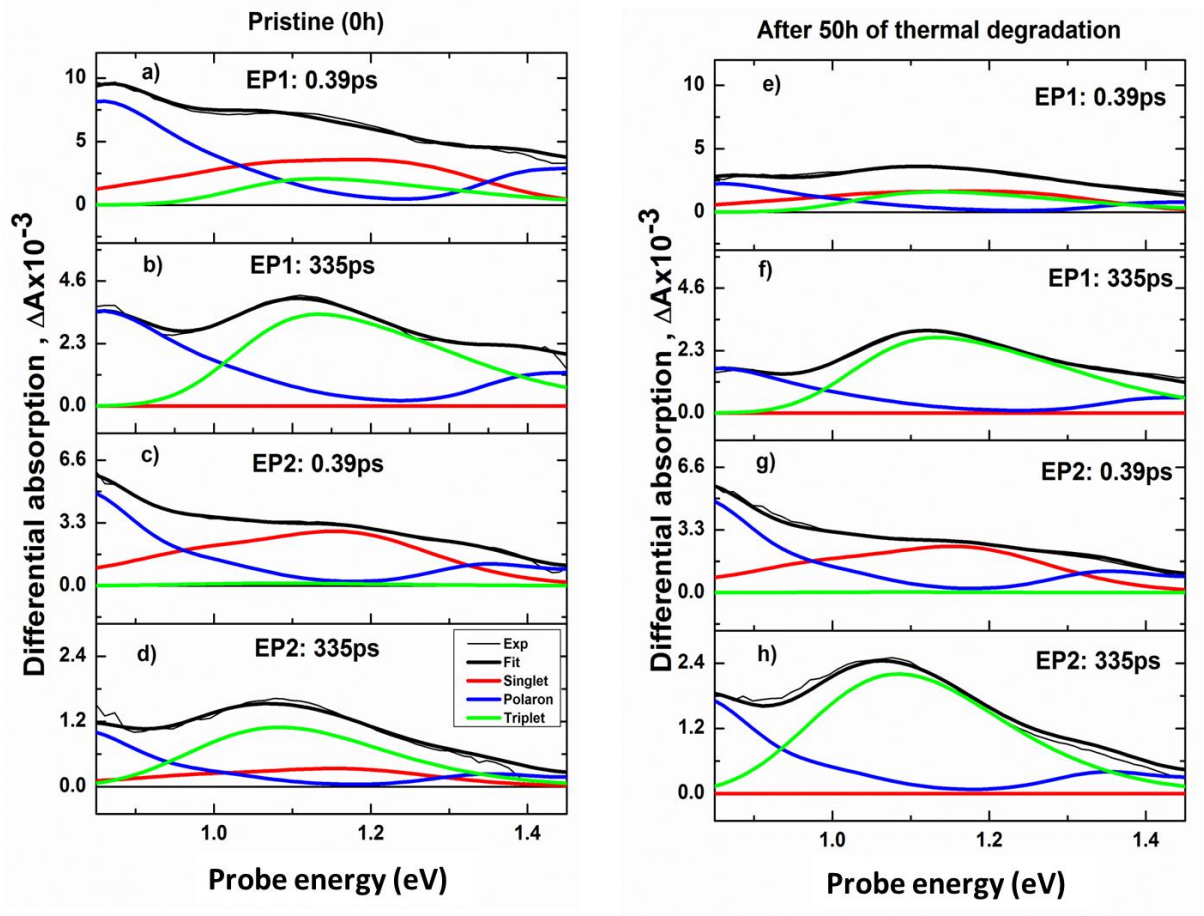

Figure 6.2: Transient absorption (TA) spectra at different pump-probe delay times (given in ps) for EP1 and EP2 (panels a, b, e, and f, and panels c, d, g, h, respectively), before and after thermal degradation (thin black curves in left and right panel, respectively). Thick black curves are global fits according to a spectral model (for details see supplementary material). Isolated contribution from singlet, triplet, and charged states are given as red, green and blue curves, respectively.

If we compare the TA spectra before and after thermal degradation at t = 335 ps for EP1 (figure 6.2 b and f, respectively), we find that the T/P ratio is much more on the side of the triplet after thermal degradation. This observation can be explained by enhanced nongeminate recombination due to the thermal treatment. In contrast to EP1, the spectral changes upon thermal treatment in EP2 are very contained, see figure 6.2. At t = 0.39 ps, the polaron band at 0.8 eV is very strong, indicating a high yield of ultrafast polaron generation and thus a high interfacial area between donor rich and acceptor rich phases, which is still the same after 50

hrs of thermal treatment. And also note that EP2 is the only one device which shows negligible ultrafast triplet generation. These findings are in agreement with the relative thermal stability of both the electrical performance and the morphology of EP2.[37]

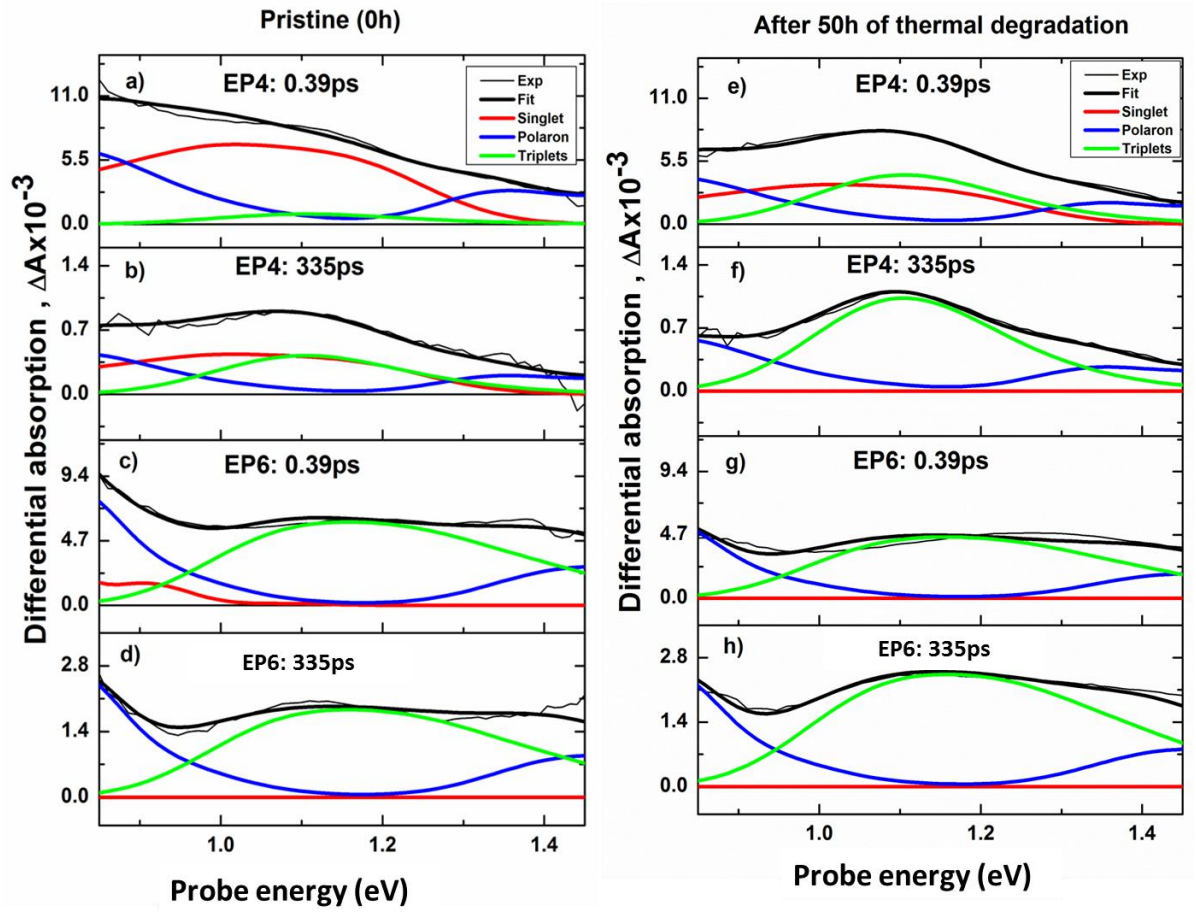

Figure 5: *Transient absorption (TA) spectra at different pump-probe delay times (given in ps) for EP4 and EP6 (panels a, b, e, and f, and panels c, d, g, h, respectively), before and after thermal degradation (thin black curves in left and right panel, respectively). Thick black curves are global fits according to a spectral model (for details see supplementary material). Isolated contribution from singlet, triplet, and charged states are given as red, green and blue curves, respectively.*

At early delay times, EP4 behaves similarly to EP1, in that the contribution of ultrafast polaron generation is reduced upon thermal treatment, compare panels *a* and *e* in figure 6.3, and that the overall amount of polarons is reduced by the thermal treatment, showing that exciton diffusion mediated polaron generation is not very efficient. However, the most striking observation in the TA spectra of EP4, even before thermal treatment, is the particularly short polaron lifetime. As we will show later by a target analysis, this is not an effect of the high fluences reached by femtosecond spectroscopy, but mainly caused by geminate recombination, which is independent of pump intensity. From this we conclude that generation losses under solar conditions are very strong in this material, explaining the fact

that in Table 6.1, EP4 has the lowest J_{sc} value of all materials in the series. In EP6 finally, we find very little evolution of the TA spectra with time, intensity or degradation. This means that very few singlet states are formed, and that thermal treatment, although resulting in the formation of major crystallites, does not cause a significant change in the charge generation mechanism.

In order to quantify these observations, especially with respect to polaron formation and decay, we performed a target analysis of the time-dependent spectral weights of S, P, and T, obtained from spectral fits like in figures 6.2 and 6.3 across the whole time scale. A complication of the numerical modelling in solid state samples is the fact that the ensemble kinetic model cannot be assumed to be homogeneous, as the pair correlation function between the reaction partners, such short time after creation of the photoexcitations, cannot be assumed to be in the stationary state.[32] Therefore, we set all rate constants to be time-dependent according to a dispersive model:

$$\frac{dp}{dt} = g + k_d(t) \cdot S - k_g(t) \cdot P - k_{ng}(t) \cdot P^2 \tag{6.1}$$

Herein, *P (S)* is the time-dependent concentration of polarons (singlet excitons), g is the rate for immediate polaron formation at the interface, k_d is the rate constant for diffusion-mediated polaron formation. Polaron decay is given by geminate monomolecular recombination and non-geminate bimolecular recombination (rate constants k_g and k_{ng}, respectively). The time dependence of all rate constants is given by;

$$k_\alpha(t) = k_\alpha^0 \cdot \left(\frac{t}{1ps}\right)^{-\gamma_\alpha}, \text{ where } \alpha \epsilon \{d, g, ng\}. \tag{6.1a}$$

We use equation 6.1 to fit the time-resolved polaron concentrations for all pump intensities globally, but separately for pristine and degraded samples. The rate constants are summarized in Table 6.2, and the time-resolved polaron yields are shown, together with the fits, in figure6.4, for the highest and lowest pump intensities only. Due to the fact that the photoexcitation dynamics have been fitted globally at different pumping intensities, we can clearly distinguish non-geminate recombination from the geminate one. Both contributions to charge recombination have a quite distinct influence on the electrical performance of the OPV device: while geminate recombinations limits the amount of extractable carriers irrespective of illumination intensity and therefore reduces J_{sc}, non-geminate recombination depends on illumination intensity; under solar irradiation this loss process occurs on a

nanosecond to microsecond time scale and therefore is in competition with charge extraction. For this reason, non-geminate recombination tends to reduce the fill factor. In the following, we will discuss the isolated contributions to the electrical performance one by one.

Figure 6.4 shows that the polaron yields in the subpicosecond regime do not significantly depend on pump intensity; this shows that at the pump fluences that we used, high intensity effects like, two-photon absorption and sequential excitation, do not contribute to the measured data, the results reflect therefore low-intensity behaviour of the samples and are significant also for operational conditions. In the following, we will first discuss the observations in the pristine device, and then we will discuss effects arising from thermal degradation.

In all panels of figure 6.4, we can clearly distinguish contributions from ultrafast charge carrier generation (occurring on a timescale of $t < 200$ fs) from exciton diffusion mediated charge carrier generation (occurring on a 1-5 ps time scale in competition with the onset of geminate recombination). We find that the ultrafast carrier yield in pristine films decreases monotonously from EP1 (40%) via EP 2 and EP4 to EP6 (< 20%). It is interesting to note that the surface roughness in AFM micrographs of the same materials follows exactly the opposite trend.[37] Although the surface roughness is not a direct measure of the domain size in the bulk of the active material, it can still be taken as an approximate measure of crystallization tendency of the respective blends. As crystallite formation decreases the effective interfacial area between donor and acceptor rich phases, the probability of singlet excitons being created close enough to the interface to be dissociated immediately, is expected to decrease, causing the reduction of the ultrafast carrier yield as observed in figure 6.4. Concomitantly, the probability of excitons to be created far from the D/A interface, is higher in materials with a higher crystallization tendency, causing an increased contribution of delayed charge carrier formation to the overall charge carrier yield. This effect can be also seen in figure 4: while in EP1 and EP2, delayed charge carrier formation increases the overall charge carrier yield by only about 5%, more than 10% increase is observed in EP4 and EP6. Under our experimental conditions, maximum charge carrier yields are reached in about 1 ps, the overall yield from both processes being in the range of 30-40 % for all materials. This finding shows that if exciton diffusion is efficient, the total charge carrier yield is relatively robust against morphological details.

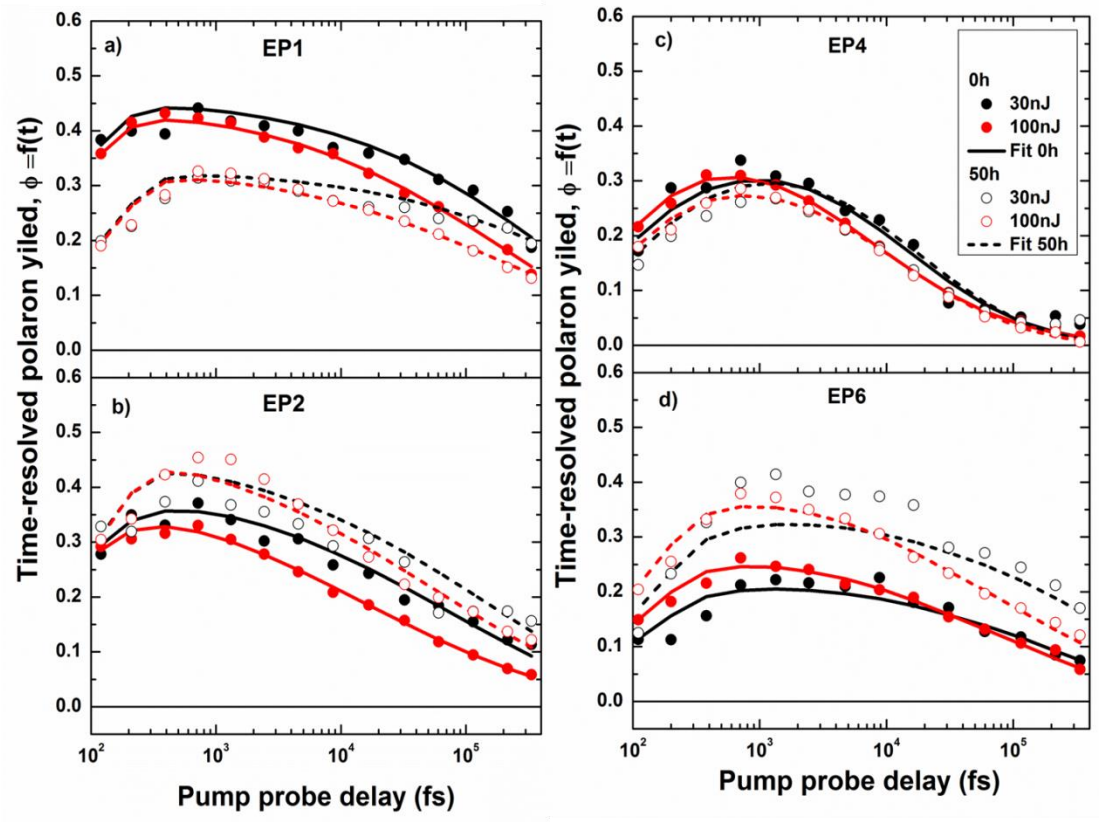

Figure 6.4: *Dynamics of charge carriers in the donor polymer after 150 fs pulses at 775 nm with low and high pump energy (black and red symbols, respectively), obtained as time-resolved spectral weights of the polaron bands in the spectral fits in Fig.2 and 3. Solid and open symbols refer to pristine and degraded samples, respectively, and are fitted by a target model comprising all significant processes occurring on a picosecond time scale (solid and dashed curves, respectively). Details of the target model are given in the supporting material*

Given the fact that all materials show overall charge carrier yields in the range of 30-40 %, it seems surprising at first sight why the J_{sc} values vary over nearly a factor of two. However, the consideration of the rate coefficients for geminate recombination k_g in Table 6.2 fully explain this discrepancy: the rate of geminate recombination increases in the order EP1 < EP6 < EP2 < EP4, while the J_{sc} values decrease exactly in the same order. Thus, we can clearly assign the low J_{sc} values in EP4 to one predominant loss mechanism, namely geminate recombination. It has been shown that geminate recombination is strongest when the domain size is small because under these conditions the probability of island formation is high.[128]However, This scenario does not explain the particularly high rate of geminate recombination in EP4, which has intermediate AFM roughness and relatively low yield of ultrafast charge formation, both arguing against a small domain size. This example shows

that electronic factors (charge mobility and influencing the precise energetics of polarons at the interface

Device	k_{ng} (p)	k_{ng} (deg)	k_g (p)	k_g (deg)	γ (p)	γ (deg)
EP1	0.0048	0.01	2.1e-5	8.3e-6	0.544	0.544
EP2	0.033	0.014	4.7e-5	4.1e-5	0.61	0.61
EP4	0.035	0.025	2.0e-3	1.7e-3	0.556	0.556
EP6	0.01	0.017	2.4e-5	1.3e-5	0.499	0.499

Table 6.2: Parameters obtained after performing a target analysis of the time-dependent spectral weights of S, P, and T. Where k_{ng} is non-geminate recombination rate, k_g is geminate recombination rate and γ is dispersiveness parameter.

compared to polarons in the bulk) can be more important than pure morphological considerations. From charge extraction measurements (vide infra, electrical measurements section), we find that the charge mobility of EP4 is not higher than in the other polymers. On the other hand, we find that also the rate coefficient for non-geminate recombination (k_{ng} in Table 6.2) is the highest of all studied samples. We therefore conclude that the sub-Langevin factor for EP4 is lower than in the other materials.[71] As it has been shown recently that pure morphological considerations can only explain a sub-Langevin factor down to 0.1, is clear that when very low sub-Langevin factors are obtained, electronic factors must play a significant role in "rejecting" a polaron that dwells in the bulk of the donor-rich phase, from reaching the interface.[169] We suggest therefore that EP4 lacks this rejecting mechanism, which enhances the rates for both geminate and non-geminate recombination.

We have shown now that the findings from femtosecond spectroscopy can explain the electrical performance of pristine devices and clearly relate sample-specific performance deficits to specific loss channels. In the following we will show how thermal degradation affects these specific loss channels.

In figure 6.4a, is shown that after 50 hrs of thermal treatment, the ultrafast carrier yield drops dramatically in EP1, from initially 40% to below 20%, while the drop is rather small in the other materials. In line with the above reasoning, this can be understood by an increase of the domain size, causing a sharp decrease of the ultrafast carrier yield only for those samples that adopt a close to optimum domain size in the pristine case. This is the case for EP1, while the other materials have a higher crystallization tendency so that already in the pristine case the delayed charge generation mechanism is dominant, and a further increase of the domain size does not lead to a strong further reduction of the ultrafast carrier yield.

In order to understand electrical performance loss upon thermal degradation, we need to take into account all three factors that govern the amount of extractable carriers, namely, ultrafast carrier generation, diffusion-mediated carrier generation and geminate recombination. We find for EP1, that diffusion-mediated charge carrier formation increases from about 5% to about 10% of the total charge carrier yield, which is however not enough to counteract the over 20% reduction of the ultrafast carrier yield. There is obviously a picosecond exciton quenching process reducing the exciton diffusion yield in the degraded EP1 sample. However, Table 6.2 shows that the amount of geminate recombination is reduced in EP1 upon thermal degradation. We can thus explain the finding in Table 6.1 that J_{sc} first increases (due to a reduction of geminate recombination) but then decreases at higher degradation times when the domains get too large for exciton diffusion to be efficient.

In EP2, neither ultrafast nor diffusion mediated charge generation change significantly upon thermal degradation. Since also the geminate recombination coefficient drops only slightly, we expect that J_{sc} be independent of thermal degradation, in agreement with experiment. In EP4, we find a small reduction of the ultrafast carrier yield which is not fully made up for by an increase of the delayed carrier yield. Since also the geminate recombination rate is only very slightly reduced, we can explain the small reduction of J_{sc} in EP4 in Table 6.1.

In EP6 finally, we do not find a significant change of the overall charge generation yield upon thermal treatment. Since the geminate recombination coefficient is strongly reduced, we would expect an increase of the extractable carrier yield (which is indeed displayed in figure6.3 at t=355 ps), which however contradicts the observation of a strong J_{sc} reduction EP6 upon thermal treatment. We note that in EP6, there is much less evolution of the relative concentrations of S, P, and T with pump intensity and degradation, such that the reliability of the spectral model – and thus of the time-resolved concentrations – is less than in the other materials. However, this uncertainty affects mainly the distinction between the contributions from singlet and triplet states while the spectral model of the polarons is quite distinct from the other photoexcitations. We therefore tend to trust in the notion of a rise of the yield of extractable carriers with thermal degradation in EP6. The discrepancy between the rise of the yield of extractable carriers and the drop of J_{sc} upon degradation is thus formally explained by a drop in the device effective area for charge extraction. In fact, AFM studies show that EP6 is the only material forming large crystallites upon thermal treatment.[37] Those device regions close to the crystallite will not show significant photocurrents (because of

delamination from the selective contacts) and thus need to be discounted from the device effective area.

Here, we relate the notions found above to the substitution pattern of the materials. We found that in the pristine case, the amount of geminate recombination is decisive for the observed J_{sc}. The rate of geminate recombination strongly decreases with increasing intermolecular interaction, leading to an increase of J_{sc}. In EP4, the only compound with a bulky C10-C12 branched aliphatic chain on the acceptor moiety of the polymer, intermolecular interaction is strongly inhibited. Moreover, the lack of substituents at the donor moiety positions induces voids which can accommodate small PCBM crystallites. Geminate recombination is therefore orders of magnitude faster than in the other materials, causing a very small J_{sc} value despite good matching with the solar spectrum. It can also be understood why the J_{sc} in EP4 does not further decrease strongly upon degradation, see Table 6.2: there simply is no driving force for morphological changes from the polymer side; only the PCBM crystallites tend to increase in size albeit limited by the voids in the donor polymer.

The other polymers have smaller branched aliphatic C4-C6 chains on the acceptor moiety of the polymer, enabling a good degree of interchain interaction and encouraging the formation of a bulk heterojunction with high J_{sc} values. It is now the choice of the substituents on the donor moiety which controls long term stability: if only n-aliphatic chains are present as in EP2, good order is induced, as in the well-known example poly-hexyl thiophene. Ordering has positive consequences on the effect of domain size growth: although morphological evolution is clearly present (see reduction of geminate recombination in Table 6.2), it doesn't seem to have any effect on the ultrafast carrier yield. This can be understood by the fact that the exciton wavefunction is extended over an ideally conjugated segment of a polymer. If the order is high, then most excitons will still have wavefunction overlap with the D/A interface, even when the domains are growing. In contrast, EP1 (with alkoxy chains) or EP6 (with an extra thiophene unit) cause strong inductive or mesomeric effects, respectively and thus lead to strong free energy losses upon further crystallization.

As noted above, the bimolecular recombination coefficient is related to FF losses. Indeed, those materials showing strong thermally induced FF losses, namely EP1 and EP6, show a strong increase of the nongeminate recombination coefficient (k_{ng} in Table 6.2) In contrast, those materials showing only a small FF loss, namely EP2 and EP4, show a thermally induced reduction of nongeminate recombination in the femtosecond experiment. We note

however, that apart from k_{ng}, a multitude of other factors contribute to FF loss, which are better analysed in the microsecond time range (vide infra).

6.3.3 Charge extraction and nongeminate recombination

Under operational conditions, the charge carrier density in the device is governed by charge generation, recombination and extraction according to;

$$\frac{dn}{dt} = G - k_L(n) \cdot n \cdot n - \mu(n) \cdot n \cdot \frac{E_{bi}}{d} \tag{6.2}$$

where $\mu(t)$ is the effective charge carrier mobility, which in disordered polymer materials usually depends on the carrier concentration $n(t)$,G is the photo-induced generation of extractable charge carriers, and k_L is the bimolecular charge recombination coefficient, assuming Langevin recombination:

$$k_L(t) = 2 \cdot e \cdot \mu(n) \cdot f_{LV} / (\varepsilon \cdot \varepsilon_0) \tag{6.3}$$

Herein, $\mu(n) = \mu_e(n) + \mu_h(n)$ is the sum of the time-dependent mobilities for positive and negative charges, respectively, ε is the relative dielectric constant, ε_0 is the dielectric constant in vacuum, and f_{LV} accounts for sub-Langevin recombination, as often observed in BHJ active layers.

In order to quantify charge recombination, we measured charge decay curves by means of microsecond TA dynamics in OSC under open circuit conditions at a probe wavelength of 1300 nm, after pumping with a pulsed LED at 780 nm for periods long enough to reach the stationary state at various different pumping intensities in the range of 0.01 sun up to 0.1 sun. For each degradation condition, we fitted the resulting charge carrier dynamics globally by numerically solving equation 6.2, setting the generation and the extraction terms to zero and describing the charge density dependence of the charge mobility empirically via its time dependence by;

$$k_L(t) = k_L^0 \cdot \left(\frac{t}{1\mu s}\right)^{-\gamma} \tag{6.4}$$

where k_L^0 is the value of k_L for t = 1 µs after termination of illumination, and γ is the dispersiveness parameter. In figure6.5, we show values for k_L^0 and γ (panel *a* and *b*, respectively) as function of annealing time, as resulting from the global. In the pristine case, the recombination values cover two orders of magnitude, EP2 showing the fastest recombination and EP4 the slowest one, see figure 6.5a for t = 0 hrs. Upon thermal annealing,

the recombination parameters for EP2 and EP6 decrease dramatically over nearly two orders of magnitude, while for EP4 only a slight decrease is obtained and EP1 even shows a slight increase of the recombination parameter. According to equation 6.3, we can associate changes of k_L with changes of either the charge mobility $\mu(n)$, or the sub-Langevin parameter f_{LV} (the relative dielectric constant, another material specific parameter present in equation 6.3, is not expected to change strongly, given the electronic similarity of the compounds).

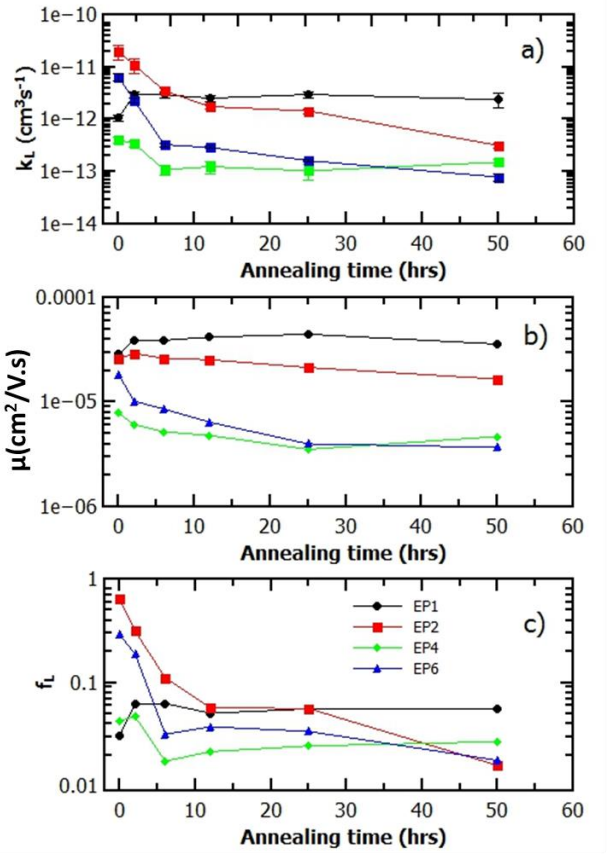

Figure 6.5: a) Charge recombination parameter k_L as obtained from global fitting to charge carrier dynamics according to equation 6.2 under open circuit conditions; b) effective mobility μ_{eff} obtained from global fitting of TPC transients according to eq. 6; c) sub-Langevin parameter f_L as obtained from equation 6.3 using the values from panels a) and b)

In order to disentangle the contributions from $\mu(t)$ and f_{LV} to the charge recombination coefficient, we measured time-resolved photocurrents (TPC) under quasi-open circuit conditions (measuring the voltage across a 50Ω termination). According to equation 6.2, the extraction current I_{extr} is given by;

$$I_{extr} = \frac{dn_{extr}}{dt} = \mu(n) \cdot n_{SS} \cdot q \cdot \frac{E_{bi}}{d} \tag{6.5}$$

In order to determine the effective charge mobility under operational conditions, we exploit the fact that under short circuit conditions the extraction time is much faster than the

recombination time. Therefore, we can ignore the recombination term in equation 6.2 and write for the normalized population decay due to extraction, considering also equation 6.5;

$$\frac{dn}{n_{ss}dt} = \frac{dI}{I_{ss}dt} = -\mu(n).(n/n_{ss})\frac{E_{bi}}{d} \tag{6.6}$$

For the population dependence of the charge mobility, we use the empirical formula;

$$\mu_{eff}(n) = \mu_{eff}(n_{ss}) \cdot \left(\frac{n}{n_{ss}}\right)^{\beta} \tag{6.7}$$

Which is due to its monotonous nature should describe the density of states distribution close to band edges reasonably. We measured TPC transients after long enough irradiation to reach the stationary current I_{ss} and fitted them globally for a series of illumination strengths between 0.01 and 0.1 sun using equation 6.6. Using a built-in voltage of 0.7 V and a thickness of the active layer of d = 250 nm, we obtain the effective extraction mobilities given in figure 6.5b. First, note that for all materials, the effective mobilities are low, typically in the range of 10^{-5} to 10^{-4} cm^2/Vs, which is about an order of magnitude less than the mobilities of high order polymers like, P3HT.[65] The second observation is that upon degradation, the effective charge mobilities in figure6.5b follow the same trend as the recombination coefficients k_L in Fig. 6.5a, but not for EP2. In EP1, both k_L and μ_{eff} are increasing with degradation time; both quantities are decreasing with degradation time for the other materials except EP2, where the change in mobility is very less and thus explains the better performance against degradation. On first glance, this notion is to be expected since in equation 6.2, both recombination and extraction depend on the charge mobility. However note that the relative change of k_L is much stronger than the change of μ_{eff} in EP6 for example, a degradation-induced reduction of k_L by two orders of magnitude corresponds to a reduction of μ_{eff} by less than one order of magnitude. In the above equations there are three candidate parameters able to explain this discrepancy:

(i) In equation 6.5, a degradation induced increase of E_{bi} (which we set constant in the global fitting of figure 6.5b) could have led to an overestimation of the mobility at higher levels of degradation. However, such an increase of E_{bi} is hard to explain in our devices. We can also exclude a degradation induced reduction of E_{bi} due to shielding of space charges, because in the modelling of TA dynamics for figure6.5a, we did not observe any evidence for the presence of space charges.[32]

(ii) Due to a degradation induced higher ordering of the materials, the anisotropy of the

relative dielectric constant ε in equation 6.3 (which given anisotropic charge mobility would lead to an increase of the effective isotropic value of ε) might have increased, contributing to the degradation induced reduction of k_L. While we cannot exclude such scenario, we note that charge recombination occurs predominantly at the D/A interface. Thermal degradation might induce crystal growth and thus a relative reduction of the interfaces is, but the electronic structure of the interface should stay the same.

(iii) A reduction of the sub-Langevin factor f_L in equation 6.3 might have contributed to the strong degradation-induced reduction of k_L. We consider scenario (iii) the most plausible one, because of the strong morphology dependence of f_L.[169] In figure6.5c, we show the evolution of f_L as function of degradation, obtained by inserting the values of figure6.5*a* and *b* into equation 6.3. As expected, the values of f_L decrease with degradation time for EP2, 4, and 6, while an initial increase of $f_L$is observed for EP1.

Various scenarios can explain a decrease of f_L with thermal degradation. An increase of the domain size will reduce the effective interfacial area and thus the recombination rate. We indeed concluded from the target analysis of the femtosecond TA spectra of EP1 and EP4 that the effective interfacial area is reduced. On the other hand, a reduction of the effective interfacial area is supposed to increase the mobility, as interfaces are reflecting barriers for charge carriers of either type, reducing the overall drift velocity and thus the mobility. We therefore favour a scenario in which thermal degradation fosters a demixing of donor and acceptor rich areas along the stack direction. Such a vertical demixing would yield a strong reduction of the interface area, while it would also reduce the number of direct percolation channels towards the extraction layers for the respective carrier types. Most carriers would therefore need to use stochastic diffusive motion between various percolation paths until one is found that is not a dead end. The effective mobility along the stack direction (which is the one measured by TPC transients - is therefore expected to be reduced upon vertical demixing.

6.4 Conclusions

In conclusion, we have quantified the elementary processes in the photovoltaic event chain of organic solar cells comprising PCBM as acceptor and a polymer of the PBDTDPP class as donor polymer, in the pristine state and after thermal degradation. Different substituents at the PBDT and/ or DPP moieties showed strong specific effects on the elementary processes, especially with respect to degradation. We therefore can now present a detailed mapping of

substitution patterns to the susceptibility to morphology evolutions and finally to the resulting stability of device performance. This leads to clear design rules for matching high initial performance with long term stability: from the above results, the crucial point seems not to avoid morphological evolution, but to provide a morphology that maintains high electrical performance even when morphology changes to a certain extent. The formation of a bi-continuous network requires significant interchain interactions, therefore the substituents should not be too bulky. N-alkyl substituents at the PBDT moiety induce ordering, leading to significant performance tolerance towards domain growth. The example EP2 showed that although the thermally induced reduction of both geminate and non-geminate recombination are clear signs of domain growth, the yield of ultrafast carrier generation remained stable. This can be understood by the fact that higher order enables a higher extension of the extension of the wavefunction of the singlet exciton, so that even in larger domains, most excitons still have wavefunction overlap with the D/A interface, allowing for ultrafast carrier generation.

The use of unsymmetric substitution patterns should be avoided, as it reduces ordering and creates voids that can be filled up with small acceptor aggregates. In the example of EP4, the absence of substituents on the PBDT moiety causes huge geminate recombination losses and concomitantly disappointing J_{sc} values.

Using substituents with inductive and/or mesomeric effects is critical as well. The examples EP1 and EP6 show that although these substituents cause high initial J_{sc} values, the devices are very unstable against thermal degradation. From the evolution of both k_L and μ_{eff}, we conclude that apart from domain size growth, these substituents might also have specific affinities to one or both of the selective contacts, leading over time to a demixing of donor and acceptor rich domains along the stack direction, penalizing the fill factor and possibly also J_{sc}. These effects are found to be of minor importance in EP2, carrying purely aliphatic substituents and showing stable mobilities, Jsc and FF values.

Chapter 7

Conclusiones y outlook

7.1 Conclusiones

El insuficiente tiempo de vida útil de las celdas solares orgánicas es un gran obstáculo para la comercialización masiva de las mismas. Los efectos de la degradación química y el estrés térmico en la capa activa de las OSC son aún poco conocidos. Teniendo lo anteriormente expuesto en consideración, esta tesis investigó los efectos de la foto-oxidación y la degradación térmica en una serie de celdas solares orgánicas construidas a partir de polímeros conjugados de pequeña y media banda prohibida tales como el P3HT, el Si-PCPDTBT, el KP115 y el BDT:DPP, todos incorporados con el $PC_{61}BM$, considerado como el receptor de electrones por excelencia. Además también fueron estudiados los cambios relacionados a los procesos fundamentales luego de la foto-oxidación. Entre las técnicas experimentales empleadas para investigar estos efectos de degradación se encuentra la espectroscopía de absorción transitoria (TAS, por sus siglas en inglés) a través de una amplia gama de escalas temporales que van desde femtosegundos a milisegundos, con el objetivo de explorar las relaciones estructura-propiedad en los dispositivos antes y luego de la degradación. Además de espectroscopía de absorción resuelta en el tiempo (TAS, por sus sigla en inglés), técnicas eléctricas transitorias complementarias como la medición del foto-voltaje resuelto en el tiempo (TPV, por sus siglas en inglés), la medición de la foto-corriente resuelta en el tiempo (TPC, por sus siglas en inglés) y la medición de la extracción de carga al incrementar linealmente el voltaje (CELIV, por sus siglas en inglés) también se utilizaron para monitorear y controlar las pérdidas de rendimiento por degradación inducida en las celdas solares orgánicas.

Estudios de absorción resuelta en el tiempo realizados en filmes y dispositivos de P3HT:PCBM mostraron que la tasa de recombinación es mayor en aproximadamente un factor de dos en los filmes que en los dispositivos. La menor tasa de recombinación en los dispositivos se explica debido a una separación parcial de portadores positivos y negativos por el campo incorporado. Por otra parte, se llevaron a cabo estudios sobre la influencia del efecto de la altamente conductora capa intermedia de PEDOT:PSS en el transporte de

portadores de cargas. Mediante la realización de estudios de absorción resuelta en el tiempo con diferentes grados de superposición espacial entre el pulso de excitación y el pulso de análisis, se encontró una clara acumulación retardada de densidad de carga cuando dichos impulsos de excitación y análisis no se encontraban superpuestos. Sin embargo, la dinámica de decaimiento final del polarón resulto ser independiente del grado de superposición alcanzado. Estos hallazgos apoyan la teoría de rápida difusión lateral a través del PEDOT, permitiendo a los polarones su difusión en toda la zona activa a su disposición. Estudios complementarios realizados en los espectros de absorción foto-inducida (PIA, por sus siglas en inglés) mostraron una clara confirmación de la ruta de recombinación ofrecida por el PEDOT:PSS en las celdas solares de P3HT:PCBM.

La influencia del oxígeno en celdas solares no encapsuladas de P3HT:$PC_{61}BM$ y Si-PCPDTBT:PCBM fue examinado mediante la exposición de los dispositivos a aire sintético bajo condiciones específicas. Se encontró que la tasa de generación de carga apenas cambia durante la foto-oxidación, lo que sugiere que el rendimiento de la extracción de cargas es prácticamente independiente del nivel de degradación. Sin embargo, la degradación inducida por el oxígeno provocó una fuerte reducción del coeficiente de recombinación de carga, que se corresponde formalmente con una reducción de la movilidad de los portadores de carga. Se observó además una desviación en el orden de recombinación (de bimolecular puro a seudomonomolecular) para el P3HT, mientras que la recombinación de Si-PCPDTBT claramente proviene de un modelo bimolecular puro incluso en el caso cuando no existe degradación de los dispositivos. La tasa de extracción de portadores de carga fue aún más seriamente reducida por la foto-degradación de lo esperado, a partir de los cambios de movilidad calculados, a partir de la expresión de recombinación, lo que conduce a la pérdida de corriente de cortocircuito en los dispositivos degradados. Mientras que la tasa de extracción es superior a la de la recombinación por dos órdenes de magnitud en las muestras sin degradación, ambas tasas son más o menos iguales en las muestras que se encuentran fuertemente degradadas. Las mediciones de foto-extracción de carga al incrementar linealmente el voltaje (photo-CELIV, por sus siglas en inglés) confirman la reducción de la movilidad y la fuerte reducción de las cargas extraíbles debido al aumento en la densidad de portadores de fondo.

El cálculo de la reducción de la eficiencia cuántica interna (IQE, por sus siglas en inglés) en función del factor de sub-Langevin (f_{LV}, por sus siglas en inglés), de la concentración de portadores de fondo foto-inducida (cb), y de la movilidad efectiva de los portadores de carga

(μ), mostró que a valores razonables de f_{LV}, la movilidad juega un papel más importante que cb, pero que ambos efectos podrían no ser suficientes para explicar la fuerte reducción de corriente de corte circuito ($J_{SC,}$ por sus siglas en inglés) observada luego de la foto-oxidación. Esto sugiere que el aumento de la densidad de portadores de fondo introducido por la irreversible degradación, contribuye a la pérdida de corriente de cortocircuito, ya que actúa como un escudo frente a la extracción en la mayor parte de los dispositivos, lo que se corresponde con una disminución de E_{bi} y por lo tanto conduce a una mengua adicional de la eficiencia de la extracción. Esta disminución adicional conduce a un tiempo de permanencia más largo de los portadores foto-generados en el dispositivo, lo que a su vez conlleva a una mejora significativa de la recombinación en la reacción de seudo-primer orden observada en las mediciones de absorción resueltas en el tiempo, lo cual constituye un efecto similar al observado en celdas solares invertidas de P3HT:PCBM altamente degradadas.

Los estudios realizados sobre la influencia de la foto-oxidación en el rendimiento eléctrico en las celdas solares de KP115:PCBM sugirieron que la enorme pérdida observada en la corriente de cortocircuito (Jsc, por sus siglas en inglés) se debe a los efectos combinados de la reducción de la movilidad y la formación de dominios aislados de donante-aceptor sin la presencia de caminos de infiltración eficaces hacia los electrodos. A diferencia de los casos anteriores en las celdas de P3HT:PCBM y Si-PCPDTBT:PCBM, la foto-oxidación de KP115:PCBM no altera el orden de recombinación y no crea portadores de fondo, que son los principales causantes del efecto de deterioro del rendimiento en el caso de las celdas de P3HT:PCBM luego de la foto-oxidación. También se observó al realizar mediciones de foto-corriente con resolución temporal, que incluso en dispositivos no degradados de KP115:PCBM , la extracción de carga es incompleta, lo que indica que la morfología no es la óptima. Estudios adicionales se deben hacer en este material con el fin de explorar y mejorar la estabilidad frente a otros desencadenantes de la degradación como son la humedad y la temperatura.

El último capítulo de esta tesis trata sobre la degradación térmica. En función de la región geográfica de empleo, las OSC pueden alcanzar hasta 80°C en condiciones operativas. Visto que la nano-morfología óptima en términos de eficiencia a menudo no es la más estable termodinámicamente, las elevadas temperaturas tienden a evolucionar la nano-morfología en la capa activa de las celdas hacia el equilibrio termodinámico, causando una pérdida del rendimiento eléctrico. Una serie de OSC que emplean novedosos polímeros de pequeña banda prohibida del tipo DPP, con diferentes cadenas laterales, fue proporcionada por Merck

Ltd, Southampton. Las cadenas laterales tienen una influencia insignificante sobre la estructura electrónica, mientras que influyen fuertemente en la interacción intermolecular, esta serie de compuestos proporcionados da una oportunidad única para abordar específicamente la influencia de la interacción intermolecular de los procesos elementales de la fotovoltaica orgánica, y su sensibilidad hacia los cambios morfológicos inducidos térmicamente. En términos generales se encontró que todos los polímeros a base de DPP muestran la generación de tripletes como canal de pérdida de la eficiencia. Por lo tanto, aunque la generación de carga conlleva a altas eficiencias externas, debido a la pequeña banda prohibida de los polímeros empleados, un alto porcentaje de las cargas foto-inducidas no puede ser extraído debido a las pérdidas por recombinación geminada y no geminada. Se observó una dependencia muy específica de las tasas de recombinación en los sustituyentes del donador de electrones benzotiofeno (BDT, por sus siglas en inglés). En ausencia de sustituyentes, se observó una tendencia muy fuerte a la recombinación geminada, mientras que en la presencia de un sustituyente aromático, se encontró que la recombinación non geminada era aquella que prevalecía. El uso de sustituyentes alifáticos, por otra parte, causa solamente una recombinación limitada, y proporciona una mayor estabilidad de rendimiento eléctrico frente a la degradación térmica.

7.2 Outlook

En esta sección, se realiza un estudio de las futuras líneas de investigación. A pesar de los notables avances logrados en el campo de las celdas solares orgánicas, el actual estado del arte es todavía primitivo en relación con el tiempo de vida operacional requerida. Uno de los grandes problemas el logro de la estabilidad a largo plazo es la comprensión de los mecanismos de degradación, especialmente bajo oxígeno, humedad y altas temperaturas. Esta tesis tiene como objetivo contribuir a desentrañar los problemas de estabilidad mediante la asignación de procesos elementales a la pérdida de rendimiento por degradación inducida en una serie de celdas solares de polímeros conjugados empleando métodos ópticos y opto-eléctricos resueltos en el tiempo.

Del examen de una amplia gama de celdas solares orgánicas con diferentes propiedades ópticas, es evidente que todas ellas sufren de degradación en distintos grados. En esta tesis se analizó como la foto-oxidación causa severa reducción de la movilidad efectiva de los portadores de carga para todos los polímeros y como además induce pérdidas de extracción debido a los portadores de fondo foto-generados en las celdas solares de P3HT:PCBM. Las

celdas solares de BDT-DPP:PCBM sufren de la formación de excitones triples incluso cuando no se encuentran degradadas y que esta situación es aún peor tras la degradación térmica. En las OSC compuestas por KP115, no se encontró evidencia de portadores de carga de fondo luego de la foto-oxidación. La pérdida de rendimiento eléctrico en esta clase de materiales se asoció tentativamente con el crecimiento de dominios aislados de material Donor-Aceptor unido a trampas de oxígeno luego de la foto-oxidación. La movilidad y la recombinación de portadores de carga juega un papel importante en el transporte de carga en todos los semiconductores. Un examen más detenido y alternativo de la movilidad y la tasa de recombinación con un modelo modificado (por ejemplo: el modelo empleado para el cálculo de la movilidad de CELIV es demasiado general y derivado de semiconductores ordenados) ofrecería una comprensión mucho más clara y profunda del origen de las pérdidas por degradación. Estos hallazgos abren nuevos caminos para la optimización de métodos para la obtención de celdas solares orgánicas que sean más estables y eficientes, un tema sumamente importante para toda la humanidad en el futuro.

Se ha demostrado en esta tesis que, todos los materiales actualmente empleados ya sean como donante o aceptor en las celdas solares orgánicas sufren de degradación, sin embargo, a partir de estudios mecanísticos detallados, un conjunto cada vez mayor de principios de diseño están surgiendo. La adición de nuevas capas, el uso de aditivos, el encontrar barreras flexibles y económicas para la encapsulación, entre otros, se despliegan para mejorar la estabilidad mientras que aproximadamente se mantenga el rendimiento en el estado sin degradación. Inventar nuevos materiales , la aplicación de nuevos métodos de procesamiento , el desarrollo de nuevos modelos para el análisis y la comprensión de los fotofísica son cuestiones altamente demandadas para seguir avanzando en el campo.

Chapter 8

Conclusions and outlook

8.1 Conclusions

Insufficient operational lifetime is a major obstacle for the massive commercialization of organic solar cells. The effects of chemical degradation and thermal stress on the active layer of OSCs are still poorly understood. Therefore this thesis investigated the photo-oxidation and thermal degradation effects in a series of low and medium band gap conjugated polymer based organic solar cells such as P3HT, Si-PCPDTBT, KP115 and BDT:DPP blended with the universal electron acceptor $PC_{61}BM$ and related changes in the fundamental processes upon photooxidation. The experimental techniques used to investigate these degradation effects were transient absorption spectroscopy (TAS) across a wide range of time scales ranging from femtoseconds to milliseconds to explore the structure-property relationships in the pristine samples and upon degradation. In addition to TAS, complementary transient electrical and opto-electrical studies such as transient photovoltage (TPV), transient photocurrent (TPC) and charge extraction by linearly increasing voltage (CELIV) with and without optical excitation were also performed to monitor and to inspect the degradation induced performance losses in the organic solar cells.

Transient absorption studies on P3HT:PCBM films and on complete devices showed that the recombination rate is higher by about a factor of two in films than in devices. The reduced recombination rate in devices is explained by a partial separation of positive and negative carriers by the built-in field. Furthermore, the influence of highly conductive (h.c.) PEDOT:PSS on charge carrier recombination has been studied. By performing transient absorption studies with different degrees of spatial overlap between pump and probe pulse, we found a clearly delayed build-up of charge density when pump and probe pulses did not overlap. However, the final polaron decay dynamics were independent on the amount of overlap. These findings supported the picture of fast lateral diffusion mediated by PEDOT, allowing the polarons to spread over the whole active area at their disposal. Supplementary studies on photo-induced absorption spectra (PIA spectra) showed a clear confirmation of the h.c.-PEDOT:PSS mediated recombination route in P3HT:PCBM solar cells.

The influence of oxygen on non-encapsulated P3HT:$PC_{61}BM$ and Si-PCPDTBT:PCBM solar cells was examined by exposure of the devices to synthetic air under specific conditions. It was found that the charge generation rate hardly changes during photo-oxidation, suggesting that the yield of extractable charges is practically independent of the level of degradation. However, the oxygen induced degradation causes a strong reduction of the charge recombination coefficient, which formally corresponds to a reduction of charge carrier mobility. A deviation in the recombination order (from pure bimolecular to pseudo monomolecular) was observed for P3HT, whereas the recombination of Si-PCPDTBT clearly deviated from a pure bimolecular model even in the pristine case. The extraction rate of charge carriers was even more seriously reduced by photo-degradation than expected from the mobility changes calculated from the recombination term. This leads to the loss of short circuit current in degraded devices. While the rate of extraction exceeds that of recombination by two orders of magnitude in pristine samples, both rates are more or less equal in strongly degraded samples. The photo-CELIV measurements confirm the mobility reduction and the strong reduction of extractable carriers due to the increase in the background carrier density.

The calculation of the IQE reduction as a function of sub-Langevin factor (f_{LV}), photo-induced background carrier concentration (c_b), and effective charge carrier mobility (μ), showed that at reasonable values for f_{LV}, mobility plays a stronger role than c_b, but both effects might not be sufficient to explain the strong J_{sc} reduction observed upon photo-oxidation. This suggests that the increased background carrier density introduced by irreversible degradation contributes to the loss of short circuit current by shielding the extraction field in the bulk of the devices, which corresponds to a decrease of E_{bi} and thus leads to an additional decrease of the extraction efficiency. This additional decrease leads to a longer dwelling time of the photo-generated carriers in the device so that in turn their recombination is significantly enhanced in the pseudo-first order reaction observed in our TA measurements, similar to the effect has been shown to be operative in reversibly degraded P3HT:PCBM solar cells.

Studies on the influence of photooxidation on the electrical performance in KP115:PCBM solar cells suggested that the observed huge loss in the short circuit current J_{sc} is due to the combined effects of reduction in the effective mobility and formation of isolated donor/acceptor islands without percolative paths towards the electrodes. Different from the above cases of P3HT:PCBM and Si-PCPDTBT:PCBM, the photooxidation of KP115:PCBM does not alter the recombination order and creates no background carriers, which are the major deteriorating effects of performance in the case of P3HT:PCBM solar cells upon

photooxidation. We also observed by measurement of time-resolved photocurrents, that even in pristine devices of KP115:PCBM, the charge extraction is incomplete, indicating that the morphology is not optimum. Further studies need to be done on this material in order to explore and improve the stability against other degradation triggers such as humidity and temperature.

The last chapter of this thesis is concerned with thermal degradation. Depending on geographical region of deployment, OSC can reach up to 80°C under operational conditions. As the optimum nanomorphology in terms of efficiency is often not the thermodynamically most stable one, elevated temperatures tend to evolve the nanomorphology in the active layer towards thermodynamic equilibrium, causing electrical performance loss. A series of OSCs comprising novel low band gap polymers of the DPP class, with different side chains was provided by Merck Ltd, Southampton, U.K. As the side chains have negligible influence on the electronic structure while strongly influencing intermolecular interaction, this series of compounds provided a unique opportunity to specifically address the influence of intermolecular interaction on the elementary processes of organic photovoltaics, and their sensitivity towards thermally induced morphology changes. In general terms it was found that all DPP based polymers show triplet generation as efficient loss channel. Thus, although charge generation proceeded at high external efficiencies, owing to the low bandgap of the polymers, a high percentage of the photo-induced carriers could not be extracted due to geminate and nongeminate recombination losses. A very specific dependence of the recombination rates on the substituents of the electron donating benzothiophene (BDT) moiety was observed. In the absence of substituents, a very strong tendency for geminate recombination was observed, while in the presence of an aromatic substituent, nongeminate recombination was found to be strong. Using aliphatic substituents on the other hand caused only limited recombination, and enhanced stability of electrical performance against thermal degradation.

8.2 Outlook

In this section, a survey of the future research directions is given. Despite of the remarkable advances achieved in the field of organic solar cells, the current state of the art is still primitive relative to the required operational lifetime. One of the long-standing issues in achieving the long term stability is the understanding of degradation mechanisms especially under oxygen, humidity and elevated temperatures. This thesis aims at contributing to

unravelling the stability issues by mapping elementary processes to degradation-induced performance loss in a series of conjugated polymer based solar cells by using transient optical, electrical and opto-electrical methods.

From the examination of a wide range of organic solar cells having different optical properties, it is clear that all organic solar cells seriously suffer from degradation to varying extent. This thesis found that photooxidation causes severe reduction in the effective mobility of charge carriers for all polymers and also induces extraction losses due to photogenerated background carriers in P3HT:PCBM solar cells. The BDT-DPP:PCBM solar cells suffer from triplet excitons even in the pristine case and to an even higher extent upon thermal degradation. In OSC comprising KP115, we did not find evidence for background carriers upon photooxidation. The electrical performance loss in this class of materials was tentatively associated with the growth of isolated D/A islands along with oxygen trap upon photooxidation. The mobility and recombination of charge carriers play important roles in the charge transport in all semiconductors. A closer and alternative examination of mobility and the recombination rate with a modified model (e.g.: the model used for calculating mobility from CELIV is too specific and derived for ordered semiconductors) would allow much clearer and deeper understanding of the origin of degradation losses. These findings pave the new ways to optimisation methods for stable and efficient organic solar cells, a topic of utmost importance for the entire mankind in the future.

It has been demonstrated in this thesis that all donor and acceptor materials currently employed in organic solar cells suffer from degradation, however, from detailed mechanistic studies an increasing set of design principles is emerging. Adding new layers, using additives, finding cheap and efficient flexible barriers for encapsulation etc., are deployed to improve the stability while approximately maintaining the performance in the pristine state. Inventing new materials, applying new processing methods, developing new models for analysing and understanding the photophysics are in high demand to further advance the field.

9. References

1. Bentley, R. W. Global oil & gas depletion: an overview. *Energy Policy* **30,** 189–205 (2002).
2. Kerr, R. A. How Urgent Is Climate Change? *Science* **318,** 1230–1231 (2007).
3. Grossiord, N., Kroon, J. M., Andriessen, R. & Blom, P. W. M. Degradation mechanisms in organic photovoltaic devices. *Org. Electron.* **13,** 432–456 (2012).
4. Hermann, W. A. Quantifying global exergy resources. *Energy* **31,** 1685–1702 (2006).
5. Deibel, C. & Dyakonov, V. Polymer–fullerene bulk heterojunction solar cells. *Rep. Prog. Phys.* **73,** 096401 (2010).
6. Sims, L., Egelhaaf, H.-J., Hauch, J. A., Kogler, F. R. & Steim, R. in *Comprehensive Renewable Energy* (ed. Sayigh, A.) 439–480 (Elsevier, 2012). at <http://www.sciencedirect.com/science/article/pii/B9780080878720001207>
7. Chapin, D. M., Fuller, C. S. & Pearson, G. L. A New Silicon p-n Junction Photocell for Converting Solar Radiation into Electrical Power. *J. Appl. Phys.* **25,** 676–677 (1954).
8. Chiang, C. K. *et al.* Electrical Conductivity in Doped Polyacetylene. *Phys. Rev. Lett.* **39,** 1098–1101 (1977).
9. Chiang, C. K. *et al.* Synthesis of highly conducting films of derivatives of polyacetylene, (CH)x. *J. Am. Chem. Soc.* **100,** 1013–1015 (1978).
10. Shirakawa, H., Louis, E. J., MacDiarmid, A. G., Chiang, C. K. & Heeger, A. J. Synthesis of electrically conducting organic polymers: halogen derivatives of polyacetylene, (CH)x. *J. Chem. Soc. Chem. Commun.* 578–580 (1977). doi:10.1039/C39770000578
11. Branker, K., Pathak, M. J. M. & Pearce, J. M. A review of solar photovoltaic levelized cost of electricity. *Renew. Sustain. Energy Rev.* **15,** 4470–4482 (2011).
12. Bagnall, D. M. & Boreland, M. Photovoltaic technologies. *Energy Policy* **36,** 4390–4396 (2008).
13. *Third Generation Photovoltaics*. **12,** (Springer Berlin Heidelberg, 2006).
14. Britt, J. & Ferekides, C. Thin-film CdS/CdTe solar cell with 15.8% efficiency. *Appl. Phys. Lett.* **62,** 2851–2852 (1993).
15. Chu, T. L. *et al.* 13.4% efficient thin-film CdS/CdTe solar cells. *J. Appl. Phys.* **70,** 7608–7612 (1991).
16. Fthenakis, V. Sustainability of photovoltaics: The case for thin-film solar cells. *Renew. Sustain. Energy Rev.* **13,** 2746–2750 (2009).
17. Fthenakis, V. M. & Moskowitz, P. D. Thin-film Photovoltaic Cells: Health and Environmental Issues in their Manufacture Use and Disposal. *Prog. Photovolt. Res. Appl.* **3,** 295–306 (1995).
18. Alonso, E. *et al.* Evaluating Rare Earth Element Availability: A Case with Revolutionary Demand from Clean Technologies. *Environ. Sci. Technol.* **46,** 3406–3414 (2012).

19. Green, M. A. Third generation photovoltaics: Ultra-high conversion efficiency at low cost. *Prog. Photovolt. Res. Appl.* **9,** 123–135 (2001).
20. Thompson, B. C. & Fréchet, J. M. J. Polymer-fullerene composite solar cells. *Angew. Chem. Int. Ed Engl.* **47,** 58–77 (2008).
21. Chamberlain, G. A. Organic solar cells - A review. *Sol. Cells* **8,** 47–83 (1983).
22. Tang, C. W. Two-layer organic photovoltaic cell. *Appl. Phys. Lett.* **48,** 183–185 (1986).
23. Smalley, R. E. Discovering the fullerenes. *Rev. Mod. Phys.* **69,** 723–730 (1997).
24. Lüer, L. *et al.* Oxygen-induced quenching of photoexcited states in polythiophene films. *Org. Electron.* **5,** 83–89 (2004).
25. Stübinger, T. & Brütting, W. Exciton diffusion and optical interference in organic donor–acceptor photovoltaic cells. *J. Appl. Phys.* **90,** 3632–3641 (2001).
26. Yu, G., Gao, J., Hummelen, J. C., Wudl, F. & Heeger, A. J. Polymer photovoltaic cells: Enhanced efficiencies via a network of internal donor-acceptor heterojunctions. *Science* **270,** 1789–1791 (1995).
27. He, Z. *et al.* Simultaneous Enhancement of Open-Circuit Voltage, Short-Circuit Current Density, and Fill Factor in Polymer Solar Cells. *Adv. Mater.* **23,** 4636–4643 (2011).
28. Service, R. F. Solar energy. Outlook brightens for plastic solar cells. *Science* **332,** 293 (2011).
29. Distler, A. *et al.* The Effect of PCBM Dimerization on the Performance of Bulk Heterojunction Solar Cells. *Adv. Energy Mater.* **4,** n/a–n/a (2014).
30. Jørgensen, M., Norrman, K. & Krebs, F. C. Stability/degradation of polymer solar cells. *Sol. Energy Mater. Sol. Cells* **92,** 686–714 (2008).
31. Jørgensen, M. *et al.* Stability of Polymer Solar Cells. *Adv. Mater.* **24,** 580–612 (2012).
32. Karuthedath, S. *et al.* The effect of oxygen induced degradation on charge carrier dynamics in P3HT:PCBM and Si-PCPDTBT:PCBM thin films and solar cells. *J. Mater. Chem. A* **3,** 3399–3408 (2015).
33. Norrman, K., Madsen, M. V., Gevorgyan, S. A. & Krebs, F. C. Degradation Patterns in Water and Oxygen of an Inverted Polymer Solar Cell. *J. Am. Chem. Soc.* **132,** 16883–16892 (2010).
34. Gavrilenko, A. V. *et al.* Optical Absorption of Poly(thienylene vinylene)-Conjugated Polymers: Experiment and First Principle Theory†. *J. Phys. Chem. C* **112,** 7908–7912 (2008).
35. Hoppe, H., Arnold, N., Sariciftci, N. S. & Meissner, D. Modeling the optical absorption within conjugated polymer/fullerene-based bulk-heterojunction organic solar cells. *Sol. Energy Mater. Sol. Cells* **80,** 105–113 (2003).
36. Liang, Y. *et al.* For the Bright Future—Bulk Heterojunction Polymer Solar Cells with Power Conversion Efficiency of 7.4%. *Adv. Mater.* **22,** E135–E138 (2010).
37. Morse, G. E. *et al.* The effect of polymer solubilizing side-chains on solar cell stability. *Phys. Chem. Chem. Phys. PCCP* **17,** 11884–11897 (2015).

38. Di Nuzzo, D. *et al.* Improved Film Morphology Reduces Charge Carrier Recombination into the Triplet Excited State in a Small Bandgap Polymer-Fullerene Photovoltaic Cell. *Adv. Mater.* **22,** 4321–4324 (2010).
39. Scholes, G. D. & Rumbles, G. Excitons in nanoscale systems. *Nat. Mater.* **5,** 683–696 (2006).
40. Brédas, J.-L., Beljonne, D., Coropceanu, V. & Cornil, J. Charge-transfer and energy-transfer processes in pi-conjugated oligomers and polymers: a molecular picture. *Chem. Rev.* **104,** 4971–5004 (2004).
41. Dyakonov, V., Rösler, G., Schwoerer, M. & Frankevich, E. L. Evidence for triplet interchain polaron pairs and their transformations in polyphenylenevinylene. *Phys. Rev. B* **56,** 3852–3862 (1997).
42. Köhler, A. & Bässler, H. What controls triplet exciton transfer in organic semiconductors? *J. Mater. Chem.* **21,** 4003–4011 (2011).
43. Cowan, S. R., Banerji, N., Leong, W. L. & Heeger, A. J. Charge Formation, Recombination, and Sweep-Out Dynamics in Organic Solar Cells. *Adv. Funct. Mater.* **22,** 1116–1128 (2012).
44. McNeill, C. R. *et al.* Efficient Polythiophene/Polyfluorene Copolymer Bulk Heterojunction Photovoltaic Devices: Device Physics and Annealing Effects. *Adv. Funct. Mater.* **18,** 2309–2321 (2008).
45. Zhou, Y. *et al.* Donor−Acceptor Molecule as the Acceptor for Polymer-Based Bulk Heterojunction Solar Cells. *J. Phys. Chem. C* **113,** 7882–7886 (2009).
46. McNeill, C. R. & Greenham, N. C. Conjugated-Polymer Blends for Optoelectronics. *Adv. Mater.* **21,** 3840–3850 (2009).
47. Shaw, P. E., Ruseckas, A. & Samuel, I. D. W. Exciton Diffusion Measurements in Poly(3-hexylthiophene). *Adv. Mater.* **20,** 3516–3520 (2008).
48. Spanggaard, H. & Krebs, F. C. A brief history of the development of organic and polymeric photovoltaics. *Sol. Energy Mater. Sol. Cells* **83,** 125–146 (2004).
49. Hwang, I.-W., Moses, D. & Heeger, A. J. Photoinduced Carrier Generation in P3HT/PCBM Bulk Heterojunction Materials. *J. Phys. Chem. C* **112,** 4350–4354 (2008).
50. Sariciftci, N. S., Smilowitz, L., Heeger, A. J. & Wudl, F. Photoinduced electron transfer from a conducting polymer to buckminsterfullerene. *Science* **258,** 1474–1476 (1992).
51. Guo, J., Ohkita, H., Benten, H. & Ito, S. Charge Generation and Recombination Dynamics in Poly(3-hexylthiophene)/Fullerene Blend Films with Different Regioregularities and Morphologies. *J. Am. Chem. Soc.* **132,** 6154–6164 (2010).
52. Clarke, T. M. & Durrant, J. R. Charge photogeneration in organic solar cells. *Chem. Rev.* **110,** 6736–6767 (2010).
53. Frankevich, E. L. *et al.* Polaron-pair generation in poly(phenylene vinylenes). *Phys. Rev. B* **46,** 9320–9324 (1992).
54. Grancini, G. *et al.* Hot exciton dissociation in polymer solar cells. *Nat. Mater.* **12,** 29–33 (2013).

55. Deibel, C. *et al.* Bulk vs. surface recombination in polymer-fullerene solar cells. in **7416,** 74160Q–74160Q–6 (2009).
56. Braun, C. L. Electric field assisted dissociation of charge transfer states as a mechanism of photocarrier production. *J. Chem. Phys.* **80,** 4157–4161 (1984).
57. Onsager, L. Initial Recombination of Ions. *Phys. Rev.* **54,** 554–557 (1938).
58. Veldman, D. *et al.* Compositional and Electric Field Dependence of the Dissociation of Charge Transfer Excitons in Alternating Polyfluorene Copolymer/Fullerene Blends. *J. Am. Chem. Soc.* **130,** 7721–7735 (2008).
59. Arkhipov, V. I., Heremans, P. & Bässler, H. Why is exciton dissociation so efficient at the interface between a conjugated polymer and an electron acceptor? *Appl. Phys. Lett.* **82,** 4605–4607 (2003).
60. Peumans, P. & Forrest, S. R. Separation of geminate charge-pairs at donor–acceptor interfaces in disordered solids. *Chem. Phys. Lett.* **398,** 27–31 (2004).
61. Deibel, C., Strobel, T. & Dyakonov, V. Origin of the Efficient Polaron-Pair Dissociation in Polymer-Fullerene Blends. *Phys. Rev. Lett.* **103,** 036402 (2009).
62. Ohkita, H. *et al.* Charge Carrier Formation in Polythiophene/Fullerene Blend Films Studied by Transient Absorption Spectroscopy. *J. Am. Chem. Soc.* **130,** 3030–3042 (2008).
63. Groves, C., Marsh, R. A. & Greenham, N. C. Monte Carlo modeling of geminate recombination in polymer-polymer photovoltaic devices. *J. Chem. Phys.* **129,** 114903 (2008).
64. Bässler, H. Charge Transport in Disordered Organic Photoconductors a Monte Carlo Simulation Study. *Phys. Status Solidi B* **175,** 15–56 (1993).
65. Pivrikas, A., Sariciftci, N. S., Juška, G. & Österbacka, R. A review of charge transport and recombination in polymer/fullerene organic solar cells. *Prog. Photovolt. Res. Appl.* **15,** 677–696 (2007).
66. Manceau, M. *et al.* Photochemical stability of π-conjugated polymers for polymer solar cells: a rule of thumb. *J. Mater. Chem.* **21,** 4132–4141 (2011).
67. Seemann, A. *et al.* Reversible and irreversible degradation of organic solar cell performance by oxygen. *Sol. Energy* **85,** 1238–1249 (2011).
68. Deschler, F. *et al.* The Effect of Ageing on Exciton Dynamics, Charge Separation, and Recombination in P3HT/PCBM Photovoltaic Blends. *Adv. Funct. Mater.* **22,** 1461–1469 (2012).
69. Seemann, A., Egelhaaf, H.-J., Brabec, C. J. & Hauch, J. A. Influence of oxygen on semi-transparent organic solar cells with gas permeable electrodes. *Org. Electron.* **10,** 1424–1428 (2009).
70. Klimov, E., Li, W., Yang, X., Hoffmann, G. G. & Loos, J. Scanning Near-Field and Confocal Raman Microscopic Investigation of P3HT−PCBM Systems for Solar Cell Applications. *Macromolecules* **39,** 4493–4496 (2006).

71. Gytis Juska, K. G. Two dimensional Langevin recombination in regioregular poly(3-hexylthiophene). *Appl. Phys. Lett.* **95,** 013303 – 013303–3 (2009).
72. Österbacka, R. *et al.* Mobility and density relaxation of photogenerated charge carriers in organic materials. *Curr. Appl. Phys.* **4,** 534–538 (2004).
73. Mihailetchi, V. D., Wildeman, J. & Blom, P. W. M. Space-Charge Limited Photocurrent. *Phys. Rev. Lett.* **94,** 126602 (2005).
74. Shuttle, C. G., Hamilton, R., Nelson, J., O'Regan, B. C. & Durrant, J. R. Measurement of Charge-Density Dependence of Carrier Mobility in an Organic Semiconductor Blend. *Adv. Funct. Mater.* **20,** 698–702 (2010).
75. Schafferhans, J., Baumann, A., Deibel, C. & Dyakonov, V. Trap Distribution and the Impact of Oxygen-induced Traps on the Charge Transport in Poly(3-Hexylthiophene). *Appl. Phys. Lett.* **93,** 093303 (2008).
76. Mozer, A. J. *et al.* Time-dependent mobility and recombination of the photoinduced charge carriers in conjugated polymer/fullerene bulk heterojunction solar cells. *Phys. Rev. B* **72,** 035217 (2005).
77. Nelson, J. Diffusion-limited recombination in polymer-fullerene blends and its influence on photocurrent collection. *Phys. Rev. B* **67,** 155209 (2003).
78. Nelson, J. Polymer:fullerene bulk heterojunction solar cells. *Mater. Today* **14,** 462–470 (2011).
79. Hoppe, H. & Sariciftci, N. S. in *Photoresponsive Polymers II* (eds. Marder, S. R. & Lee, K.-S.) 1–86 (Springer Berlin Heidelberg, 2007). at <http://link.springer.com/chapter/10.1007/12_2007_121>
80. Saive, R., Mueller, C., Schinke, J., Lovrincic, R. & Kowalsky, W. Understanding S-shaped current-voltage characteristics of organic solar cells: Direct measurement of potential distributions by scanning Kelvin probe. *Appl. Phys. Lett.* **103,** 243303 (2013).
81. Roland Steim, S. A. C. Formation and impact of hot spots on the performance of organic photovoltaic cells. *Appl. Phys. Lett.* **94,** (2009).
82. Kalowekamo, J. & Baker, E. Estimating the manufacturing cost of purely organic solar cells. *Sol. Energy* **83,** 1224–1231 (2009).
83. Turkovic, V. *et al.* Multiple stress degradation analysis of the active layer in organic photovoltaics. *Sol. Energy Mater. Sol. Cells* **120, Part B,** 654–668 (2014).
84. Hermenau, M. *et al.* Water and oxygen induced degradation of small molecule organic solar cells. *Sol. Energy Mater. Sol. Cells* **95,** 1268–1277 (2011).
85. Bertho, S. *et al.* Effect of temperature on the morphological and photovoltaic stability of bulk heterojunction polymer:fullerene solar cells. *Sol. Energy Mater. Sol. Cells* **92,** 753–760 (2008).
86. Brabec, C. J. *et al.* Polymer–Fullerene Bulk-Heterojunction Solar Cells. *Adv. Mater.* **22,** 3839–3856 (2010).

87. Yang, Y.-H., Bolling, L., Priolo, M. A. & Grunlan, J. C. Super Gas Barrier and Selectivity of Graphene Oxide-Polymer Multilayer Thin Films. *Adv. Mater.* **25,** 503–508 (2013).
88. Yoshihide Santo, I. J. Mixture of [60] and [70]PCBM giving morphological stability in organic solar cells. *APL Org. Electron. Photonics* **6,** (2013).
89. Kumar Barik, U., Srinivasan, S., Nagendra, C. L. & Subrahmanyam, A. Electrical and optical properties of reactive DC magnetron sputtered silver oxide thin films: role of oxygen. *Thin Solid Films* **429,** 129–134 (2003).
90. Lloyd, M. T. *et al.* Impact of contact evolution on the shelf life of organic solar cells. *J. Mater. Chem.* **19,** 7638–7642 (2009).
91. Dyer-Smith, C. *et al.* Interplay Between Side Chain Pattern, Polymer Aggregation, and Charge Carrier Dynamics in PBDTTPD:PCBM Bulk-Heterojunction Solar Cells. *Adv. Energy Mater.* **5,** n/a–n/a (2015).
92. Etzold, F. *et al.* The Effect of Solvent Additives on Morphology and Excited-State Dynamics in PCPDTBT:PCBM Photovoltaic Blends. *J. Am. Chem. Soc.* **134,** 10569–10583 (2012).
93. Krebs, F. C. Fabrication and processing of polymer solar cells: A review of printing and coating techniques. *Sol. Energy Mater. Sol. Cells* **93,** 394–412 (2009).
94. Yang, X. *et al.* Crystalline Organization of a Methanofullerene as Used for Plastic Solar-Cell Applications. *Adv. Mater.* **16,** 802–806 (2004).
95. Seck, M. *et al.* Characterization of the degradation process of Si-PCPDTBT:PC70BM(1:2) blend layers deposited on ITO/glass substrate. *Sol. Energy Mater. Sol. Cells* **132,** 210–214 (2015).
96. Wang, X. *et al.* Morphology Related Photodegradation of Low-Band-Gap Polymer Blends. *Adv. Energy Mater.* **4,** n/a–n/a (2014).
97. Brabec, C. J. Organic photovoltaics: technology and market. *Sol. Energy Mater. Sol. Cells* **83,** 273–292 (2004).
98. Krebs, F. C., Tromholt, T. & Jørgensen, M. Upscaling of polymer solar cell fabrication using full roll-to-roll processing. *Nanoscale* **2,** 873–886 (2010).
99. Kaduwal, D. *et al.* ITO-free organic solar cells with roll-to-roll coated organic functional layers from non-halogenated solvents. *Sol. Energy Mater. Sol. Cells* **124,** 92–97 (2014).
100. Espinosa, N., García-Valverde, R., Urbina, A. & Krebs, F. C. A life cycle analysis of polymer solar cell modules prepared using roll-to-roll methods under ambient conditions. *Sol. Energy Mater. Sol. Cells* **95,** 1293–1302 (2011).
101. Krebs, F. C. All solution roll-to-roll processed polymer solar cells free from indium-tin-oxide and vacuum coating steps. *Org. Electron.* **10,** 761–768 (2009).
102. Krebs, F. C., Alstrup, J., Spanggaard, H., Larsen, K. & Kold, E. Production of large-area polymer solar cells by industrial silk screen printing, lifetime considerations and lamination with polyethyleneterephthalate. *Sol. Energy Mater. Sol. Cells* **83,** 293–300 (2004).

103. Aernouts, T. *et al.* Printable anodes for flexible organic solar cell modules. *Thin Solid Films* **451–452,** 22–25 (2004).
104. Yulia Galagan, J.-E. J. M. R. ITO-free flexible organic solar cells with printed current collecting grids. *Sol. Energy Mater. Sol. Cells - Sol. ENERG MATER Sol. CELLS* **95,** (2011).
105. Zimmermann, B., Würfel, U. & Niggemann, M. Longterm stability of efficient inverted P3HT:PCBM solar cells. *Sol. Energy Mater. Sol. Cells* **93,** 491–496 (2009).
106. Manceau, M., Angmo, D., Jørgensen, M. & Krebs, F. C. ITO-free flexible polymer solar cells: From small model devices to roll-to-roll processed large modules. *Org. Electron.* **12,** 566–574 (2011).
107. Angmo, D. *et al.* Scalability and stability of very thin, roll-to-roll processed, large area, indium-tin-oxide free polymer solar cell modules. *Org. Electron.* **14,** 984–994 (2013).
108. Alzoubi, K., Hamasha, M. M., Lu, S. & Sammakia, B. Bending Fatigue Study of Sputtered ITO on Flexible Substrate. *J. Disp. Technol.* **7,** 593–600 (2011).
109. Angmo, D. *et al.* Outdoor Operational Stability of Indium-Free Flexible Polymer Solar Modules Over 1 Year Studied in India, Holland, and Denmark. *Adv. Eng. Mater.* **16,** 976–987 (2014).
110. Hintz, H., Egelhaaf, H.-J., Peisert, H. & Chassé, T. Photo-oxidation and ozonization of poly(3-hexylthiophene) thin films as studied by UV/VIS and photoelectron spectroscopy. *Polym. Degrad. Stab.* **95,** 818–825 (2010).
111. Manceau, M., Rivaton, A., Gardette, J.-L., Guillerez, S. & Lemaître, N. The mechanism of photo- and thermooxidation of poly(3-hexylthiophene) (P3HT) reconsidered. *Polym. Degrad. Stab.* **94,** 898–907 (2009).
112. Pacios, R. *et al.* Effects of Photo-oxidation on the Performance of Poly[2-methoxy-5-(3′,7′-dimethyloctyloxy)-1,4-phenylene vinylene]:[6,6]-Phenyl C61-Butyric Acid Methyl Ester Solar Cells. *Adv. Funct. Mater.* **16,** 2117–2126 (2006).
113. Hintz, H. *et al.* Photodegradation of P3HT−A Systematic Study of Environmental Factors. *Chem. Mater.* **23,** 145–154 (2011).
114. Abdou, M. S. A., Orfino, F. P., Son, Y. & Holdcroft, S. Interaction of Oxygen with Conjugated Polymers: Charge Transfer Complex Formation with Poly(3-alkylthiophenes). *J. Am. Chem. Soc.* **119,** 4518–4524 (1997).
115. Rivaton, A. *et al.* Light-induced degradation of the active layer of polymer-based solar cells. *Polym. Degrad. Stab.* **95,** 278–284 (2010).
116. Billingham, N. C., Calvert, P. D., Foot, P. J. S. & Mohammad, F. Stability and degradation of some electrically conducting polymers. *Polym. Degrad. Stab.* **19,** 323–341 (1987).
117. McCullough, R. D. The Chemistry of Conducting Polythiophenes. *Adv. Mater.* **10,** 93–116 (1998).
118. Liang, Z., Nardes, A., Wang, D., Berry, J. J. & Gregg, B. A. Defect Engineering in π-Conjugated Polymers. *Chem. Mater.* **21,** 4914–4919 (2009).

119. Liang, Z., Reese, M. O. & Gregg, B. A. Chemically Treating Poly(3-hexylthiophene) Defects to Improve Bulk Heterojunction Photovoltaics. *ACS Appl. Mater. Interfaces* **3,** 2042–2050 (2011).
120. Tapponnier, A., Biaggio, I. & Günter, P. Ultrapure C60 field-effect transistors and the effects of oxygen exposure. *Appl. Phys. Lett.* **86,** 112114 (2005).
121. Hamed, A., Sun, Y. Y., Tao, Y. K., Meng, R. L. & Hor, P. H. Effects of oxygen and illumination on the \textit{in} \textit{situ} conductivity of ${\mathrm{C}}_{60}$ thin films. *Phys. Rev. B* **47,** 10873–10880 (1993).
122. Norrman, K., Larsen, N. B. & Krebs, F. C. Lifetimes of organic photovoltaics: Combining chemical and physical characterisation techniques to study degradation mechanisms. *Sol. Energy Mater. Sol. Cells* **90,** 2793–2814 (2006).
123. Madsen, M. V., Norrman, K. & Krebs, F. C. Oxygen- and water-induced degradation of an inverted polymer solar cell: the barrier effect. *J. Photonics Energy* **1,** 011104–011104–6 (2011).
124. Schäfer, S. *et al.* Influence of the indium tin oxide/organic interface on open-circuit voltage, recombination, and cell degradation in organic small-molecule solar cells. *Phys. Rev. B* **83,** 165311 (2011).
125. Shuttle, C. G. *et al.* Bimolecular recombination losses in polythiophene: Fullerene solar cells. *Phys. Rev. B* **78,** 113201 (2008).
126. Cabanillas-Gonzalez, J., Grancini, G. & Lanzani, G. Pump-Probe Spectroscopy in Organic Semiconductors: Monitoring Fundamental Processes of Relevance in Optoelectronics. *Adv. Mater.* **23,** 5468–5485 (2011).
127. van Stokkum, I. H. M., Larsen, D. S. & van Grondelle, R. Global and target analysis of time-resolved spectra. *Biochim. Biophys. Acta BBA - Bioenerg.* **1657,** 82–104 (2004).
128. Howard, I. A., Mauer, R., Meister, M. & Laquai, F. Effect of Morphology on Ultrafast Free Carrier Generation in Polythiophene:Fullerene Organic Solar Cells. *J. Am. Chem. Soc.* **132,** 14866–14876 (2010).
129. O'Regan, B. C. & Durrant, J. R. Calculation of Activation Energies for Transport and Recombination in Mesoporous TiO2/Dye/Electrolyte FilmsTaking into Account Surface Charge Shifts with Temperature. *J. Phys. Chem. B* **110,** 8544–8547 (2006).
130. Shuttle, C. G. *et al.* Experimental determination of the rate law for charge carrier decay in a polythiophene: Fullerene solar cell. *Appl. Phys. Lett.* **92,** 093311 (2008).
131. M Stephen, S. K. Degradation Effects on Charge Carrier Transport in P3HT:PCBM Solar Cells Studied by Photo-CELIV and ToF. (2014).
132. Ohkita, H. & Ito, S. Transient absorption spectroscopy of polymer-based thin-film solar cells. *Polymer* **52,** 4397–4417 (2011).
133. Li, G. *et al.* 'Solvent Annealing' Effect in Polymer Solar Cells Based on Poly(3-hexylthiophene) and Methanofullerenes. *Adv. Funct. Mater.* **17,** 1636–1644 (2007).

134. Padinger, F., Rittberger, R. s. & Sariciftci, N. s. Effects of Postproduction Treatment on Plastic Solar Cells. *Adv. Funct. Mater.* **13,** 85–88 (2003).
135. Ma, W., Yang, C., Gong, X., Lee, K. & Heeger, A. J. Thermally Stable, Efficient Polymer Solar Cells with Nanoscale Control of the Interpenetrating Network Morphology. *Adv. Funct. Mater.* **15,** 1617–1622 (2005).
136. Li, G. *et al.* High-efficiency solution processable polymer photovoltaic cells by self-organization of polymer blends. *Nat. Mater.* **4,** 864–868 (2005).
137. Koppe, M. *et al.* Charge Carrier Dynamics in a Ternary Bulk Heterojunction System Consisting of P3HT, Fullerene, and a Low Bandgap Polymer. *Adv. Energy Mater.* **3,** 949–958 (2013).
138. Juška, G. *et al.* Charge transport in $\ensuremath{\pi}$-conjugated polymers from extraction current transients. *Phys. Rev. B* **62,** R16235–R16238 (2000).
139. Carsten Deibel, D. R. Order of decay of mobile charge carriers in P3HT:PCBM solar cells. *Appl. Phys. Lett.* **103,** 043307 (2013).
140. Shockley, W. & Read, W. T. Statistics of the Recombinations of Holes and Electrons. *Phys. Rev.* **87,** 835–842 (1952).
141. Movaghar, B., Grünewald, M., Ries, B., Bassler, H. & Würtz, D. Diffusion and relaxation of energy in disordered organic and inorganic materials. *Phys. Rev. B* **33,** 5545–5554 (1986).
142. Silva, C. *et al.* Efficient exciton dissociation via two-step photoexcitation in polymeric semiconductors. *Phys. Rev. B* **64,** 125211 (2001).
143. Nenashev, A. V. *et al.* Role of Diffusion in Two-dimensional Bimolecular Recombination. *Appl. Phys. Lett.* **96,** 213304 (2010).
144. Clarke, T. M. *et al.* Significantly Reduced Bimolecular Recombination in a Novel Silole-Based Polymer: Fullerene Blend. *Adv. Energy Mater.* **1,** 1062–1067 (2011).
145. Heumueller, T. *et al.* Disorder-Induced Open-Circuit Voltage Losses in Organic Solar Cells During Photoinduced Burn-In. *Adv. Energy Mater.* n/a–n/a (2015). doi:10.1002/aenm.201500111
146. Clarke, T. M. *et al.* Photodegradation in Encapsulated Silole-Based Polymer: PCBM Solar Cells Investigated using Transient Absorption Spectroscopy and Charge Extraction Measurements. *Adv. Energy Mater.* **3,** 1473–1483 (2013).
147. McNeill, C. R., Hwang, I. & Greenham, N. C. Photocurrent transients in all-polymer solar cells: Trapping and detrapping effects. *J. Appl. Phys.* **106,** 024507 (2009).
148. Etzold, F. *et al.* Sub-ns triplet state formation by non-geminate recombination in PSBTBT:PC70BM and PCPDTBT:PC60BM organic solar cells. *Energy Environ. Sci.* **8,** 1511–1522 (2015).
149. Bundgaard, E. & Krebs, F. C. Low band gap polymers for organic photovoltaics. *Sol. Energy Mater. Sol. Cells* **91,** 954–985 (2007).

150. He, Z. *et al.* Enhanced power-conversion efficiency in polymer solar cells using an inverted device structure. *Nat. Photonics* **6,** 591–595 (2012).
151. You, J. *et al.* 10.2% Power Conversion Efficiency Polymer Tandem Solar Cells Consisting of Two Identical Sub-Cells. *Adv. Mater.* **25,** 3973–3978 (2013).
152. Adams, J. *et al.* Water Ingress in Encapsulated Inverted Organic Solar Cells: Correlating Infrared Imaging and Photovoltaic Performance. *Adv. Energy Mater.* n/a–n/a (2015). doi:10.1002/aenm.201501065
153. Bagienski, W. & Gupta, M. C. Temperature dependence of polymer/fullerene organic solar cells. *Sol. Energy Mater. Sol. Cells* **95,** 933–941 (2011).
154. Roberts, A. P. *et al.* Gas permeation in silicon-oxide/polymer (SiOx/PET) barrier films: role of the oxide lattice, nano-defects and macro-defects. *J. Membr. Sci.* **208,** 75–88 (2002).
155. Sachs-Quintana, I. T. *et al.* Electron Barrier Formation at the Organic-Back Contact Interface is the First Step in Thermal Degradation of Polymer Solar Cells. *Adv. Funct. Mater.* **24,** 3978–3985 (2014).
156. Kwon, M.-H. Stability of Bulk Heterojunction Organic Solar Cells with Different Blend Ratios of P3HT:PCBM. *Trans. Electr. Electron. Mater.* **13,** 98–101 (2012).
157. Xiao, Z. *et al.* Effect of molecular weight on the properties and organic solar cell device performance of a donor–acceptor conjugated polymer. *Polym. Chem.* **6,** 2312–2318 (2015).
158. Kim, J.-H., Lee, M., Yang, H. & Hwang, D.-H. A high molecular weight triisopropylsilylethynyl (TIPS)-benzodithiophene and diketopyrrolopyrrole-based copolymer for high performance organic photovoltaic cells. *J. Mater. Chem. A* **2,** 6348–6352 (2014).
159. Ochsmann, J. R. *et al.* Triplet State Formation in Photovoltaic Blends of DPP-Type Copolymers and PC71BM. *Macromol. Rapid Commun.* **36,** 1122–1128 (2015).
160. Brinkmann, M. Structure and morphology control in thin films of regioregular poly(3-hexylthiophene). *J. Polym. Sci. Part B Polym. Phys.* **49,** 1218–1233 (2011).
161. Kwong, C. Y., Djurišić, A. B., Chui, P. C., Cheng, K. W. & Chan, W. K. Influence of solvent on film morphology and device performance of poly(3-hexylthiophene):TiO2 nanocomposite solar cells. *Chem. Phys. Lett.* **384,** 372–375 (2004).
162. Zhang, L. *et al.* Vertical phase separation in bulk heterojunction solar cells formed by in situ polymerization of fulleride. *Sci. Rep.* **4,** (2014).
163. Jeranko, T., Tributsch, H., Sariciftci, N. S. & Hummelen, J. C. Patterns of efficiency and degradation of composite polymer solar cells. *Sol. Energy Mater. Sol. Cells* **83,** 247–262 (2004).
164. Gevaerts, V. S., Furlan, A., Wienk, M. M., Turbiez, M. & Janssen, R. A. J. Solution Processed Polymer Tandem Solar Cell Using Efficient Small and Wide bandgap Polymer:Fullerene Blends. *Adv. Mater.* **24,** 2130–2134 (2012).
165. Kouijzer, S. *et al.* Efficient Inverted Tandem Polymer Solar Cells with a Solution-Processed Recombination Layer. *Adv. Energy Mater.* **2,** 945–949 (2012).

166. Kesters, J. *et al.* Enhanced intrinsic stability of the bulk heterojunction active layer blend of polymer solar cells by varying the polymer side chain pattern. *Org. Electron.* **15,** 549–562 (2014).
167. Dimitrov, S. D. *et al.* Polaron pair mediated triplet generation in polymer/fullerene blends. *Nat. Commun.* **6,** (2015).
168. Virgili, T. *et al.* Spectroscopic Signature of Trap States in Assembled CdSe Nanocrystal Hybrid Films. *J. Phys. Chem. C* **116,** 16259–16263 (2012).
169. Heiber, M. C., Baumbach, C., Dyakonov, V. & Deibel, C. Encounter-Limited Charge-Carrier Recombination in Phase-Separated Organic Semiconductor Blends. *Phys. Rev. Lett.* **114,** 136602 (2015).

Appendix 1

A.1 Derivation of the fitting function for charge decay in degraded samples

Photooxidation in P3HT and Si-PCPDTBT can cause a background of space charge even in the absence of irradiation, by introducing deep traps for one carrier type. These background carriers do not give rise to a transient absorption (TA) signal (because they are not photo-induced), but they do influence the decay kinetics of the photo-induced polarons, because they are at the disposal for recombination.

We assume degradation-induced defects in the donor (P3HT or Si-PCPDTBT) phase that act as acceptors for electrons.[h] The auto-dissociation equilibrium, given by the dissociation and recombination coefficients k_d and k_a, respectively, cause an excess density of positive polarons that, upon photoexcitation of negative and positive polarons, causes a deviation of polaron recombination kinetics from simple bimolecular behavior. The kinetic scheme is given by

$$\begin{bmatrix} 0 \underset{k_L}{\overset{g(L)}{\rightleftharpoons}} p + n \\ A \underset{k_a}{\overset{k_d}{\rightleftharpoons}} A^- + p \end{bmatrix}, \tag{A1. 1}$$

where 0 signifies a neutral polymer strand, p and n are negative polarons in the donor and acceptor phase, respectively, A and A^- are neutral and negatively charged defects in the donor phase. The generation term g(L) in our experimental setup is a boxcar function that depends on light intensity L. Since the density of negative polarons in the donor phase can be neglected, an interaction between these latter species and A can be neglected. Electro-neutrality then requires that at all times,

[h]The assumption of electron donors would lead to the same concentration-time law for P3HT polarons, under the given assumptions.

$$A^- + n = p \tag{A1. 2}$$

Assuming complete ionization of defect sites, we get $A^- = const = A_{tot}$ (A_{tot} being the total density of degradation-induced defect sites) and therefore

$$p(t) = n(t) + A_{tot} \tag{A1. 3}$$

For equation A1.3 to hold during the experimentally accessible time range, we also require the autoionization equilibrium to be faster than the typical recombination times, i.e. in A1.1, $k_d + k_a \gg k_L$. This assumption is different from the one by Seemann et.al [1]., who assume that k_a is very slow and thermally activated, which is justified in their system by the observation of a photo-induced build-up of persistent background carriers. Here, we do not observe such a phenomenon, and we are concerned with an unknown electrochemistry (i.e. we do not know the redox potentials of the irreversible photoinduced defects while Seemann et al, studying reversible oxygen effects, can rely on the known redox potential of the O_2/O_2^- system).

The rate equation for negative polarons is thus given by

$$\frac{dn}{dt} = G(L) - k_L(t) \cdot (n(t) + A_{tot}) \cdot n(t) \tag{A1. 4}$$

In order to account for dispersive effects, we choose a polynomial ansatz for the recombination coefficient:

$$k_L(t) = k_L^0 \cdot t^{-\gamma} \tag{A1. 5}$$

The experimentally obtained differential absorption ΔA(t), is related to the polaron concentration via the Beer-Lambert law,

$$\Delta A(t) = A(t)_{pumpon} - A(t)_{pumpoff} = \sigma_p^{970\,nm} \cdot \Delta p(t) \cdot d, \tag{A1. 6}$$

Where $\sigma_p^{970\,nm}$ is the positive polaron absorption cross-section at the probe wavelength of 970 nm, d is the film thickness, and Δp(t) is given by ;

$$\Delta p(t) = p(t)p_{pumpon} - p(t)_{pumpoff} \quad \text{(A1. 7)}$$

When the pump pulse is off, n(t)=0; from A1. 3 we then obtain;

$$p(t)_{pumpoff} = A_{tot} \quad \text{(A1. 8)}$$

Inserting A1.3 and A1.8 into A1.7, we obtain;

$$\Delta p(t) = n(t), \quad \text{(A1. 9)}$$

And inserting A1.9 into A1.6 and rearranging gives;

$$n(t) = \Delta A(t)/\left(\sigma_p^{970\,nm} \cdot d\right) \quad \text{(A1. 10)}$$

We insert A1.10 into A1.4 and obtain after rearranging;

$$\frac{d\Delta A(t)}{dt} = \sigma_p^{970\,nm} \cdot d \cdot g(L) - \frac{k_L(t)}{\left(\sigma_p^{970\,nm} \cdot d\right)} \cdot \left[\Delta A(t) + \sigma_p^{970\,nm} \cdot d \cdot A_{tot}\right] \cdot \Delta A(t) \quad \text{(A1. 11)}$$

We define a spectroscopic recombination rate constant $k_r'(t) = \frac{k_r(t)}{\left(\sigma_p^{970\,nm} \cdot d\right)}$ and a spectroscopic generation term $G'(L) = \sigma_p^{970\,nm} \cdot d \cdot g(L)$. From A1.6 and A1.8, we learn that the absorption caused by the "background polarons" is $A_P^{background} = \sigma_p^{970\,nm} \cdot d \cdot A_{tot}$. Inserting these relations into A1.11, we obtain finally

$$\frac{d\Delta A(t)}{dt} = G'(L) - k_r'(t) \cdot \left[\Delta A(t) + A_p^{background}\right] \cdot \Delta A(t) \quad \text{(A1. 12)}$$

Equation A1.12 is solved numerically by standard ODE (ordinary differential equation) solvers. By variation of $G'(L)$, $k_r'(t)$, and $A_p^{background}$, we fit the calculated transient absorption profile to the experimental one. For each sample and degradation level, we fit all measured dynamics at different light intensities globally. Minimizing the global error squared with standard non-linear optimization techniques, checking that no systematic deviations are present, and using $\sigma_p^{970\,nm} \approx 10^{-16} cm^2$and d=250 nm, we obtain the device parameters $k_r(t)$ and A_{tot} quantitatively at each degradation level.

In equation A1.12, the fitting parameters $A_p^{background}$ and γ (inside $k_L(t)$) both act on the long term asymptotic form of the concentration-time dependence. This raises the question how strong the cross talk between these parameters is expected to be in the fits. Below, we give some simulations that show quite distinct long-time behaviors for variation of γ and $A_P^{background}$, respectively.

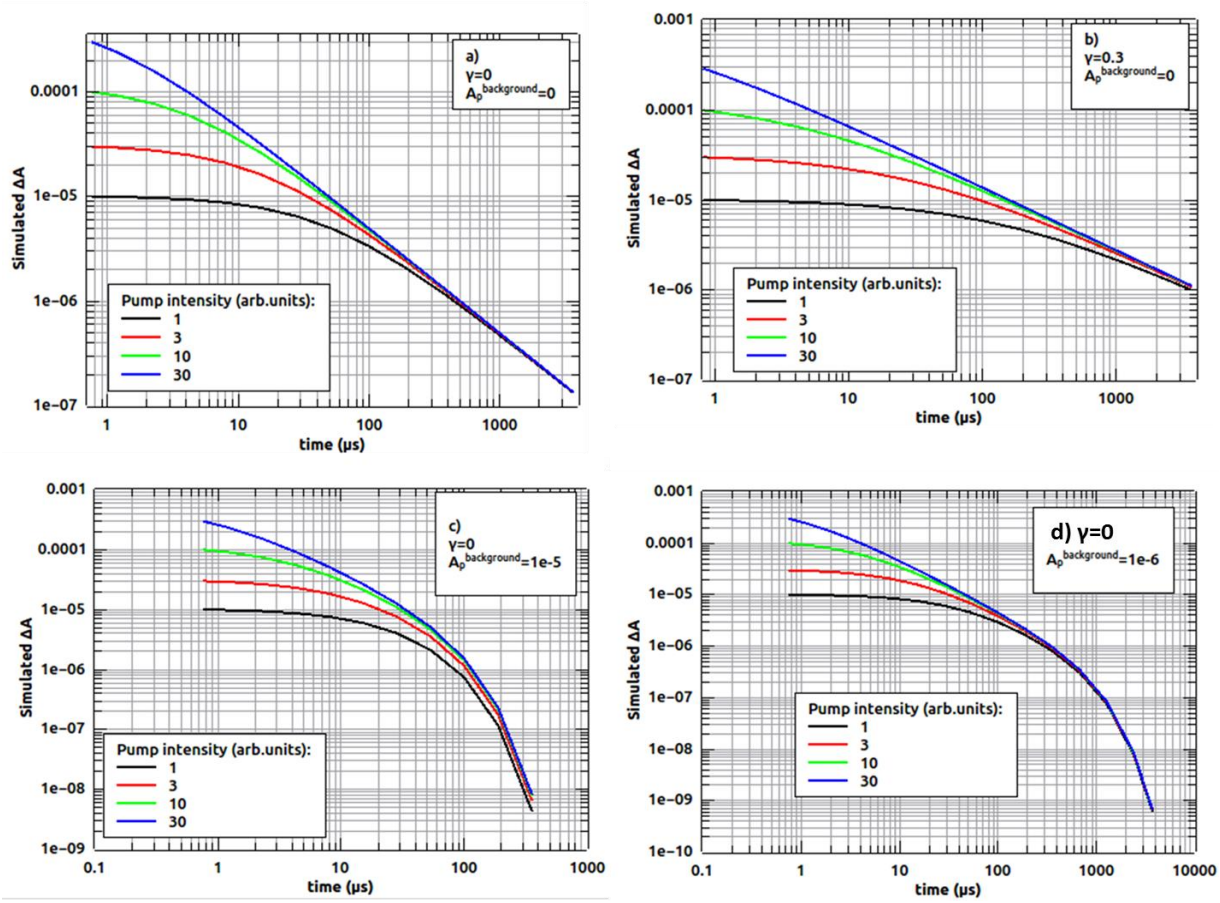

Figure A1.1: Simulated transient absorption traces for different γ values and for background carrier concentrations at different intensities.

In figure A1.1a, both γ=0 and $A_p^{background}$= 0. In this case, equation A1.12 has the following solution:

$$\Delta A(t) = \left[{}^{1}/_{A(0)} + k_L t\right]^{-1}, \qquad \text{(A1. 13)}$$

which has an intensity independent long-time asymptote of $\Delta A(t) = [k_L t]^{-1}$, which is the same for all starting concentrations and has a slope of -1 in a double logarithmic

representation. In figure A1.1b, we leave $A_p^{background}= 0$ but set $\gamma = 0.3$. As can easily be shown, the long-time asymptote is still linear in a double logarithmic representation and independent of the starting concentration, but the slope is now $1-\gamma = 0.7$. Finally, in figure A1.1c, we set $\gamma = 0$ and $A_p^{background}= 10^{-5}$. In this case, an entirely different long-time solution is obtained: At a time when $A_p^{background}$ becomes comparable to the remaining polaron absorption $\Delta A(t)$, the decay trace deviates from bimolecular recombination. After very long times, $A_p^{background} >> \Delta A(t)$, so the bracket in A1.12 becomes a constant, and the solution is a stretched exponential. As can be seen in figure A1.1c, such a stretched exponential does not have a linear long-time asymptote, instead it bends towards infinite slope in a double logarithmic representation, nor is the long-term behavior intensity independent: for long times, all curves in figure A1.1c are y-shifted replicas of each other meaning that they deviate by a constant factor. In figure A1.1d finally, $A_p^{background}= 10^{-6}$. The condition $A_p^{background} >> \Delta A(t)$ is now obtained at a much later time than in figure A1.1c. For this reason, the two regimes (linear slope and final stretched exponential) can both be observed separately, at least at high intensities. When the stretched exponential part sets in after the intensity independent asymptote of the bimolecular decay has already been reached, it follows that also all stretched exponentials are independent of the initial concentration. The amount of intensity dependence still present in the stretched exponential part is therefore a probe for the background carrier concentration. Therefore, a global fitting of various curves at different starting concentrations, as performed here, is mandatory to disentangle γ from $A_p^{background}$.

Summarizing this curve discussion, a variation of γ causes a change in the slope of the linear asymptote, while a change in $A_p^{background}$ changes the time at which $A_p^{background}$ and $\Delta A(t)$ become comparable, which results in a deviation from the straight line behavior and in turn controls how much of the initial intensity variation is still visible in the long time exponential

decay phase. These phenomena are well distinguished and therefore both $A_p^{background}$ and γ can be fitted at the same time with low cross talk, but only if several curves of different starting concentration are fitted at the same time. This justifies the procedure we adopted for the analysis of the charge dynamics in of figures in Chapter 4 and 5 of this thesis.

Appendix 2

A.2.1 List of figures:

Figure 1.1: Different categories of photovoltaic technology

Figure 1.2: Schematics of single layer and bi-layer organic solar cell

Figure 1.3: Schematic architecture of a) normal b) inverted bulk hetero junction solar cell

Figure 1.4 Schematic representation of elementary processes in organic solar cell

Figure 1.5 Fundamental processes towards the photocurrent generation in a BHJ solar cell.

Figure 1.6 : Schematic representation of polaron pair dissociation in organic solar cells

Figure 1. 7 Schematic current-voltage curve representation of a BHJ solar cells

Figure 1.8 Major degradation triggers and types of degradation

Figure 1.9 Pictorial representation of possible degradation triggers in organic solar cells

Figure 2.1: a) Chemical structure of P3HT and b) UV-Vis absorption spectrum of P3HT:PCBM film

Figure 2.2: a) Chemical structure of Si-PCPDTBT and b) UV-Vis absorption spectrum of Si-PCPDTBT:PCBM film

Figure 2.3: a) Chemical structures of KP115 and b) UV-Vis absorption spectrum of KP115:PCBM film

Figure 2.4: Chemical structures of BDT-DPP polymers and b) UV-Vis absorption spectrum of BDT-DPP:PCBM film with different side chains

Figure 2.5: Chemical structure of $PC_{60}BM$

Figure 2.6: Chemical structures of (a) PEDOT:PSS and (b) PEI.

Figure 2.7: Structure of investigated organic solar cells

Figure 2.8: Scheme of pump-probe experiment

Figure 2.9: Schematics of femtosecond pump probe spectroscopy

Figure 2.10: Figure 2.10: A typical evolution associated differential spectra (EADS) obtained from a global fit for P3HT:PCBM film

Figure 2.11: Schematics of microsecond transient absorption spectroscopy

Figure 2.12: Simplified experimental setup for transient photo voltage and transient photo current measurements.

Figure 2.13: Experimental arrangements for CELIV (a) and photo-CELIV (b)

Figure2.14: The pulse sequence and schematic response of CELIV and photo-CELIV transients

Figure 3.1: Schematic diagram of working principle of organic solar cells.

Figure 3.2: Evolution associated differential spectra (EADS) at 10nJ pump intensity for P3HT:PCBM

Figure 3.3: Charge carrier recombination traces in P3HT:PCBM films at different light intensities and at 970 nm probing wavelength, upon termination of illumination.

Figure 3.4: Transient absorption (black) and transient photo-voltage (red) traces at different background intensities.

Figure 3.5 : (a) The variation of charge carrier density and in the open circuit voltage upon incease in the background light intesnity obtained form the TAS. (b) Changes in recombiation time ($t_{\Delta n}$) of charge carriers extracted by applying mono exponential fits to TA and TPV traces.

Figure 3.6: (a) Transient absorption decay traces for film (balck) and for complete device (red) and (b) normlalized transient absorption traces.

Figure 3.7: Schematic representation of charge carrier distribution in film

Figure 3.8: Schematic representation of charge carrier distribution in solar cells

Figure 3.9:Normalized transient absorption traces for P3HT:PCBM film without PEDOT:PSS layer and for the whole device having PEDOT:PSS layer

Figure 3.10:Detecting lateral diffusion of charge carriers

Figure 3.11: Photo induced absorption (PIA) spectra with full overlap between pump and probe (black, represented as 0) and pump and probe are separated by a distance of 2 times the probe diameter (red curves) of (a) of (a)P3HT:PCBM solar cell and (b) P3HT:PCBM film

Figure 4.1 : Current density–voltage (J–V) characteristics for P3HT:PCBM and for Si-PCPDTBT:PCBM

Figure 4.2: Charge generation in P3HT:PCBM and Si-PCPDTBT:PCBM as a function of photo-oxidation

Figure 4.3: Charge transients in polymer:PCBM films at different light intensities at 970 nm probing wavelength, upon termination of illumination

Figure 4.4: a) Dark CELIV transienst at diferent levels of degradation at 1V applied voltage with a ramp rate 10^5V/s. b) Corresponding photo-CELIV transients with a ramp rate 10^4V/s for mobility measurements and carreir density measurements. c) Photo-CELIV transients with respect to delay time without any offset for the pristine sample with 1V pulse and ramp rate of $5*10^3$ V/s for pristine sample

Figure 4.5: Fitting parameters from fitting of the curves in Fig. 4.3 (panel a) and Fig. 4.4 (panels b–d) using eqn (4.5)

Figure 4.6: TA traces in P3HT:PCBM solar cells under open circuit (OC) and short circuit (SC) conditions, at various stages of photo-degradation, as given in the legends.

Figure 4.7: Simulation of internal quantum efficiency (IQE) as a function of effective charge carrier mobility for various values of the sub-Langevin parameter fLV, according to eqn (1a) and (4)

Figure 4.8: a)Equilibrium carrier density with degradation, from dark-CELIV transients with ramp rate 10^5V/S (black curves) and corresponding loss the mobility obtained from photo-CELIV with ramp rate 10^4V/S. b) Calculated extracted carriers at different delay time for different degradation levels.

Figure 5.1: Current density-voltage curves for pristine and photo-oxidised KP115:PCBM (1:2) solar cells measured at AM 1.5 sun. a) Before reannealing and b) after reannealing at 130^{o}C for 5 min in glove box.

Figure 5.2: Parameters extracted from figure 5.1. a) Short circuit current density, b) open circuit voltage, c) fill factor and d) power conversion efficiency before and after reannealing (black and red curves respectively) at 130^{o}C in glovebox for all photooxidation levels.

Figure 5.3: a) UV-Vis absorption spectra of KP115:PCBM for all photo-oxidation levels, inset shows the zoomed in region where the KP115 absorption peak changes. b) Comparing normalized optical density loss (black spheres) with loss in short circuit current (red squares) for all degardation levels.

Figure 5.4: Evolution associated differential spectra (EADS) at 200nJ pump intensity for KP115:PCBM, as obtained from a global analysis of using a 3 sequential step model

Figure 5.5: Difference in the EADS a) for pristine and b) for photooxidized KP115:PCBM thin films.

Figure 5.6: Charge transients KP115:PCBM solar cells a) at different degradation levels and at 9mW and b) at different pumping intensities for 2hrs photooxidation. The symbols are measured curve and solid lines are corresponding fit with eqn.5.1.

Figure5.7: Parameters obtained from the global fits of figure 5.4a using equation 5.1. a)Evolution of bimolecular recombination coefficient at 1μs, and b) dispersive parameter, γ for all degradation levels.

Figure5.8: TA traces in KP115:PCBM solar cells under open circuit (OC) and short circuit (SC) conditions

Figure 5.9: Disruption of percolation pathways in KP115:PCBM solar cells upon photooxidation. a)Sub-optimal morphology in pristine solar cell and b) islands formation upon photooxidation.

Figure 5.10: a) Normalized transient photovolatge traces of KP115:PCBM solar cells at different levels of degardation. b) Time taken to drop 100mV of initial Voc for at each degradation levels

Figure5.11: a)Transient photocurrent decays of KP115:PCBM solar cells upon photooxidation and b)normalized TPC traces of a.

Figure 5.12: a) Amount of extrcatble charge carriers with photooxidation obtained by integarating the area under the curve of each TPC transients and b) time taken to drop 60% of initial carrier density for at each degradation levels.

Figure 6.1: Chemical structure donor polymers studied (a) and inverted device architecture (b).

Figure 6.2: Transient absorption (TA) spectra at different pump-probe delay times (given in ps) for EP1 and EP2

Figure 6.3: Transient absorption (TA) spectra at different pump-probe delay times (given in ps) for EP4 and EP6

Figure 6.4: Dynamics of charge carriers in the donor polymer after 150 fs pulses at 775 nm with low and high pump energy (black and red symbols, respectively), obtained as time-resolved spectral weights of the polaron bands in the spectral fits in Fig.6.2 and 6.3.

Figure 6.5: a) charge recombination parameter k_L as obtained from global fitting to charge carrier dynamics according to eq.2 under open circuit conditions; b) effective mobility μ_{eff} obtained from global fitting of TPC transients according to eq. 6; c) sub-Langevin parameter f_L as obtained from eq. 3 using the values from panels a) and b)

A.2.2 List of tables:

Table 2.3: Characteristic values of the EP polymers

Table 2. 4: Elementary processes in an organic solar cell and their approximate lifetimes.

Table 6.1: : Electrical parameters of OSC comprising materials EP1,2,4, and 6 under AM1.5 conditions, in the pristine state (p) and after 50 hrs at 50°C (deg). An asterisk marks values that have been reached after an intermediate increase of the respective parameter at short degradation times.

Table 6.2: Parameters obtained after performing a target analysis of the time-dependent spectral weights of S, P, and T. Where k_{ng} is non-geminate recombination rate, k_g is geminate recombination rate and γ is dispersiveness parameter.

Appendix 3

A.3 Acronyms

PV	Photovoltaic
OSC	Organic Solar Cells
OPV	Organic Photovoltaic
1G	1st Generation solar cells
2G	Second Generation solar cells
3G	Third Generation solar cells
CdTe	Cadmium Telluride
LCOE	Levelized Cost Of Electricity
CIGS	Copper Indium Gallium Selenide
DSSC	Dye Sensitized Solar Cells
BHJ	Bulk Heterojunction
HOMO	Highest Occupied Molecular Orbital
LUMO	Lowest Unoccupied Molecular Orbital
AM 1.5	Air Mass 1.5
Vis	Visible
NIR	Near Infra-Red
P3HT	Poly [3-hexyl thiophene]
PCBM	[6,6]-Phenyl-C61-butyric acid methyl ester
MEH-PPV	Poly [2-methoxy-5-(2-ethylhexyloxy)-1,4-phenylenevinylene]
TEM	Transmission Electron Microscopy
PP	Polaron Pair
CTS	Charge Transfer State
OB	Onsager-Braun
CELIV	Charge Extraction by Linearly Increasing Voltage

HTL	Hole Transport Layer
ETL	Electron Transport Layer
J-V	Current-Voltage
EQE	External Quantum Efficiency
IQE	Internal Quantum Efficiency
PCE	Power Conversion Efficiency
FF	Fill Factor
Voc	Open Circuit Voltage
Jsc	Short Circuit Current
Tg	Glass transition temperature
R2R	Roll to Roll
ITO	Indium Tin Oxide
PET	Poly Ethylene Terephthalate
PEDOT:PSS	Poly(3,4-ethylenedioxythiophene) polystyrene sulfonate
ISOS	International Summit on OPV Stability
XPS	X-ray Photon Spectroscopy
ToF-SIMS	time-of-Flight Secondary Ion Mass Spectrometry
PAL	Photoactive Layer
TCE	Transparent Conducting Electrode
TPV	Transient Photovoltage
TPC	Transient Photocurrent
TAS	Transient Absorption Spectroscopy
PDI	Polydispersity Index
Si-PCPDTBT	Poly [(4,4 0-bis(2-ethylhexyl) dithieno[3,2-b:2 0,3 0-d]silole)-2,6-diyl-alt-(4,7-bis(2-thienyl)-2,1,3-benzothiadiazole)-5,5 0-diyl]
PDTSTzTz (KP115)	Poly [(4,4′ - bis (2-ethylhexyl) dithieno [3,2-b:2′,3′-d] silole) - 2,6-diyl-alt-(2,5-bis 3-tetradecylthiophen-2-yl thiazolo 5,4-d thiazole)-2,5diyl]
BDT-DPP	Poly (benzodithiophene–diketopyrrolopyrrole)

Mw	Molecular Weight
UV/Vis	Linear optical absorption spectroscopy in the Ultraviolet and Visible spectral region
HOMO	Highest Occupied Molecular Orbital
LUMO	Lowest Unoccupied Molecular Orbital
AOM	Acousto-Optic Modulator
PIA	Photoinduced Absorption
D/A	Donor-Acceptor
BIPV	Building Integrated Photovoltaics
OD	Optical Density
ΔA	Differential Absorption
CW	Continuous Wave
OC	Open Circuit
SC	Short Circuit
UV	Ultra Violet
RR	Regio Regular
RRa	Regio Random
DOS	Density Of States
SMU	Source Measure Unit

Publications

[1] M. Stephen, **S. Karuthedath**, T. Sauermann, K. Genevičius, G. Juška :Degradation effects on charge carrier transport in P3HT: PCBM solar cells studied by Photo-CELIV and ToF**, Proc. SPIE 9184, Organic Photovoltaics XV, 918424, (2014).**

[2] **S. Karuthedath**, T. Sauermann, H-J. Egelhaaf, R. Wannemacher, C. J. Brabec, L. Lüer : The effect of oxygen induced degradation on charge carrier dynamics in P3HT: PCBM and Si-PCPDTBT: PCBM thin films and solar cells. **Journal of Material Chemistry A**, **3, 3399-3408, (2015).**

[3] **S. Karuthedath**, G. Morse, L. Lüer: Improved thermal stability of low band gap polymer solar cells: Relating device performance to blend morphology. To be submitted.

[4] A. Isakova, S. Dowland, **S. Karuthedath**, P. Topham, Larry Lüer: Decoupling blend morphology segregation from other degradation effects in organic photovoltaics using time-resolved techniques. Submitted, **Energy& Environmental Science,(2015).**

[5] **S. Karuthedath**, J. Cabanillas-Gonzalez, T. Sauermann, R. Wannemacher, H.-J. Egelhaaf, C. Brabec, L. Lüer: Lateral diffusion in P3HT:PCBM solar cells induced by high-conductivity PEDOT. To be submitted.

[6] **S. Karuthedath**, D. Deribew, H-J. Egelhaaf, A. Distler, L. Lüer: Tracing photo-oxidation effects in Silole based polymer solar cells. In preparation.